UNIVERSITY OF SOUTHAMPTON

DEPARTMENT OF ELECTRONICS AND COMPUTER SCIENCE

OPTICAL FIBRE LASERS AND AMPLIFIERS

by

ROBERT JOSEPH MEARS

A Thesis Submitted for the Degree of

Doctor of Philosophy

July 1987

UNIVERSITY OF SOUTHAMPTON

ABSTRACT

FACULTY OF ENGINEERING AND APPLIED SCIENCE

ELECTRONICS AND COMPUTER SCIENCE

Doctor of Philosophy

OPTICAL FIBRE LASERS AND AMPLIFIERS

by Robert Joseph Mears

Abstract

This thesis describes the development and characterisation of single-mode optical fibre lasers and amplifiers. Although the fibre laser configuration was first employed over twenty years ago, its application to conventional optical fibre technology has not been demonstrated previously.

The new devices are based on single-mode fibres doped with rare-earth ions, notably neodymium and erbium. The combination of strong absorption bands, long fluorescence lifetimes, low fibre losses in the infra-red and small fibre cores have made possible very low threshold and efficient fibre lasers. Experiments on the tunability, output spectra and pulsed operation of these devices are described. A number of world firsts, including the lowest threshold and widest tuning range of a doped glass laser, and the efficient CW operation of an erbium-doped three level laser, have been achieved. High-gain amplification at 1.54μm, the preferred wavelength for optical communication, has also been demonstrated. The results have been modelled by adapting conventional laser theory to the single-mode fibre configuration, and some simple design criteria are considered.

LIST OF CONTENTS

Acknowledgements

Grateful acknowledgement is made to many members of the Optical Fibre Group, past and present, for their support and guidance. In particular I would like to thank Professor Alec Gambling for his patient advice and encouragement and Dr. David Payne for his helpful direction throughout the course of my studies.

The investigation of rare-earth-doped fibre lasers and amplifiers was made possible by the fabrication expertise of Simon Poole. Laurence Reekie, who joined the Group in the early days of doped-fibres, has proved a constant source of support and enthusiasm. I would also like to thank Ian Jauncey and Lin Jin-Tong, whose presence in the labs during the past year has added greatly to the spirit of innovation.

The majority of the experiments on fibre couplers were done in collaboration with Dr. Cathy Ragdale, although the ideas on modelling their behaviour are my own. Since I started my study of fibre lasers and amplifiers, Sam Yataki has further developed fused tapered couplers, and special thanks are owed to him for the fabrication to my specification of the couplers used in the amplifier and ring laser experiments. Other members of the Group who deserve a grateful mention are Dr. Frank Payne for many helpful discussions, and Drs. Robin Birch and Martin Gold for their continual encouragement.

No acknowledgements would be complete without a big thank-you to Nicki Pink for typing the manuscript and Chris Nash for patiently helping to prepare the figures.

Over the past few months my parents have sacrificed their dining room table to find a home for my writing, so I know how much this thesis means to them!

Finally I would like to thank Kathy for her continual love, support and encouragement.

CHAPTER 1 : INTRODUCTION

1.1 Active Fibres

One of the most striking features of the optical fibre is its ability to convey light for long distances within a core of glass dimensionally similar to the optical wavelength. The potential for lightwave communication was first recognised in the 1960's[1], following the advent of the laser[2], and the large bandwidth of optical signals (greater than 1THz [3]) has served to establish the optical fibre as a major long-distance telecommunications medium. This progess has been made possible by significant advances in fibre fabrication techniques[4,5,6] which have resulted in a reduction in fibre loss from many hundreds of dB/km to the state-of-the-art level of 0.15dB/km at a wavelength of 1.55μm [7]. The optical fibre is not simply a transmission medium. The high light intensities that can be generated within the small core of the fibre make it possible to design optical fibres which actively process light. The idea behind the majority of the work described in this thesis is the design of a fibre which amplifies light rather than attenuating it[8]. The critical difference is in the glass composition. Whereas the current trend is towards greater material purification in order to minimise losses, the key to the amplifying fibre described here is the addition of small amounts of special dopants to the silica glass[9].

In its simplest form the optical fibre amplifier is a step-index single-mode fibre with a doped core region. When light of an appropriate wavelength (the pump) is launched into the fibre, the dopant ions absorb strongly and fluoresce at a characteristic wavelength. At sufficient pump powers, the fluorescence is amplified by stimulated emission as it passes along the fibre. If feedback is provided (usually in the form of mirrors butted to the fibre ends), then at a particular pump power

(threshold), the round trip gain will overcome the round trip losses, and the fibre will lase at the fluorescence wavelength. Without the feedback, the fibre simply acts as an amplifier.

The dopants which have been exploited to date in optical fibre lasers and amplifiers are rare-earth ions, notably neodymium (Nd^{3+})[8], erbium (Er^{3+})[10,11] and praseodymium (Pr^{3+})[12]. The ions differ in their absorption and fluorescence wavelengths, and span much of the optical wavelengths of interest for communications. There remain a wide variety of other dopant materials to be investigated, including the transition metal ions, and research is continuing. The level of doping need only be a few parts per million (ppm), and the most heavily doped fibre used in this work has an ion concentration of a few hundred ppm. It is possible, however, to add dopant ions up to tens of thousands of ppm whilst maintaining the glass structure. These heavily-doped fibres have exciting prospects for future research.

1.2 Review of Fibre Lasers and Amplifiers

1.2.1 Background

The neodymium glass laser was one of the first solid state lasers to be demonstrated[13]. Since then, glass lasers have received considerable attention, and reviews of much of the work are to be found in papers by Snitzer and Young[14,15]. Many rare-earth ions have been made to lase in glass, including neodymium[13], erbium[16] and holmium[17]. Of these ions neodymium has received the most attention, because it can be operated at room-temperature with high efficiency.

Glass lasers differ from crystal lasers in a number of respects. The fluorescence linewidths of dopant ions are considerably broader in glass, than in crystal hosts, resulting in higher thresholds for lasing. In

return, glass lasers are tunable[18,19] and can produce pulses of shorter duration and higher energy[20]. The thermal conductivity of glass is much smaller than that of crystals, resulting in considerable thermal problems for continuous wave (CW), or high repetition rate, glass lasers. For this reason, the majority of CW solid-state lasers commercially available are based on crystalline hosts. Glasses and crystals can be doped with a variety of ions, but glasses are the more versatile in their physical properties, and can accommodate a large number of different ions.

The two disadvantages of glass lasers are thus higher thresholds and thermal problems. Both of these can be overcome in the optical fibre laser configuration. The threshold power for laser oscillation is generally proportional to the cross-sectional area of the active medium. Fibre lasers have thresholds which are orders of magnitude smaller than their bulk counterparts. In order to absorb the pumping radiation effectively, a longitudinal pump scheme and a relatively long interaction length are required. The fibre waveguide is ideal in this respect. Furthermore, the extremely large length/diameter ratio (up to 10^8), and efficient pumping, act together to eliminate thermal problems.

1.2.2 New fibre from old

Snitzer's first glass laser[13] employed a cladded glass rod, i.e. a crude optical waveguide, in order to reduce the oscillation threshold, and some of the early observations of fibre waveguide modes were made in such devices[21]. If the field of fibre optics is dated from Kao and Hockham's proposal to use dielectric waveguides for optical communication[1], then fibre lasers could be argued to pre-date fibre optics! Nevertheless, since that time, glass lasers have played little part in optical fibre research and vice versa. The few exceptions include the

demonstration of lasing in a multimode Nd^{3+}-doped fibre with a GaAlAs diode laser pump, by Stone and Burrus[22] in 1973, and a paper by Galant et al[23] in the same year.

The fabrication techniques for optical fibres have progressed dramatically since the early 70's. The invention of the modified chemical vapour deposition technique (MCVD) in 1975 [5,6], and further refinements in purification and drying have resulted in a reduction in fibre losses by orders of magnitude. It is timely, therefore, that a re-examination of the advantages of fibre lasers be made, in particular with emphasis on the application of active fibres to the expanding fields of optical fibre devices and circuitry.

1.3 Contents

The thesis is divided into five main chapters which describe the most important aspects of optical fibre lasers and amplifiers. Chapter Two begins with a review of the properties of rare-earth ions in glass and a description of the optical fibre laser configuration. The gain in three-level and four-level fibre lasers is evaluated using a simple model which includes the mixed homogenous/inhomogenous broadening mechanisms. The model is applied to the CW operation of lasers and the calculation of the threshold power, output power and spectral broadening. Temporal relaxation and Q-switching are also considered.

Chapter Three describes the fabrication and characterisation of doped-fibres, concentrating specifically on neodymium-doped and erbium-doped fibres. Measurements on ground-state and excited-state absorption as well as spectral and temporal fluorescence are provided, and the chapter ends with a description of the fibres studied in laser and amplifier experiments.

Chapter Four deals exclusively with CW single-mode fibre lasers. The operation and optimisation of 3-level and 4-level neodymium-doped and erbium-doped lasers is first described. The threshold and slope efficiency results are amongst the best achieved for these systems. It has also been possible to fully exploit the tunability of the doped-glass lasers, which approach the performance of dye lasers. The chapter ends with a description of line-narrowing experiments.

Fibre lasers can be Q-switched and mode-locked to produce pulses of short duration and high peak power. Results on these topics are described in Chapter Five. Amplification is particularly suited to the fibre configuration because of its very small active area (typically 10^{-11} m^2). The chapter continues with a description of the properties of fibre amplifiers at 1.088μm (neodymium) and 1.54μm (erbium). The latter wavelength is of particular interest for optical communications. Other power-dependent effects described in this chapter are Raman generation from pulsed fibre lasers and a pump-dependent bistability.

The majority of the laser experiments described so far have been based on bulk optical components in conjunction with optical fibres. There is, however, considerable scope for the application of optical fibre components to create all-fibre laser devices[8].

Chapter Six describes the fundamental fibre component, the coupler, and its application to all-fibre ring lasers. During the work, a new model of operation of fused fibre couplers was developed, which accurately describes the influence of wavelength and refractive-index changes. Wavelength-selective couplers have been employed in efficient ring lasers, which are particularly robust, and fully compatible with other fibre devices.

Finally, in Chapter Seven, the future prospects for fibre lasers and amplifiers are considered, and conclusions drawn.

REFERENCES TO CHAPTER 1

1. K.C. Kao and G.A. Hockham:
"Dielectric-fibre surface waveguides for optical frequencies",
Proc. IEE., 1966, 113, pp. 1151-1158.

2. T.H. Maiman,
"Optical Maser Action in Ruby",
Brit. Comm. & Electronics, 1960, 7, pp. 674.

3. N.A. Olsson, J. Hegarty, R.A. Logan, L.F. Johnson, K.L. Walker, L.C. Cohen, B.L. Kasper and J.C. Campbell:
"Transmission with 1.37 Tbit km/sec capacity using ten wavelength division multiplexed lasers at 1.5μm",
Technical Digest OFC 1985, Paper WB6.

4. F.P. Kapron, D.B. Keck and R.D. Maurer:
"Radiation losses in glass optical waveguides",
Appl. Phys. Lett., 1970, 17, p. 423.

5. D.N. Payne and W.A. Gambling:
"New silica-based low-loss optical fibre",
Electron. Lett., 1974, 10, pp. 289-290.

6. J.B. MacChesney, P.B. O'Connor and H.M. Presby:
"A new technique for the prepration of low-loss and graded-index optical fibres",
Proc. IEEE, 1974, 62, pp. 1280-1281.

7. T. Miya, Y. Teranuma, T. Hosaka and T. Miyashita:
"Ultimate low-loss single-mode fibre at 1.55μm",
Electron. Lett., 1979, 15, pp. 106-108.

8. R.J. Mears, L. Reekie, S.B. Poole and D.N. Payne:
"Neodymium-doped silica single-mode fibre lasers",
Electron. Lett., 1985, 21, pp. 738-740.

9. S.B. Poole, D.N. Payne and M.E. Fermann:
"Fabrication of low-loss optical fibres containing rare-earth ions",
Electron. Lett., 1985, 21, pp. 737-738.

10. R.J. Mears, L. Reekie, S.B. Poole and D.N. Payne:
"A low threshold tunable CW and Q-switched fibre laser at 1.55μm",
Electron. Lett., 1986, 22, pp. 159-160.

11. R.J. Mears, L. Reekie, I.M. Jauncey and D.N. Payne:
"High gain rare-earth-doped fibre amplifier at 1.54μm",
Proc. OFC, 1987, Reno.

12. L. Reekie, R.J. Mears, S.B. Poole and D.N. Payne:
"A Pr^{3+}-doped single-mode fibre laser",
IOP/IEE Symposium on Advances in Solid State Lasers, Imperial College, 7th May 1986.

13. E. Snitzer:
"Optical maser action of Nd^{3+} in a barium crown glass",
Phys. Rev. Lett., 1961, 7, pp. 444-446.

14. E. Snitzer and C.G. Young:
"Glass lasers",
Advances in Lasers, Vol. 2, A. Levine Ed.,
New York: Dekker 1968, pp. 191-256.

15. C.G. Young:
"Glass Lasers",
Proc. IEEE, 1969, 57, pp. 1267-1289.

16. E. Snitzer and R. Woodcock:
"Yb^{3+}-Er^{3+} glass laser",
Appl. Phys. Lett., 1965, 6, pp. 45-46.

17. H.W. Gandy and R.J. Ginther:
"Stimulated emission from holmium activated silicate glass",
Proc. IRE, 1962, 50, pp. 2113-2114.

18. E. Snitzer:
"Frequency control of a Nd^{3+} glass laser",
Appl. Opt., 1966, 5, pp. 121-125.

19. P.C. Magnante:
"A high spectral-radiance neodymium glass laser",
IEEE Journal of Quant. Electron., 1968, QE-4,
pp. 363-364.

20. A.J. DeMaria, W.H. Glenn, M.J. Brienza and M.E. Mack:
"Picosecond Laser Pulses",
Proc. IEEE, 1969, 57, pp. 2-25.

21. E. Snitzer:
"Cylindrical dielectric waveguide modes",
J. Opt. Soc. Amer., 1961, 51, pp. 491.

22. J. Stone and C.A. Burrus:
"Neodymium doped silica laser in end-pumped fibre geometry",
Appl. Phys. Lett., 1973, 23, pp. 388-389.

23. E.I. Galant, Y.N. Kondrat'ev, A.K. Przevuskii, M.N. Tolstoi and V.N. Shapovalov:
"Stimulated emission of neodymium ions in quartz glass",
JETP Lett., 1974, 18, pp. 372.

CHAPTER 2 : THEORY OF OPTICAL FIBRE LASERS

The aim of this chapter is to outline a model for the operation of fibre lasers and amplifiers, based on conventional solid-state laser theory[1,2]. A number of analyses of waveguide lasers have been made previously[3,4], the most pertinent to the optical fibre laser being the paper by Digonnet and Gaeta. Although the question of modal overlap is addressed, their analysis is aimed at crystal fibre lasers and is restricted to homogenously-broadened four-level systems with negligible pump saturation. It was considered necessary in the present work to outline a theory which includes the effects of inhomogenous broadening, pump saturation and amplified spontaneous emission for both three-level and four-level transitions.

The chapter begins with a review of the properties of rare-earth ions in glass, followed by a description of the optical fibre laser configuration. The gain of three-level and four-level transitions in the glass fibre and the effect of amplified spontaneous emission are evaluated. The analysis is applied to the CW operation of fibre lasers and the chapter ends with a brief description of relaxation oscillations and Q-switching.

2.1 Rare-earth ions in glass

The new fibre lasers and amplifiers are based on silica optical fibres which have been doped with one, or more, rare-earth ions. This section reviews the properties of rare-earth ions in glass.

2.1.1 Rare-earth energy levels

An energy level diagram for selected trivalent rare-earth ions is shown in Figure 2.1. The information is taken from a study of the free ions summarised in a paper

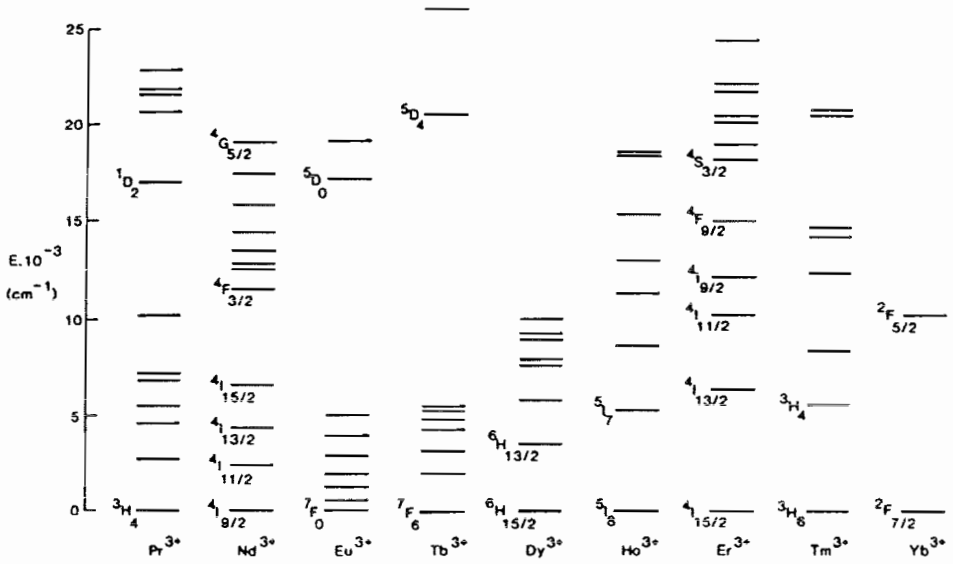

Figure 2.1 Energy level diagram for trivalent rare-earth ions

by Dieke and Crosswhite[5]. The electronic configuration of these ions is $(Xe)^4f_N$, where (Xe) represents the closed shell electronic configuration of xenon, and N is the number of 4f electrons (N = 3 for Nd^{3+} and 11 for Er^{3+}). The partially-filled 4f shell is shielded by the closed outer shells of the xenon configuration and thus the rare-earth ions have similar physical and chemical properties. The shielding also reduces the influence of the local electric fields when the ions are incorporated into a solid material. The energy shifts relative to the free ion levels are only of the order of a few hundred cm^{-1} (one cm^{-1} is equal to 2.0×10^{-23} joules) and thus the information in Figure 2.1 is sufficient to identify the transitions observed in the solid-state.

The labelling of the energy levels or "terms" (e.g. $^4F_{3/2}$) follows the standard LS coupling notation. The presuperscript represents the value of 2S+1; the capital letter indicates the value of L according to the sequence

L = 0, 1, 2, 3, 4, 5, 6
S, P, D, F, G, H, I

and the postscript is the value of J. The quantum numbers S, L and J describe the spin, orbital angular momentum, and total angular momentum, for atoms in which the coupling between individual electron spins and between the orbital angular momenta exceeds the coupling between the total spin (S) and total orbital angular momentum (L). The reader is referred to any text on atomic physics (e.g. Woodgate[6]) for a more detailed discussion of atomic spectra. The importance of the angular momentum J is that it determines the multiplicity of the term i.e. the number of different orientations of the angular momentum in an external field. The multiplicity is given by the value of 2J+1.

When rare-earth ions are placed in a glass matrix, the local electric fields remove the 2J+1 -order degeneracy of the individual energy terms. The number of possible sublevels (known as Stark levels) is given by Kramer's rule for electric fields as J+½ for half integral J and 2J+1 for integral J. The actual number observed depends on the symmetry of the material, but the full number is usually observed in glass since it is of lower than tetragonal symmetry[7]. The magnitude of the splitting depends on the glass composition and is typically of the order of $100cm^{-1}$.

The ground state (unexcited state) of an ion is determined by thermal equilibrium between the lowest lying energy levels. The relative electronic populations in these levels is given by the Boltzmann distribution

$$\frac{g_i n_i}{g_j n_j} = \exp\left[\frac{-\Delta E_{ij}}{kT}\right] \qquad (2.1)$$

where

$n_{i,j}$ are the populations of the i^{th} and j^{th} energy levels

$g_{i,j}$ are the remaining degeneracies of these levels

k is Boltzmann's constant

T is the absolute temperature.

At room temperature kT is approximately $200cm^{-1}$ and so only the first few Stark levels of the lowest term are significantly populated.

2.1.2 Rare-earth transitions, cross-sections and lifetimes

Although the rare-earth energy levels are adequately described by the L-S notation, the probability for electron dipole transitions within the $4f^N$ configuration is zero. In order to permit dipole transitions between the levels, the states of the $4f^N$ configuration

must be perturbed by those of the higher lying $4f^{N-1}5d$ configuration. Details of the perturbation calculations are given in papers by Judd[8] and Ofelt[9]. The transition probabilities are typically three to four orders of magnitude smaller than for allowed transitions between electronic configurations. A further discussion of rare-earth spectra can be found in Reisfeld and Jorgensen[10].

The results of transition probability calculations are usually given in terms of the oscillator strength f_{ij} (see reference 6) which is related directly to the Einstein B_{ij} coefficient for absorption[11] by

$$f_{ij} = \frac{2\ \varepsilon_o\ m}{\pi\ e^2}\ B_{ij}\ \hbar\ \omega_{ij} \qquad (2.2)$$

where

ε_o is the vacuum dielectric permittivity
m is the electron rest mass
e is the electron charge
$\hbar = h/2\pi$ where h is Planck's constant
ω_{ij} is the angular frequency of the transition

In the solid state, the energy levels are considerably broadened (see section 2.1.3) and it is usually more convenient to consider an absorption (or stimulated emission) cross-section $\sigma(\nu)$ defined by

$$\frac{dS}{dz} = n\ \sigma(\nu)S \qquad (2.3)$$

where

S is the photon intensity at frequency ν
z is the direction of propagation
n is the number density of absorbing or emitting ions)

The cross section $\sigma(\nu)$ has the dimensions of area and can be considered in a ballistic sense as the area subtended by the absorbing or emitting ion. The relationship between the oscillator strength and the cross section is given by[12]

$$f_{ij} = \frac{\pi e^2 h^2}{g m c} \frac{n}{(n^2+2)^2} \int_{\text{over band ij}} \sigma(\nu) d\nu \qquad (2.4)$$

where n is the refractive index

The importance of the cross-section is that it is the parameter most closely related to experimental measurements of absorption (or gain). The results of the fibre laser theory are expressed in terms of the cross-section wherever possible.

Once a particular rare-earth ion has absorbed energy, it can relax to the ground-state by a variety of mechanisms. The most direct route is the emission of a photon corresponding to the energy difference between the excited level and the ground-state. In the majority of cases, however, the probability of this occurence is far outweighed by the probability of relaxation to an intermediate level via the excitation or one or more vibrational modes (optical phonons) of the host matrix. The lifetime of a level under multi-phonon decay is proportional to the energy difference with the next lowest level, and rises rapidly for larger energy differences. The lifetime is typically 1ns for energy gaps of $1000cm^{-1}$ or less, rising to 1ms for a gap of $4000\text{-}5000cm^{-1}$ [10].

A further decay mechanism is the transfer of energy from one ion to another, either resonantly (energy levels of the two ions significantly overlap) or

non-resonantly (energy difference accounted for by excitation or absorption of phonon(s)). The dependence of the resonant transfer rate p on the inter-ionic distance r, goes as[7]

$$p \propto \left(\frac{r_o}{r} \right)^6 \qquad (2.5)$$

where r_o is typically 4×10^{-9}m.

For a concentration of 10^{19} ions/cm^3, p is approximately 1 s^{-1} and is thus much smaller than either the radiative or non-radiative rates (typically $10^3 s^{-1}$ or greater). At higher concentrations, or if there is significant clustering of ions, inter-ion relaxation can be significant. For Nd^{3+}-doped glass the critical concentration is usually about 2×10^4 ppm Nd^{3+} ions, i.e. approximately two orders of magnitude greater than for the glass fibres studied here (see Chapter 3).

Certain levels in the rare-earth ions are sufficiently removed from other, lower, levels that the probability for radiative emission (fluorescence) becomes significant. Because the radiative probabilities are relatively small, these levels have lifetimes ranging from a few microseconds to many milliseconds, and are called metastable levels. The most important levels from which fluorescence is observed in Nd^{3+} and Er^{3+} ions are the $^4F_{3/2}$ and $^4I_{13/2}$ levels respectively. Fluorescence measurements on doped fibres are described in Chapter 3.

2.1.3 Homogenous and inhomogenous broadening

The fluorescence emitted by the rare-earth ions consists of broad bands, typically tens of nanometres wide. It is important to understand the origins of this broadening. As an example, the fluorescence resulting from the $^4F_{3/2}$ - $^4I_{9/2}$ transition in Nd^{3+} is considered.

The local energy fields in the glass matrix split the $^4F_{3/2}$ and $^4I_{9/2}$ levels into two components, and five components, respectively. The splitting of the $^4F_{3/2}$ level is typically of the order of kT at room temperature, so that, in accordance with equation (2.1), both sublevels are significantly populated. There are thus a full ten components in the fluorescence spectrum. Each component is thermally broadened by the absorption or creation of low-energy phonons (acoustic phonons) during the transition. This broadening is determined by the temperature and by the material properties of the glass, in particular the velocity of sound[13], and is typically of the order of $50cm^{-1}$. It is known as homogenous broadening because it is common to all ions in the glass.

Glass is an "inorganic product of fusion cooled to a rigid condition without crystallising[7]". It is characterised by a high short-range order corresponding to the constituent molecules, a low long-range order and a low symmetry[7]. The local electric fields which give rise to the Stark levels vary between ionic sites and thus so do the magnitudes of the level splittings. The resultant variation in transition energies is typically of the order of $100cm^{-1}$. The broadening is called inhomogenous, and makes it possible to distinguish between classes of ions in different sites. A schematic of the effects of the different broadening mechanisms is given in Figure 2.2.

2.1.4 Basic 3- and 4-level lasers

The various relaxation rates determine the pumping rate required to significantly populate the metastable level. If this population is larger than that to which a transition is allowed (i.e. there is a population inversion), then stimulated emission of that transition will produce gain. A four-level system is one in which the terminal level of the transition is not normally populated at the operational temperature. Thus any population of the metastable level can give rise to gain. In a

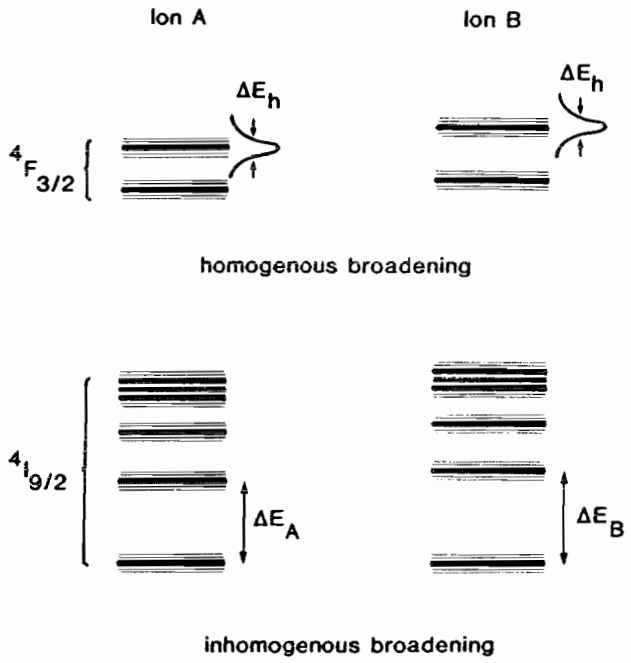

Figure 2.2 Line-broadening mechanisms in a typical rare-earth ion

three-level system, the terminal level is the ground state. The pumping rate must be sufficient to deplete the ground state before a population inversion can be achieved. The CW operation of a three-level glass laser is usually prohibited by the very high pump power that is required and the associated thermal problems. However, because of the intense and efficient pumping scheme for a fibre laser, its large length/diameter ratio which minimises thermal effects, and the long lifetimes of the metastable levels, efficient CW laser operation of three-level systems has been achieved[14], and is described in Chapter 4.

2.2 Optical Fibre Laser Cavities

In this section a number of features particular to optical fibre laser cavities are described. It is assumed that the reader has a basic knowledge of optical fibres (see, for example, references 1 and 15). An excellent description of the theory of optical waveguides is to be found in Snyder and Love[16].

2.2.1 Modal considerations

The fibre laser can be designed to operate intrinsically and continuously in a single transverse mode at both the pump and laser wavelengths. This property offers unparalleled pumping efficiency. Because of the small modal spot-size (typically $10^{-11}m^2$), low pump powers of a few milliwatts can maintain high intensities for long distances, and thus very low oscillation thresholds can be achieved.

Since the pump and laser wavelengths differ, it is unlikely that a perfect overlap will exist between the excited gain medium and the oscillating mode. The evolution of a pump or laser mode along the fibre can be expressed in terms of the local intensity of the mode using equation (2.3)

$$\frac{dP}{dz} = P\,\sigma \int_{A\infty} \hat{S}\, n(x,y,z)\,dxdy \qquad (2.6)$$

where $\hat{S}$ is the normalised mode intensity[16] ($S = P\hat{S}$). The overlap integral between the mode intensity and the population inversion arises because the gain at any point in the fibre is proportional to both the local intensity and the local inversion.

Strictly speaking, the modes of the absorbing, or amplifying, waveguide are not the same as in an ideal lossless waveguide, since the loss or gain adds an imaginary component n_i to the refractive index, n. For the relatively low-doped fibres described in this thesis;

$$\left|\frac{n_i}{n}\right| < 10^{-5} \qquad (2.7)$$

and so the influence on propagation is negligible.

2.2.2 Polarisation

The evolution of a mode, j, in an optical fibre can be expressed by[16]

$$E = E_0 \exp j(\beta_j z - \omega t) \qquad (2.8)$$

where E is the electric field, β_j is the propagation constant (complex for absorbing or amplifying fibres) and ω is the optical (angular) frequency.

In the circularly-symmetric, step-index, fibre, the propagation constant β_j is independent of polarisation. For any real fibre, however, core asymmetry, material anisotropy and external perturbations such as bends or

pressure, act to make the fibre birefringent (i.e. $\beta_{jx} \neq \beta_{jy}$ where x and y describe two orthogonal polarisations). Fibre birefringence can cause problems whenever a fibre is used interferometrically, since the interference conditions for the two polarisations are different.

The coupling between the polarised modes is a function of the difference in propagation constants $\Delta\beta$, and is strongest for perturbations with period $2\pi/\Delta\beta$[17]. The value of $2\pi/\Delta\beta$ is called the beat length L_p. By designing a fibre to have a high intrinsic birefringence, the beat length can be reduced to be much less than the typical period of any external perturbations. Thus light launched in one polarised mode remains in that mode and cannot give rise to modal interference.

The fibre laser frequently has a polarised laser as the pump source. It is usually assumed that information about the pump polarisation is lost as the ion relaxes to the upper lasing level, and that the cross-section for stimulated emission is independent of polarisation. The availability of doped high-birefringence fibres makes it possible to test this hypothesis closely. The theory developed in the remainder of this chapter is chosen, for clarity, to be independent of polarisation, but can be extended to include polarisation phenomena with the definition of two cross sections, σ_x and σ_y, for the two orthogonal polarisations[18]. Polarisation phenomena in fibre lasers will be discussed in more detail in a future report[19]. It should be noted that for the majority of fibre laser measurements (e.g. efficiency, spectral broadening, output power and wavelength), polarisation anisotropy is a second-order effect, and that very good agreement between (polarisation independent) theory and experiment has been obtained.

2.3 CW Gain Evaluation

In this section the basic equations for the gain of three-level and four-level fibre lasers are derived under some simplifying assumptions and consideration is given to the effect of amplified spontaneous emission.

2.3.1 Gain in four-level fibre lasers

A four-level laser system (such as Nd^{3+} at 1.088μm) is shown schematically in Figure 2.3. The usual starting point for analysis is the simplified rate equation

$$\frac{dn_3}{dt} = \eta n_1 R - \frac{n_3}{T_{32}} - n_3 W \qquad (2.9)$$

and the expression for the total ion population per unit volume n_T

$$n_1 + n_3 = n_T \qquad (2.10)$$

where n_j is the population of level j per unit volume
R is the pumping rate from level 1; $R=S_p\sigma_p/h\nu_p$
σ_p is the absorption cross-section (see equation (2.3))
ν_p is the pump frequency
W is the stimulated emission rate
T_{32} is the lifetime of level 3
and η is the excitation efficiency from level 1 to level 3

Implicit in these equations is the assumption that the lifetimes of levels 2 and 4 are so short that their populations may be neglected. For Nd^{3+} ions the 4-level scheme at 1.088μm is shown in Figure 2.4. The lifetimes of the $^4G_{5/2}$ - $^4F_{3/2}$ and $^4I_{11/2}$ - $^4I_{9/2}$ transitions (non-radiative) have both been estimated to be of the order of

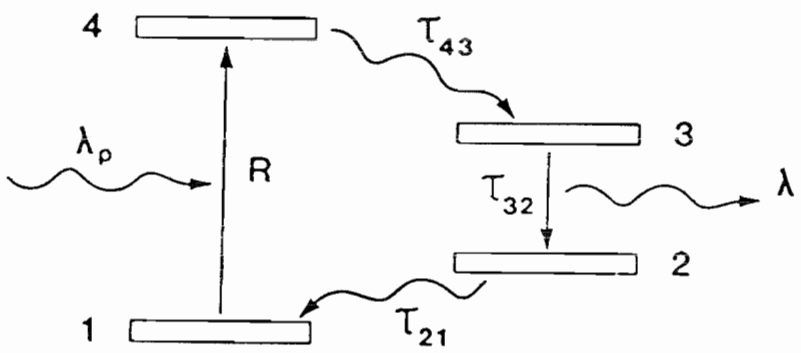

Figure 2.3. Four-level laser

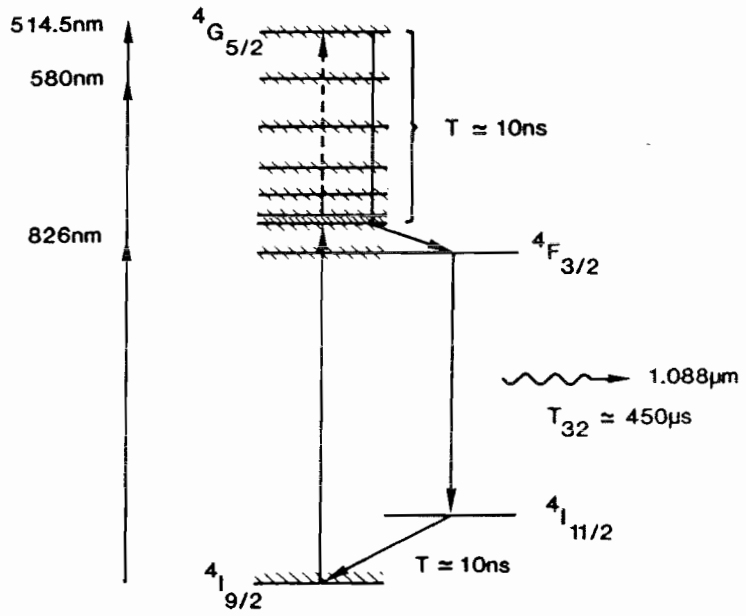

Figure 2.4. Neodymium four-level laser scheme

a few nanoseconds[10] i.e. much smaller than the fluorescence lifetime of ~450μs, and so the assumption is good for CW operation. The finite lifetime of the $^4I_{11/2}$ - $^4I_{9/2}$ transition has been known to cause bottlenecking in Q-switched operation[20], but this has not been observed in the fibre laser to date.

The rate equations are complicated by the different broadening mechanisms discussed in Section 2.1.3. In the Nd^{3+} system, the $^4F_{3/2}$ level is split by the crystal field into a doublet and the $^4I_{11/2}$ is a sextet. Transitions between these multiplets are characterised by a homogenous broadening due to vibration of the ion (phonon interaction) and an inhomogenous broadening because the crystal field, and hence the Stark splitting, varies considerably from site to site in the disordered glass matrix.

Following a standard technique for a description of inhomogenous broadening (see for example Yariv[1]) the ionic population is divided into sublevels labelled f, containing indistinguishable ions (i.e. ions in identical sites). The probability of an ion being characterised in class f is given by p(f) where

$$\int_{-\infty}^{\infty} p(f)\, df = 1 \qquad (2.11)$$

Within each class the ions are homogenously broadened with a lineshape $g^f(\nu)$ such that

$$\int_{-\infty}^{\infty} g^f(\nu)\, d\nu = 1 \qquad (2.12)$$

The overall lineshape $g(\nu)$ is then

$$g(\nu) = \int_{-\infty}^{\infty} p(f) g^f(\nu) df \qquad (2.13)$$

Equation (2.5) can be rewritten as

$$\frac{dn_3^f}{dt} = \eta n_1^f R - \frac{n_3^f}{T_{32}} - n_3^f W^f \qquad (2.14)$$

Strictly speaking, the probability distribution p(f) is determined by the pump wavelength; if the ions are pumped in the wings of an absorption rather than the centre, the selection of ionic sites changes and so does the distribution. By restricting the sites selected, the effective inhomogenity can be reduced[21]. However, at room temperature the relatively large homogenous broadening ensures that a broad distribution of sites is selected.

The stimulated transition rate $W_f(\nu)$ due to an intensity (per unit frequency interval) $S(\nu)$ can be expressed as[1]

$$W_f(\nu) = \frac{\lambda^2}{8\pi n^2 h\nu t_{spont}} g_f(\nu)\ S(\nu) \qquad (2.15)$$

where

n is the refractive index

t_{spont} is the contribution of the lifetime of level 3 that is due to spontaneous emission

The relationship between equation (2.15) and the semi-empirical expression of (2.3) is given by the Fuchbauer-Ladenburg relationship,

$$\sigma(\nu) = \frac{\lambda^2}{8\pi n^2\ t_{spont}} g(\nu) \qquad (2.16)$$

An experimental determination of the spectral and temporal fluorescence characteristics of a particlar ion can therefore be used to calculate the stimulated cross-section (see Chapter 3).

Integration of equation (2.15) gives the total stimulated rate W_f;

$$W_f = \frac{\lambda^2}{8\pi n^2 h\nu t_{spont}} \int_{-\infty}^{\infty} S(\nu) g_f(\nu)\, d\nu \qquad (2.17)$$

The steady-state population inversion $n_3{}^f$ is given by putting d/dt = 0 in equation (2.10);

$$n_3{}^f = \frac{\eta n_1{}^f R\ T_{32}}{1 + W^f\ T_{32}} \qquad (2.18)$$

The power generated per unit volume, due to stimulated emission from subset f, is $n_3{}^f W_f(\nu) h\nu$. In order to calculate the power generation per unit length this expression must be integrated over the cross-section of the fibre, and over all possible values of f. Substituting from equations (2.18) and (2.15) gives

$$\frac{dP(\nu)}{dz} = \int_{A\infty} \int_{f} \frac{\eta n_1{}^f R\ T_{32}}{1 + W^f\ T_{32}} \frac{\lambda^2}{8\pi n^2 t_{spont}} g_f(\nu) S(\nu)\, df\, dA \qquad (2.19)$$

Writing $S(\nu)$ as $P\hat{S}(\nu)$ and integrating over the length of the fibre, we obtain an expression for the single pass gain $G(\nu)$

$$G(\nu) = \ell n \frac{S(\nu)_{out}}{S(\nu)_{in}} = \int_{0}^{\ell} \int_{A\infty} \hat{S}(\nu) R \int_{f} \frac{\eta n_1{}^f T_{32}}{1+W^f\ T_{32}} \frac{\lambda^2}{8\pi n^2 t_{spont}} g_f(\nu)\, df\, dA\, dz \qquad (2.20)$$

2.3.2 Neodymium laser gain

As it stands, equation (2.20) is somewhat unwieldy. In order to derive a simple expression for four-level systems, such as the Nd^{3+}-doped fibre laser at 1.088μm, some simplifying assumptions must be made. The first is the small-signal approximation,

$$W^f T_{32} \ll 1 \tag{2.21}$$

In the case of lasers, equation (2.21) is only true at, or below, threshold.

The second approximation is that

$$n_1{}^f = n_1 p(f) \tag{2.22}$$

This is equivalent to the statement that the distribution of ionic sites selected by the pump (p(f)) is independent of pump power. In order to evaluate the area integral it is further assumed that the dopant is restricted uniformly to the fibre core. Using these assumptions the expression for the single-pass gain is then

$$G(\nu) = \frac{P_{abs}}{A_{eff}} \eta \frac{\sigma(\nu)\, T_{32}}{h\nu_p} \tag{2.23}$$

where use has been made of equations (2.6), (2.13) and (2.16),

$$P_{abs} = \int_0^{\ell} \left[\frac{dP}{dz} \right] dz$$

is the absorbed pump power (due to population n_1) in length ℓ, and the effective area, A_{eff}, is given by

$$\frac{1}{A_{eff}} = \int_{core} \hat{S}_l \hat{S}_p \, dA \qquad (2.24)$$

Equation (2.23) has proved remarkably accurate in determining the gain, and hence the threshold, of the Nd^{3+}-doped fibre lasers described in this thesis. The equation illustrates the dependence of the gain on the effective area of the fibre waveguide, which is defined by the overlap of the pump and laser intensities. It is evident that the single-mode fibre, which can maintain throughout its length a diffraction limited spot-size for the pump and signal, offers the optimum gain/power ratio for any laser cavity.

2.3.2.1 Gain Optimisation

The most important factor determining the laser gain is the effective area, A_{eff}. The overlap integral of equation (2.24) has been evaluated by Digonnet[3] for the lowest-order modes of a fibre. In the region of single-mode operation at the signal (laser) wavelength the greatest overlap occurs (as would be expected) for the pump in the lowest-order mode. Under these conditions, equation (2.24) reduces to

$$\frac{1}{A_{eff}} = \frac{4(n_{co}^2 - n_{cl}^2)}{\lambda^2} \int_0^1 \left[\frac{W \, W_p \, J_o(U \, R') J_o(U_p R')}{V^2 \, V_p \, J_1(U) J_1(U_p)} \right]^2 2\pi R' dR' \qquad (2.25)$$

$$= \frac{4(n_{co}^2 - n_{cl}^2)}{\lambda^2} \, \eta_{eff} \, (V, \, \lambda_p/\lambda) \qquad (2.26)$$

where

n_{co}, n_{cl} are the core and cladding refractive indices

U, W, V are the modal parameters for the laser mode

U_p, W_p, V_p are modal parameters for the pump mode

$R' = r/\rho$ is the normalised radius, where ρ is the core radius

J_o, J_1 are Bessel functions

The advantage of equation (2.26) is that the V-value dependence and laser parameter dependence are clearly separated (NB this is not the case for the F coefficients of reference 3). The variation of $1/A_{eff}$ with signal V-value is shown in Figure 2.5. The optimum V-value depends on the ratio of the pump and signal wavelengths, and is 1.7 for a Nd^{3+}-laser pumped at 820nm.

Equation (2.26) also illustrates the importance of the fibre numerical aperture, N.A., (i.e. $(n_{co}^2 - n_{cl}^2)^{\frac{1}{2}}$ in determining the gain. It is evident that the N.A. should be made as high as possible. In practice a limit is set by the minimum pump spot size (ω_o) attainable from the launch optics. Thus if the numerical aperture is inceased too far, the pump spot size in the fibre (ω_p) falls below ω_o and the launch efficiency is impaired. Equating ω_o to ω_p at the optimum V-value yields an expression for the minimum effective area $A_{eff,\ min}$

$$A_{eff\ min} \simeq 1.5\pi\omega_o^2 \qquad (2.27)$$

It should be noted that since the launch efficiency depends on the ratio ω_p/ω_o whereas the threshold depends on ω_p^2 (via $(n_{co}^2 - n_{cl}^2)$), a further reduction in spot size results in an even higher gain. However, the absorbed power, and hence the maximum attainable output power, is reduced.

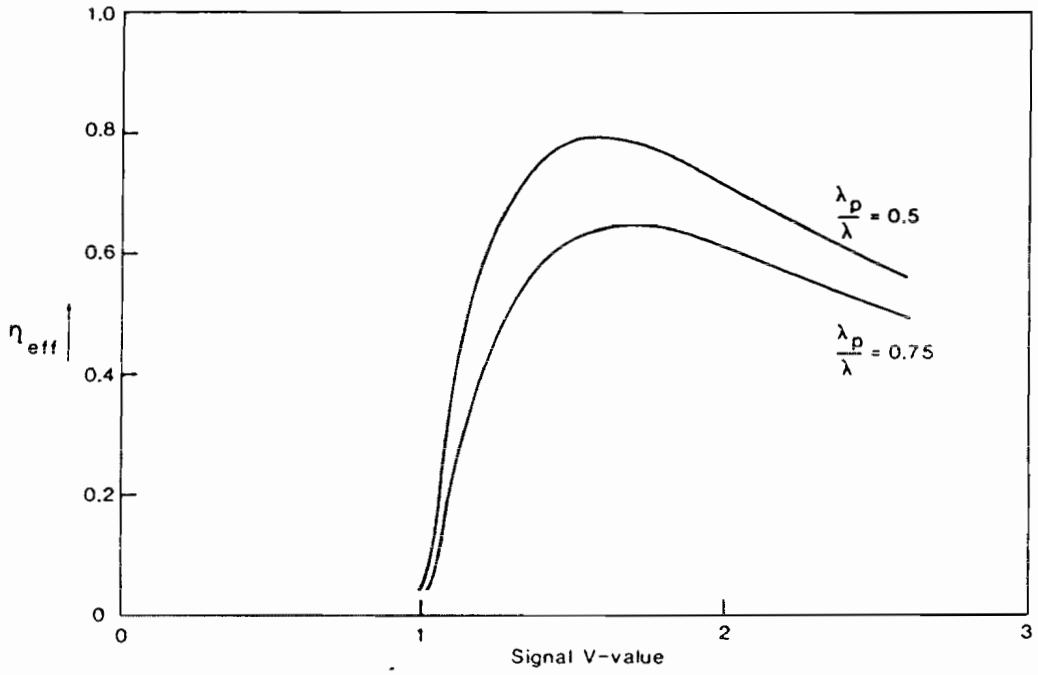

Figure 2.5. V-value dependence of waveguide effective area for a four-level laser

$$\eta_{eff} = \frac{\lambda^2}{4(n_{co}^2 - n_{cl}^2)} \frac{1}{A_{eff}}$$

The optimum length depends mainly on the excess loss of fibre α, which is usually very small. If α is given by $n_T\sigma_p/K$ then the optimum length is

$$\ell_{opt} = \frac{1}{n_T\sigma_p} \ln\left[K\ G_{max}\right] \qquad (2.28)$$

where

G_{max} is the gain resulting from total absorption of the pump power

2.3.3 Gain in three-level lasers

The analysis for a three-level system such as Er^{3+} at 1.54μm proceeds in a similar manner.

The simplified rate equation can be written

$$\frac{dn_2^f}{dt} = \eta n_1^f R - \frac{n_2^f}{T_{21}} - W_f(n_2^f - n_1^f) \qquad (2.29)$$

$$n_1^f + n_2^f = n_T^f \qquad (2.30))$$

A schematic of the three-level laser is shown in Figure 2.6. It is assumed that T_{32} is much smaller than T_{21}. An estimate of T_{32} for the Er^{3+} system (shown in Figure 2.7) is put at $T_{32} \approx 10\mu s$ (see Chapter 3) i.e. $T_{32} < 10^{-3}\ T_{21}$.

In a three-level system both the upper and lower levels of the lasing transition are populated. Gain is only available when the rate from level 2 exceeds that of level 1 i.e. $n_2^f > n_1^f$.

From equation (2.29)

$$n_2^f - n_1^f = \frac{\eta R - 1/T_{21}}{\eta R + 1/T_{21} + 2W_f}\ n_T^f \qquad (2.31)$$

By analogy with equation (2.20) the gain is expressed as

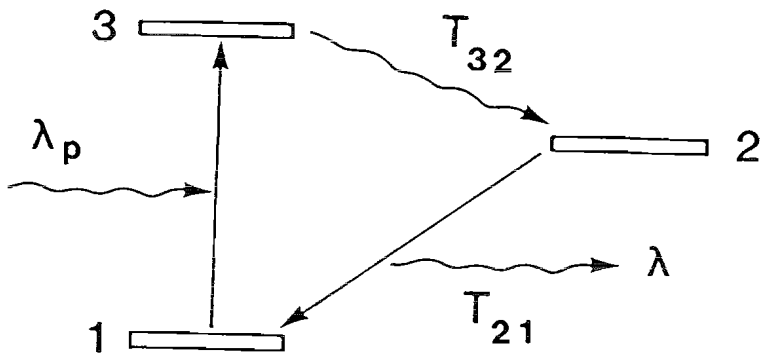

Figure 2.6. Three-level laser

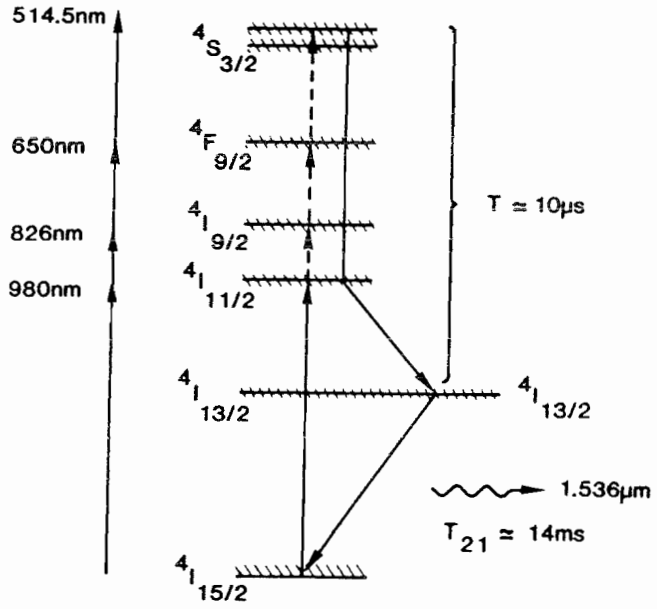

Figure 2.7. Erbium three-level laser scheme

$$G(\nu) = \int_0^{\ell} \int_{A\infty} \hat{S}(\nu) \int_f \frac{\eta R - 1/T_{21}}{\eta R + 1/T_{21} + 2\bar{w}_f} n_T p(f) \frac{\lambda^2}{8\pi n^2 t_{spont}} g_f(\nu) df dA dz \qquad (2.32)$$

2.3.4 Erbium laser gain

Under the small-signal approximation, equation (2.32) reduces to

$$G(\nu) = \xi(R, \ell, V)\, n_T \sigma(\nu) \ell \qquad (2.33)$$

where

$$\xi(R, \ell, V) = \int_0^{\ell} \int_{core} \hat{S}_{\ell} \frac{\eta R - 1/T_{21}}{\eta R + 1/T_{21}} dA dz \qquad (2.34)$$

The gain is thus expressed as a fraction, ξ, of the maximum gain available if the total ground state were inverted. The value of the pump intensity for which ηR is equal to $1/T_{21}$ is known as the saturation intensity. This value determines a pump threshold which must be exceeded if a three-level system is to exhibit gain. The small core of the single-mode optical fibre makes it possible to achieve the necessary intensity at relatively low power levels.

2.3.4.1 Gain optimisation

In Figure 2.8 the dependence of ξ on the signal V-value is plotted for various values of the pump rate. In order to illustrate the V-dependence, equation (2.34) is evaluated for incremental z, i.e. R is constant. It

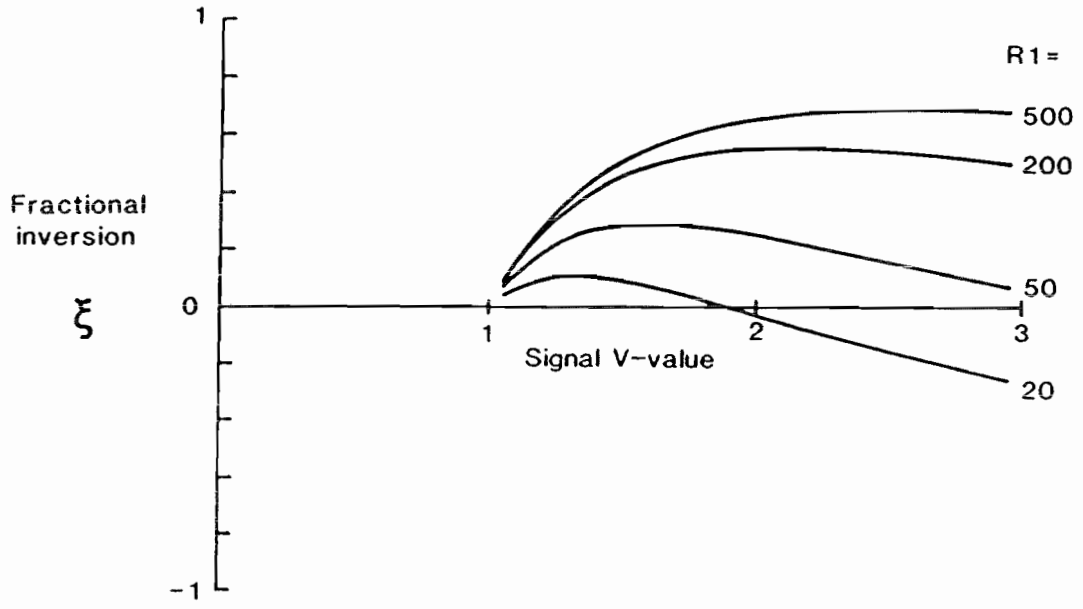

Figure 2.8. V-value dependence of fractional inversion for a three-level laser as a function of pump-rate ($R1=P\eta\frac{4\pi(n_{co}^2-n_{cl}^2)}{\lambda_p^2}\frac{\sigma_p\tau}{h\nu_p}$)

can be seen that the optimum V-value is a function of the available pump rate, and lies typically in the range 1.3-2.3. At low pump rates (R1=50, P ≈ 5mW for a typical device) the optimum V is approximately 1.6. At higher pump rates the optimum value increases to above 2, largely because the excited population is assumed to be confined to the core. (The fraction of laser power confined to the core increases as V is increased). Before the total gain in the fibre can be computed, the dependence of the pump rate on the length must be accurately known. It is shown in Chapter 3 that pump absorption from the excited-state population should be taken into account in addition to the usual ground-state absorption. The pump absorption coefficient is given by

$$\alpha(\ell) = n_T\sigma_p\left[\int_{core}\hat{S}_p\left[\frac{1/T_{21}}{\eta R\hat{S}_p+1/T_{21}}\right]dA + \frac{\sigma_a}{\sigma_p}\int_{core}\hat{S}_p\left[\frac{\eta R\hat{S}_p}{\eta R\hat{S}_p+1/T_{21}}\right]dA\right] \tag{2.35}$$

where

$dR/dz = -\alpha(\ell)R$

σ_p is the pump absorption cross-section

σ_a is the excited-state absorption cross-section

The dependence of the overall gain in the fibre on the pump rate is shown in Figure 2.9. Note that, in practice, the ratios of the cross-sections are provided by absorption measurements (see Chapter 3) and that the maximum gain $n_T\sigma(\nu)\ell$ can be compared to the small-signal absorption at the laser wavelength (see Chapter 5). From the figure it can be seen that the presence of excited-state absorption seriously reduces the available gain. The maximum length that can usefully be employed in the laser or amplifier is governed by the value of the pump rate, R, for which $\xi(\ell)$ is zero. Once the pump rate falls below this value the additional fibre length contributes loss,

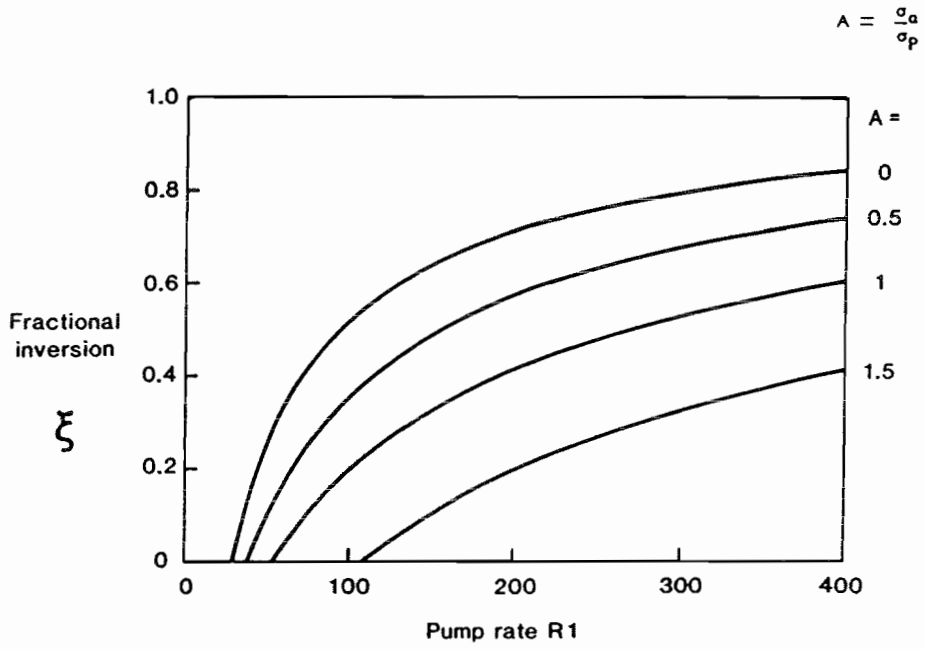

Figure 2.9 Fractional inversion versus pump-rate for erbium fibre laser.

rather than gain to the device (see Chapter 5, Appendix A). The value of ℓ at which $\xi(\ell)$ is zero depends on the threshold pump rate, R, and the absorption coefficient α, and thus the fibre length needs to be optimised for each device.

2.3.5 Amplified spontaneous emission and gain saturation

The expressions of Sections 2.2.1 and 2.2.3 for the single-pass gain contain the term W, the stimulated emission rate. Even in the absence of feedback there is always radiation in the fibre which contributes to W because of the fraction of spontaneous emission that is captured by the fibre core. It is the purpose of this section to evaluate the effect of spontaneous emission on the fibre gain.

The fluorescence, as discussed in Section 2.2, results primarily from dipole radiation.

The standard result for the fractional power emitted by a dipole aligned to the x, or y axis into a fibre mode is given by[16]

$$B = \frac{3\lambda^2}{16\pi n_{co} n_{cl}} \hat{S}_{\ell} \qquad (2.36)$$

where n_{co} = core index
n_{cl} = cladding index

The fractional power emitted by a dipole aligned to the z axis is of order $(NA)^2/2$ smaller (typically 2%) and is neglected here.

Thus the total capture fraction averaged over all possible directions of the dipole is given by

$$B = \frac{\lambda^2}{8\pi n_{co} n_{cl}} \hat{S}_{\ell} \qquad (2.37)$$

The power captured per unit length and unit frequency interval $dP(\nu)$ is given by

$$dP(\nu) = h\nu\, g(\nu) \int_{A\infty} \int_{f} \frac{n_i}{T_{ij}}^{f} g_f(\nu) B dA\, dz \qquad (2.38)$$

where $i = 3$, $j = 2$ for a 4 level laser
$i = 2$, $j = 1$ for a 3 level laser

The captured fluorescence experiences gain as it passes along the fibre. The total power at frequency ν at one end of the fibre is given by multiplying equation (2.38) by the gain (from z to one end) and integrating this over the entire fibre length

$$P_{out}(\nu) = \int_{o}^{\ell} h\nu g(\nu) \int_{A\infty} \frac{n_i}{T_{ij}} B dA \exp\left[\int_{z}^{o} \int_{A\infty} \int_{f} n_i^{f} \frac{W_f(\nu)}{S(\nu)} dfdAdz \right] dz \qquad (2.39)$$

where $n_1^f = n_3^f$ for 4 level laser
$= n_2^f - n_1^f$ for 3 level laser.

2.3.6 Amplified spontaneous emission in Nd^{3+} lasers

For the approximation of section 2.3.2

$$P_{out}(\nu) = \int_{o}^{\ell} h\nu\, g(\nu) \int_{A\infty} n_T R B dA$$

$$\exp\left[\int_{z}\int_{A\infty} n_T R T_{32}\sigma(\nu)\,\hat{S}_{\ell}\,dA\right]\,dz \qquad (2.40)$$

Since the differential of the exponent of the above equation also occurs in the integrand, the equation can be partially integrated, yielding

$$P_{out}(\nu) = \frac{B'}{\sigma(\nu)}\frac{g(\nu)h\nu}{T_{32}}\{\exp G(\nu,W) - 1\} \qquad (2.41)$$

where

$$B' = \frac{\lambda^2}{8\pi n_{co} n_{cl}} \qquad (2.42)$$

If the average stimulated emission rate $W(\nu)$ in the fibre is taken to be equal to the value at one end then

$$W(\nu) = \frac{B}{T_{32}}\frac{g(\nu)}{}\{\exp G(\nu,W) - 1\} \qquad (2.43)$$

where $G(\nu,W)$ is given by equation (2.20). Expression (2.43) indicates that the amplified spontaneous emission rate in the fibre is given by the capture fraction multiplied by the lineshape and gain, divided by the upper level lifetime. Amplified spontaneous emission is thus significant (i.e. greater than the spontaneous emission rate) when

$$W_{TOT} = \int_{\nu}\frac{Bg(\nu)}{T_{32}}\{\exp G(\nu,W) - 1\}d\nu \geqslant 1/T_{32} \qquad (2.44)$$

Typically, amplified spontaneous emission can be neglected (has less than 10% effect on gain) provided $G \leqslant 3$. This criterion is well met by the majority of fibre laser cavities, except for those relying on feedback simply from the fibre ends. In that case expression (2.44) can be used in an iterative program with equation (2.20) to calculate the saturated gain.

2.4 Threshold and Output Power of Fibre Lasers

Whenever a doped fibre fluoresces there is a contribution to the stimulated emission rate W from the spontaneous emission captured by the fibre. If the feedback is present, either from mirrors or fibre circuits or from Fresnel reflection at the fibre ends, and if the gain in the fibre initially exceeds the round trip losses, the stimulated rate will grow until the gain is saturated. This is the basis of laser action. For a given cavity configuration there is a particular pump level, the threshold, at which the small-signal gain reaches the round trip loss. Any increase in power beyond this point results in a corresponding increase in the stimulated (laser) output. The ratio of these two is known as the slope efficiency. In this section the threshold and output power of both three-level and four-level fibre lasers are evaluated.

2.4.1 Fibre laser threshold

The gain of the fibre laser is given by equation (2.20) (four-level system) or equation (2.32) (three-level system). At threshold this value is equal to the round-trip loss. If we consider the cavity shown in Figure 2.10 with a fibre of length ℓ and attenuation α(Np/m), reflectivities R_1 and R_2 and excess internal loss L_i, then at threshold;

$$G(\nu) = G_T = \alpha\ell - \ln \sqrt{R_1 R_2 (1-L_i)} \qquad (2.45)$$

where G_T is the threshold gain.

The threshold is optimised by maximising $G(\nu)$ according to Section 2.3 and by reducing the cavity loss, and hence G_T. Although the threshold is reduced as the output reflectivity is increased, the slope efficiency is also related to the reflectivity, and it is usually necessary to

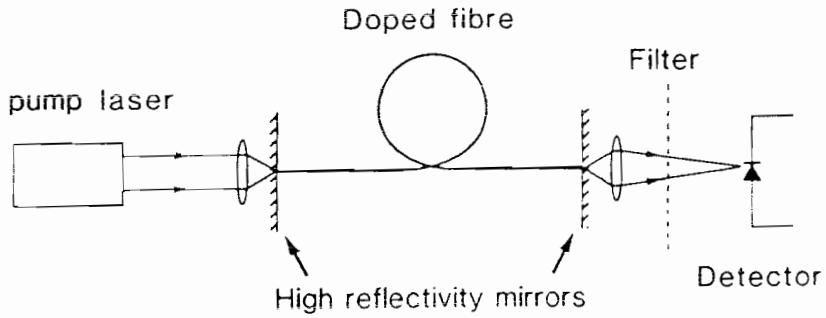

Figure 2.10 Fabry-Perot laser cavity.

compromise the threshold in order to operate the laser efficiently. A comparison between the predictions of the models described here and experimental measurements is in Chapter 4.

2.4.2 Power output and spectral broadening

One of the major reasons for developing a model which includes the effects of homogenous and inhomogenous broadening is to describe the spectral characteristics of fibre lasers. Two cases are considered here; the free-running (spectrally-broad) laser; and the line-narrowed laser.

2.4.2.1 Spectrally-broad lasers

In the free-running laser, oscillation at a single frequency is not sufficient to saturate the gain uniformly over the laser bandwidth because of (a) the inhomogenous broadening and (b) spatial hole-burning. As a result, a large number of modes reach oscillation threshold, and compete for gain. The spectral profile is particularly sensitive to the frequency dependence of the feedback (see Chapter 4). In the interest of simplicity it is assumed here that the feedback is independent of wavelength.

The free spectral range of the resonator, $\Delta\nu_{FSR}$, is given by

$$\Delta\nu_{FSR} = \frac{c}{2nL} \qquad (2.46)$$

where

n is the effective index of the oscillating mode

L is the fibre resonator length.

For a typical fibre cavity of 1m length, the mode spacing is 10^3-10^4 times smaller than the homogenous linewidth; so that any variations in the modal amplitudes do not affect the overall gain saturation.

When the pump power is raised above threshold, the stimulated emission rate W_f increases, so as to clamp the gain to the value G_T over a bandwidth $\Delta\nu$. In general, both W_f and $\Delta\nu$ increase as the pump power is raised. Calculation of the output power and spectral width proceeds by assuming a profile for $P(\nu)$ (the internal stimulating power in the definition of W_f) and iterating the profile height and width to match the required gain saturation. Further details of the model are given in Appendix A.

The predicted variation in the linewidth of the neodymium fibre laser as the pump rate is increased above its threshold value is shown in Figure 2.11. It can be seen that considerable linewidth broadening is achieved if the laser is pumped far above threshold, the limit being set by the magnitude of the inhomogenous broadening.

The total power generated from stimulated emission, P_{TOT}, is given by the expression

$$P_{TOT} = \int_{\nu}\int_{\ell}\int_{A}\int_{f} h\nu W_f(\nu)\, n_{if}\, df\, dA\, dz\, d\nu \qquad (2.47)$$

The dependence of P_{TOT} on pump rate for a Nd^{3+}-doped fibre laser is shown in Figure 2.12. The output power is given by

$$P_{out} = \frac{T}{T+L} P_{TOT} \qquad (2.48)$$

where

T is the output transmission
L is the excess cavity loss

In keeping with standard laser analyses, the stimulated power P_{TOT}, can be expressed as a function of the excitation efficiency, η, the quantum efficiency ν_ℓ/ν_p, a parameter, f, or order unity, which accounts for the reduction in efficiency due to the line broadening

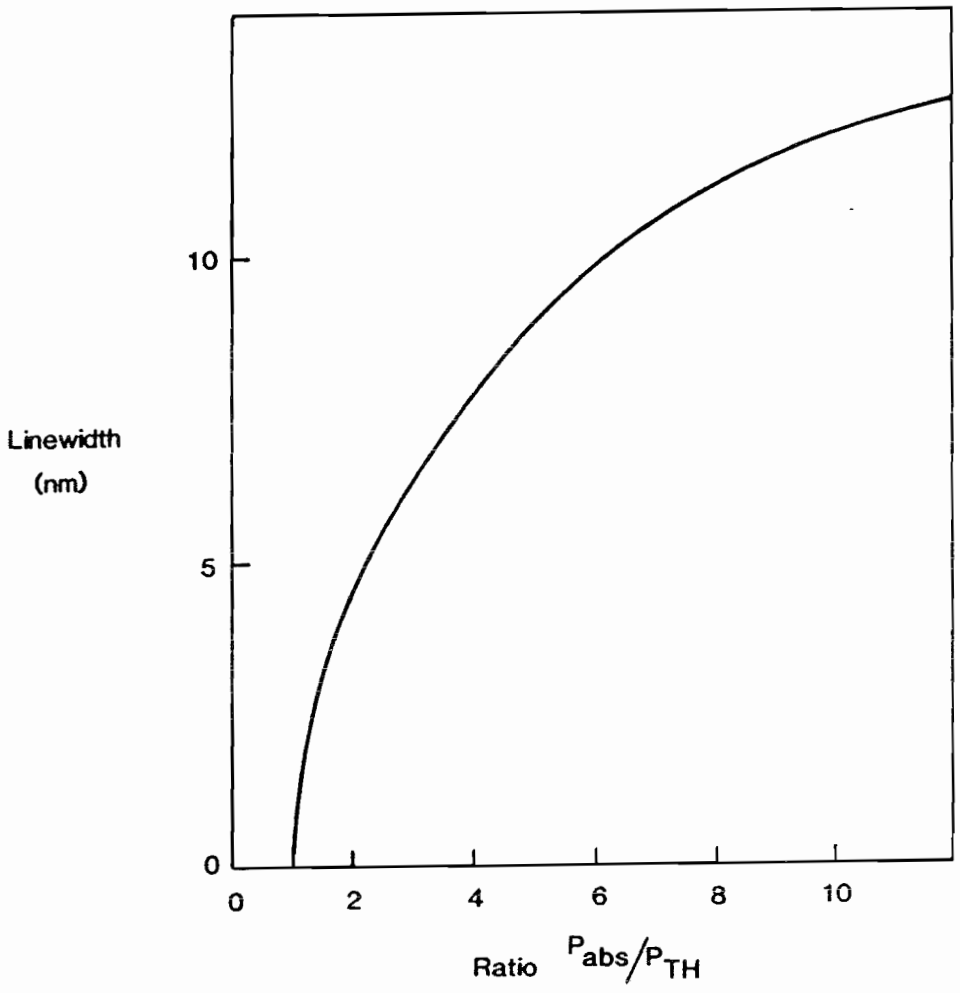

Figure 2.11 Power broadening of neodymium laser linewidth.

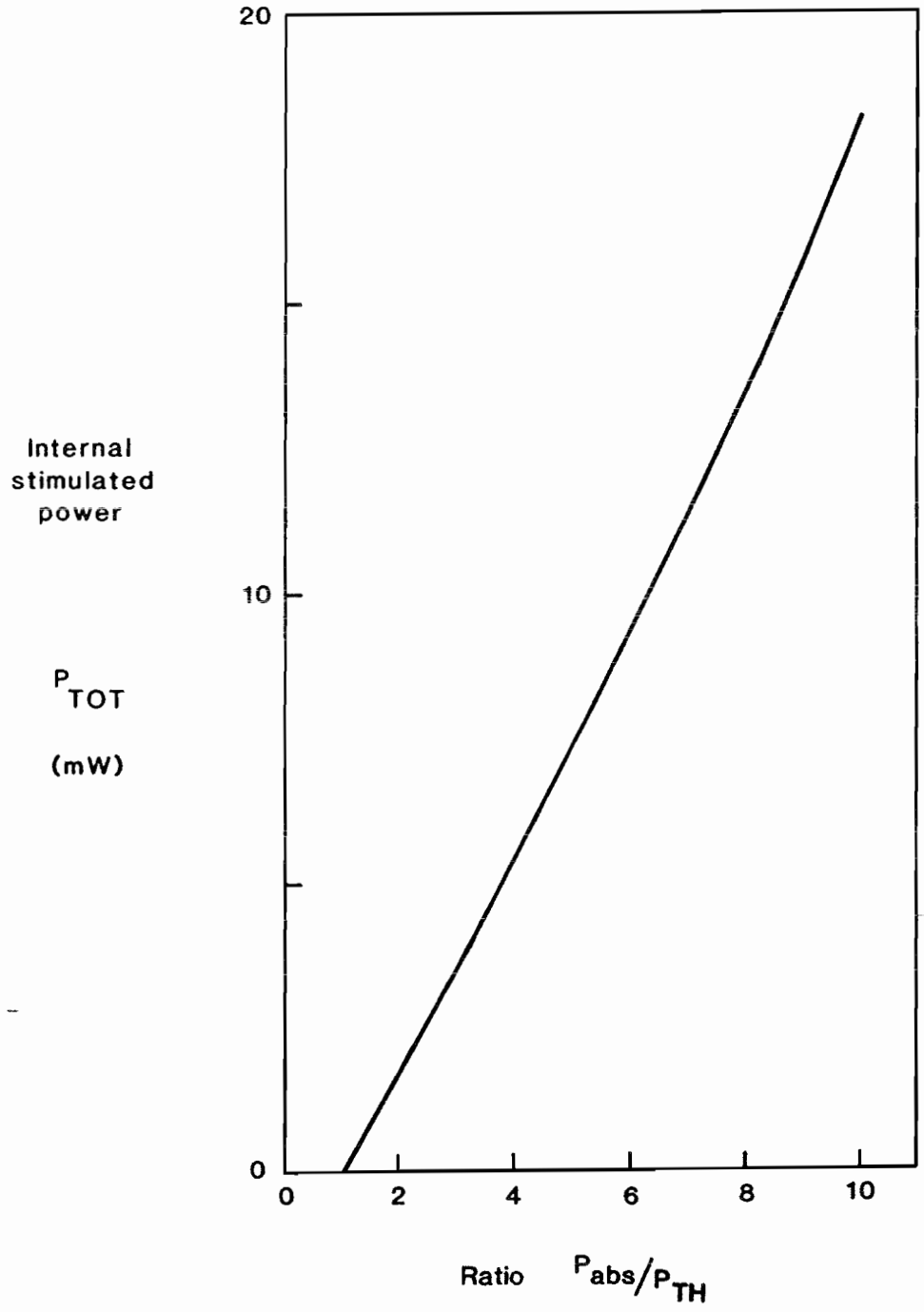

Figure 2.12 Internal stimulated power versus pump rate for neodymium-doped fibre laser.

mechanisms, and the difference between the absorbed power, P_{in} and the threshold power, P_{TH}. The output power is thus expressed

$$P_{out} = \frac{T}{T+L} \eta \frac{\nu_\ell}{\nu_p} f\left[\frac{\Delta\nu_{IH}}{\Delta\nu_H}\right](P_{in}-P_{TH}) \qquad (2.49)$$

The slope efficiency increases slightly as the pump rate is raised, Figure 2.12, due to the linewidth broadening, which increases the energy extraction from the inhomogenously-broadened inversion. The dependence of $f(\Delta\nu_{IH}/\Delta\nu_H)$, and hence the efficiency, on the magnitude of the broadening mechanisms, is discussed in the next section.

In three-level lasers, such as the Er^{3+}-doped fibre laser, the threshold is largely determined by the saturation intensity (cf Section 2.3.4). The variation of slope efficiency with output transmission for various values of the internal cavity loss is shown in Figure 2.13. The highest slope efficiencies are expected for low-gain (high reflectivity) lasers, but this advantage is rapidly lost if there are additional loss mechanisms in the cavity. Since high gains are readily achievable in erbium-doped fibre lasers (Chapter 5) it is possible to maintain efficient operation with 4% Fresnel reflection from the fibre end. The increased efficiency expected from a reduced output coupling is offset by the increased cavity loss incurred by the application of a mirror (typically 5%). Note that whereas in four-level lasers the threshold varies considerably with reflectivity, little penalty is paid in three-level lasers since the threshold is mainly determined by the saturation intensity rather than the cavity loss.

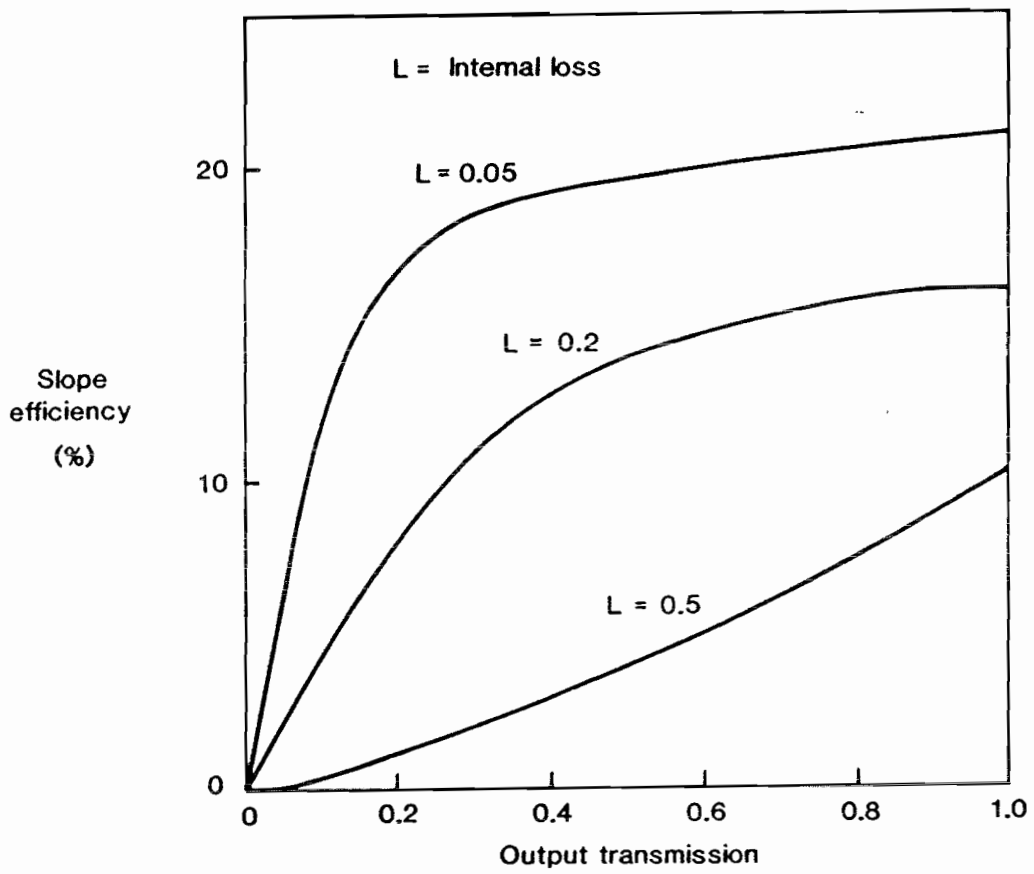

Figure 2.13 Slope-efficiency of erbium-doped fibre laser as a function of output transmission and internal loss.

2.4.2.2 Line-narrowed lasers

Line-narrowing of a fibre laser can be achieved with wavelength-selective feedback which restricts the oscillation bandwidth. Because of the various broadening mechanisms it is important to ascertain the influence of the feedback on the threshold and efficiency of the laser.

It is assumed that the laser bandwidth is now determined by the cavity, and is much smaller than the homogenous broadening, $\Delta\nu_H$. Equation (2.17) becomes

$$W_f = \frac{\lambda^2}{8\pi n^2 t_{spont} h\nu} S_{av} g_f(\nu_1) \qquad (2.50)$$

where

$$S_{av} = \int_{\substack{\text{laser}\\\text{line}}} S(\nu)d\nu$$

and

ν_1 is the centre frequency determined by the cavity

The threshold is determined by condition (2.41)

$$G(\nu_1) = G_T$$

where $G(\nu_1)$ is given by equation (2.20) or (2.32). Since the threshold is calculated for W_f=0, it is unchanged from the line-broadened case provided that ν_1 corresponds with the natural centre frequency of the laser.

In order to analyse the influence of the broadening mechanisms, the relative slope efficiency has been calculated for different ratios of the inhomogenous to homogenous linewidths ($\Delta\nu_{IH}/\Delta\nu_H$). The calculation was

made by adjusting the absolute magnitudes of the broadening so as to maintain the same threshold (via equation (2.16)). The results are plotted in Figure 2.14.

It can be seen that the efficiency relative to a purely homogenously-broadened laser is approximately 80% for a laser with $\Delta\nu_{IH}/\Delta\nu_{H} = 2$. This ratio is typical for a neodymium-doped silica fibre laser. The narrow spectral line at 1.536μm in erbium-doped silica (see Chapter 3) suggests that the ratio may be even lower for this laser. Thus it is expected that the efficient operation of line-narrowed laser should be readily achievable.

2.5 Temporal Effects

The foregoing analysis relies on a state of equilibrium being established in the fibre such that $dn_f/dt=0$. In this section, the conditions under which the equilibrium is attained, and the methods for exploiting the rate equations to produce short pulses of light are outlined.

2.5.1 Relaxation oscillations

When the pumping light is switched on, the laser responds in a damped oscillatory fashion, (see Figure 4.3). From standard laser theory[1] the oscillation period τ_{osc} for a four-level laser is given approximately by

$$\tau_{osc} = 2\pi \left[\frac{t_c T_{32}}{(r-1)} \right]^{\frac{1}{2}} \qquad (2.51)$$

where $r = G(o)/G_T$, $G(o)$ is the gain at zero stimulating rate ($W_f=0$), $t_c = n\ell/cG_T$, ℓ is the fibre length.

The oscillation is damped at a rate $\exp(-\alpha t)$ where

$$\alpha = \frac{r}{2T_{3/2}} \qquad (2.52)$$

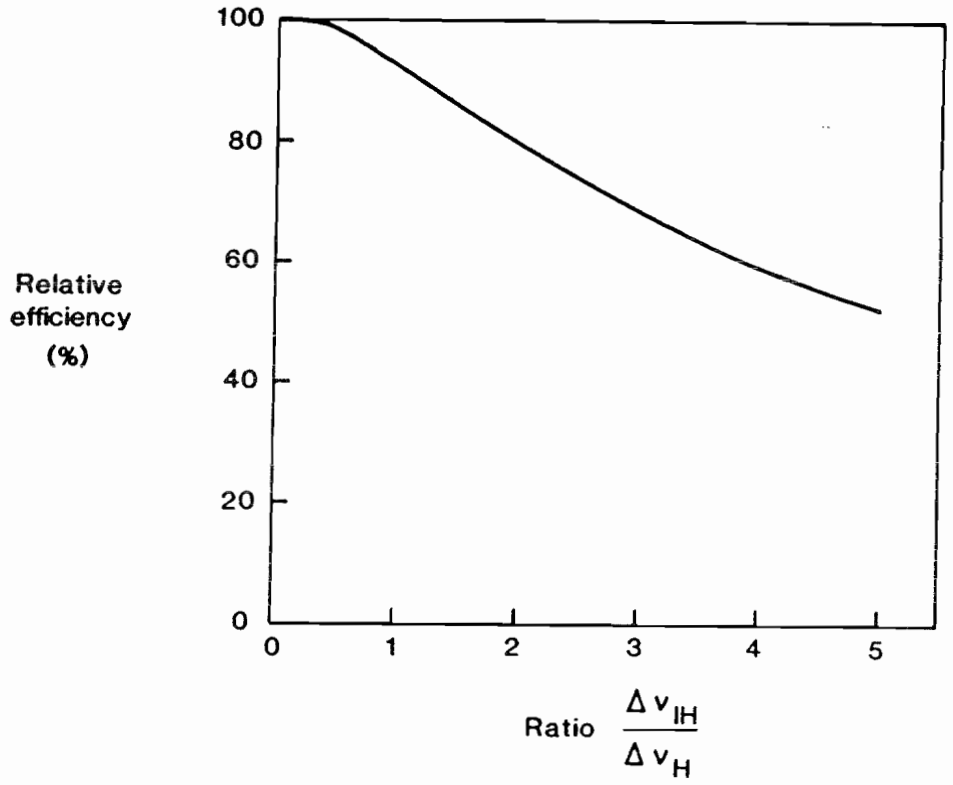

Figure 2.14 Efficiency of line-narrowed fibre laser as a function of the ratio of the inhomogenous and homogenous linewidths.

If the pump is not constant, but has an intensity fluctuation spectrum with a significant component close to $\omega_m = 2\pi/\tau_{osc}$, then the oscillation is driven. Modulation of the pump can thus produce a pulsed output. Typical modulation rates for fibres lasers are of the order of 100kHz-1MHz and pulse widths range from 5μs - 0.5μs. Relaxation oscillations are discussed further in Chapters 4 and 5.

2.5.2 Q-switched fibre laser

In the preceding section the oscillatory response of the laser to small changes in the gain was described. Unless this oscillation is driven, the laser gain tends towards the steady-state value G_T determined by the cavity losses. The technique of Q-switching[23] is based on an instantaneous reduction of G_T to a value much less than the single-pass gain. The laser intensity builds up rapidly and is usually sufficient to completely sweep out the population inversion. Thus the energy stored in the active medium prior to switching is released as a single intense pulse.

Following a standard analysis of Q-switching[1], the differential equation describing the laser intensity is

$$\frac{dS(\nu)}{dt} = \frac{c}{n\ell} [G(\nu) - G_T] S(\nu) \qquad (2.53)$$

where c/n is the speed of light in the fibre
ℓ is the fibre length.

The gain $G(\nu)$ is related to the population inversion through equation (2.20) (four-level laser) or equation (2.28) (three-level laser).

The rate equation for the population inversion is given by equation (2.14) (four-level) and equation (2.25) three-level), where W_f is defined by (2.17). Since the Q-switched pulse is typically of 10ns-100ns duration i.e.

much less than the spontaneous lifetime, the effect of the pump rate R and spontaneous emission during Q-switching is negligible (<0.1%). Q-switched Nd^{3+}-doped and Er^{3+}-doped fibre lasers have both been modelled using equation (2.53) and the appropriate expressions for the gain from Section 2.3. A typical Q-switched pulse for a Nd^{3+}-doped laser is shown in Figure 2.15. The inhomogenous broadening results in a small temporal broadening of the overall pulse since the gain for different spectral components is slightly different. Nevertheless, for a laser with a ratio $\Delta\nu_{IH}/\Delta\nu_{H} = 2$, the penalty is less than 1%. Thus the homogenous broadening ensures a relatively even depletion of the population inversion.

In three-level lasers the rate of depletion of the population inversion is twice that of an equivalent four-level system since stimulated emission results in an increase in the ground-state absorption. The maximum energy extraction is thus limited to less than 50% of the excited population energy. Fortunately the level lifetime of erbium ions is rather long ($T_{21} \sim$ 12ms), enabling greater storage of energy from a CW pump source than for neodymium ions ($T_{32} \sim$ 450μs). A high-power Q-switched Er^{3+}-doped fibre laser is described in Chapter 4.

Summary

A model has been developed for three- and four-level optical fibre lasers and amplifiers. The analysis takes account of the homogenous and inhomogenous broadening mechanisms in glass hosts, the high degree of pump saturation and the significant variation of pump power along the fibre. Previous analyses of waveguide lasers have been restricted to four-level homogenously broadened transitions, and are therefore not applicable to the optical fibre configuration.

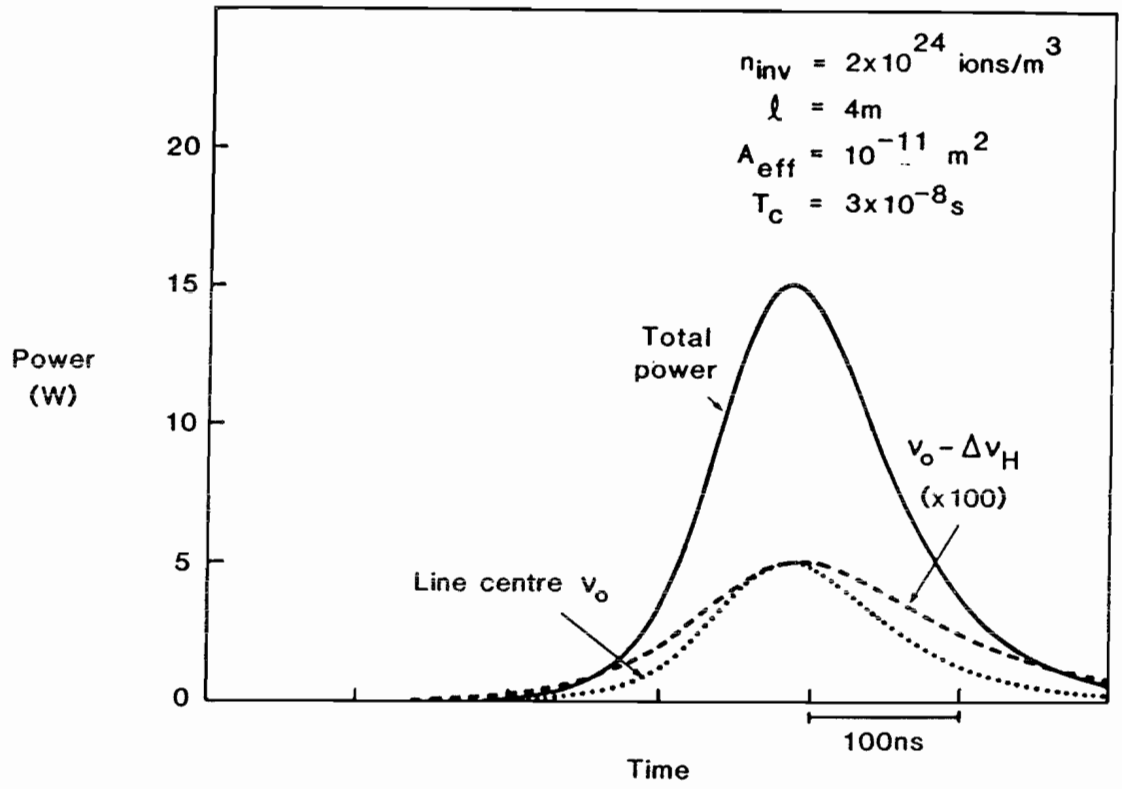

Figure 2.15. Typical Q-switched pulse for a neodymium-doped fibre laser

The remainder of this thesis is devoted to the study of two particular laser ions; neodymium, which is a four-level system at a wavelength of 1.088μm; and erbium, which is a three-level system at a wavelength of 1.54μm. Predictions of laser threshold, efficiency and certain spectral and temporal characteristics have therefore been made, and are compared with experiment in Chapters Four and Five. It is hoped that the theory presented here will prove useful in the continuing process of rare-earth-doped fibre laser development and optimisation.

APPENDIX 2A : SPECTRAL BROADENING IN SLOPE FIBRE LASERS

The homogenous broadening $g_f(\nu)$ is assumed to take a Lorentzian profile

$$g_f(\nu) = \frac{\Delta\nu_H}{2\pi[(\nu-f)^2 + (\frac{\Delta\nu_H}{2})^2]} \qquad (A2.1)$$

where $\Delta\nu_H$ is the homogenous linewidth.

This broadening is appropriate to a damped oscillator of decay time τ (e.g. an atom interrupted by a phonon) where

$$\tau = \frac{1}{\pi\Delta\nu_H} \qquad (A2.2)$$

The distribution of sites is assumed to correspond to a Gaussian

$$p(f) = \frac{2(\ln 2)^{\frac{1}{2}}}{\pi^{\frac{1}{2}}\Delta\nu_{IH}} \exp - \left[4(\ln 2) \frac{(f-\nu_o)^2}{\Delta\nu_{IH}^2} \right] \qquad (A2.3)$$

where ν_o is the centre frequency
$\Delta\nu_{IH}$ is the inhomogenous linewidth

For Nd^{3+}-ions, $\Delta\nu_H$ and $\Delta\nu_{IH}$ are taken to be $60cm^{-1}$ and $120cm^{-1}$ respectively[13]. These values correspond with a stimulated cross-section, σ, (equation (2.16)) of $1.5\times10^{-24}m^2$ (for $t_{spont} = 2T_{32}$ and $T_{32} = 450\mu s$). In order to compare the influence of the broadening mechanisms the ratio of $\Delta\nu_{IH}/\Delta\nu_H$ is varied whilst maintaining a constant value of σ.

Experimental data on the ratio of homogenous and inhomogenous broadening in erbium ions is not readily available. The narrow fluorescence and absorption linewidths at $1.536\mu m$ suggest a smaller value of $\Delta\nu_{IH}$ than in

neodymium, whereas the homogenous broadening is a more fundamental glass property, (it depends on the phonon spectrum of the material and hence the acoustic velocity) and is expected to be similar in magnitude (i.e. $\sim 60 cm^{-1}$).

References to Chapter 2

1. A. Yariv:
"Optical Electronics",
Holt Saunders ISBN 4-8337-0274-6.

2. W. Koechner:
"Solid-State Laser Engineering",
Springer-Verlag.

3. M.J. Digonnet and C.J. Gaeta:
"Theoretical analysis of optical fibre laser amplifiers and oscillators",
Appl. Opt. 1985, 24, pp. 333-342.

4. K. Kubodera and K. Otsuka:
"Single transverse mode $LiNdP_4O_{12}$ slab waveguide laser",
J. Appl. Phys., 1979, 50, p. 653.

5. G.H. Dieke and H.M. Crosswhite:
"The spectra of the doubly and triply ionised rare earths",
Appl. Opt., 1963, 2, pp. 675.

6. G.K. Woodgate:
"Elementary Atomic Structure",
Clarendon Press ISBN 0-19-851146-9.

7. K. Patek:
"Glass Lasers",
London Iliffe Books, ISBN 0-592-02778-3.

8. B.R. Judd:
"Optical absorption intensities of rare-earth ions",
Phys. Rev., 1962, 127, pp. 750.

9. G.S. Ofelt:
"Intensties of crystal spectra of rare-earth ions",
J. Chem. Phys., 1962, 37, pp. 511.

10. R. Reisfeld and C.K. Jorgensen:
"Lasers and excited states of rare earths",
Springer-Verlag, ISBN 3-540-08324-3.

11. A. Einstein:
"On the quantum theory of radiation",
Physikalische Zeitschrift, 1917, 18, pp. 121-128.

12 D. Curie
"Luminescence cristalline",
Dunod, Paris, 1960.

13. J.M. Pellegrino, W.M. Yen and M.J. Weber:
"Composition dependence of Nd^{3+}-homogenous linewidths in glasses",
J. Appl. Phys., 1980, 51, pp. 6332-6336.

14. R.J. Mears, L. Reekie, S.B. Poole and D.N. Payne:
"A low-threshold tunable CW and Q-switched fibre laser operating at 1.55μm",
Electron. Lett., 1986, 22, pp. 159-160.

15. S.E. Miller and A.G. Chynoweth:
"Optical Fibre Telecommunication",
Academic Press, New York, 1979.

16. A.W. Snyder and J.D. Love:
"Optical Waveguide Theory",
Chapman and Hall, ISBN 041209950 0.

17. D.N. Payne, A.J. Barlow and J.J. Ramskov Hansen:
"Development of low- and high-birefringence optical fibres",
IEEE J. Quant. Electron., 1982, QE-18,
pp. 477-488.

18. D.W. Hall, R.A. Haas, W.F. Krupke and M.J. Weber:
"Spectral and polarisation hole burning in neodymium glass lasers",
IEEE J. Quant. Electron., 1983, QE-19,
pp. 1704-1717.

19. J.T. Lin:
Minithesis,
The University of Southampton, to be submitted.

20. E. Snitzer and C.G. Young:
"Glass Lasers",
Advances in Lasers, Vol. 2, A. Levine Ed.,
New York : Dekker, 1968, pp. 191-256.

21. O.K. Alimov et al:
"Selective laser excitation study of the structure of inhomogeneously broadened spectra of Nd^{3+} ions in glass",
Sov. Phys. JETP., 1978, 47, pp. 29-34.

22. L.F. Stokes, M. Chodorow and H.J. Shaw:
"All-single-mode fiber resonator",
Opt. Lett., 1982, 7, pp. 288-290.

23. F.J. McClung and R.N. Hellwarth:
"Giant optical pulsations from ruby",
J. Appl. Phys., 1962, 33, p. 828.

CHAPTER 3 : CHARACTERISATION OF RARE-EARTH DOPED FIBRES

The optical fibre lasers and amplifiers described in this thesis are based on low-loss silica fibres doped with rare-earth ions. Chapter 3 describes the fabrication and characterisation of the doped fibres. Before efficient devices can be constructed, it is essential to have a knowledge of the absorption and fluorescence characteristics of the laser material. Section 3.1 reviews the doped-fibre fabrication process developed by S.B. Poole and D.N. Payne. Although the technique has recently been superceded, it has proved successful in producing high-quality doped-fibres. Section 3.2 covers the absorption and fluorescence properties pertinent to the subsequent laser and amplifier experiments. Measurement of the metastable level lifetime in Nd^{3+}-doped, and Er^{3+}-doped, silica and modelling of the non-exponential decay according to the inhomogenous broadening is also presented. The chapter ends with a description of excited-state absorption and the problems this causes in laser design.

3.1 Review of Doped-Fibre Fabrication

One of the most important developments in the application of optical fibres to telecommunications was the invention of the Modified Chemical Vapour Deposition process[1-3] (MCVD), which resulted in the production of very-high-quality optical waveguides. The original aim of the doped-fibre fabrication research was to produce fibres of telecommunications quality incorporating low levels of rare-earth dopant. It was thus essential to base the fabrication technique on the MCVD process.

Rare-earth-doped silica has received relatively little attention as a laser material[4,5] because of its high fictive temperature (~ 1800^{o}C) and poor ionic solubility. Nevertheless, its high transparency, high

durability and low thermal expansion coefficient make it an excellent host. The fluorescence linewidths of the rare-earth ions in silica are amongst the broadest in any glass[6]. A chemical vapour deposition system for the production of neodymium-doped silica was described by Namikawa[7]. The technique has been adapted to the MCVD process by S.B. Poole and D.N. Payne.

3.1.1 Gas phase deposition of rare-earth ions

The first technique to achieve low-loss doped fibres is based on a modified MCVD process[8]. The basic reaction for the production of high purity waveguides is the oxidation of silicon tetrachloride,

$$SiCl_4 + O_2 \rightarrow SiO_2 + 2Cl_2$$

which is deposited as a soot on the inside of a silica substrate tube and then fused to form a glass. The refractive index of the deposited glass is changed by the addition of germanium tetrachloride, boron trichloride or phosphorus pentachloride to the silicon tetrachloride /oxygen mixture. All these reagents are gaseous at the deposition temperature, enabling the use of mass flow controllers to determine the precise composition.

The starting materials for the deposition of rare-earth ions are the rare-earth halides (e.g. $NdCl_3$). Unfortunately these materials are solid at room temperature, and have low vapour pressures even at the deposition temperature. A separate chamber in the deposition tube which permitted the independent heating of the rare-earth halides was therefore designed, Figure 3.1. A major contaminant of optical waveguides at infra-red wavelengths is the water molecule, H_2O, which has absorption bands at 950nm and 1380nm. Fusion of the rare-earth halides to the chamber walls in a chlorine atmosphere removes the water of crystallisation and also permits a more even deposition. Any rare-earth chloride/ oxides deposited in the tube during this process are removed by passing a SF_6 etching gas through the tube.

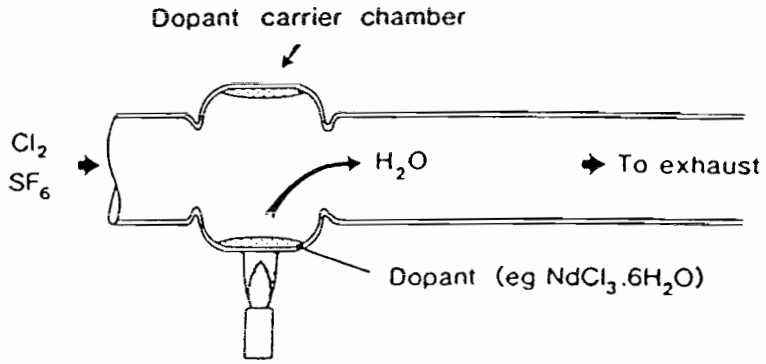

Figure 3.1 Dehydration of rare-earth halide.

Fabrication of the preform proceeds in the usual manner, except that the "core" of germania-doped silica is left unfused. The dopant chamber is then heated to approximately 1300°C (the precise temperature determines the dopant concentration) and rare-earth oxide deposits in the core according to the oxidation reaction

$$4RCl_3 + 3O_2 \rightarrow 2R_2O_3 + 6Cl_2$$

where R is the trivalent rare-earth ion. The deposition process is shown in Figure 3.2.

In order to produce low-loss fibres, a further drying stage using Cl_2 was found to be necessary before fusing and collapsing the tube into a solid preform.

The fibre drawing is accomplished using a graphite element furnace designed by D.N. Payne. A schematic of the drawing process is shown in Figure 3.3. The preform is heated to between 2100 and 2200°C and fibre is given a UV-cured acrylate coating before reaching the take-up drum. The diameter of the fibre is measured with an Anritsu laser diameter-measuring system, and controlled via a feedback loop to the drum motor.

3.1.2 Results and limitations

The fabrication technique described above has proved successful in producing low-loss fibres with dopant concentrations of up to a few hundred parts per million (ppm). At this doping level, absorptions of up to 100dB/m can be attained, whilst at wavelengths where ionic absorption is negligible, the fibre loss is comparable to conventional silica fibres. The fibre has made it possible to study laser devices ranging in length from a few tens of centimetres to many hundreds of metres.

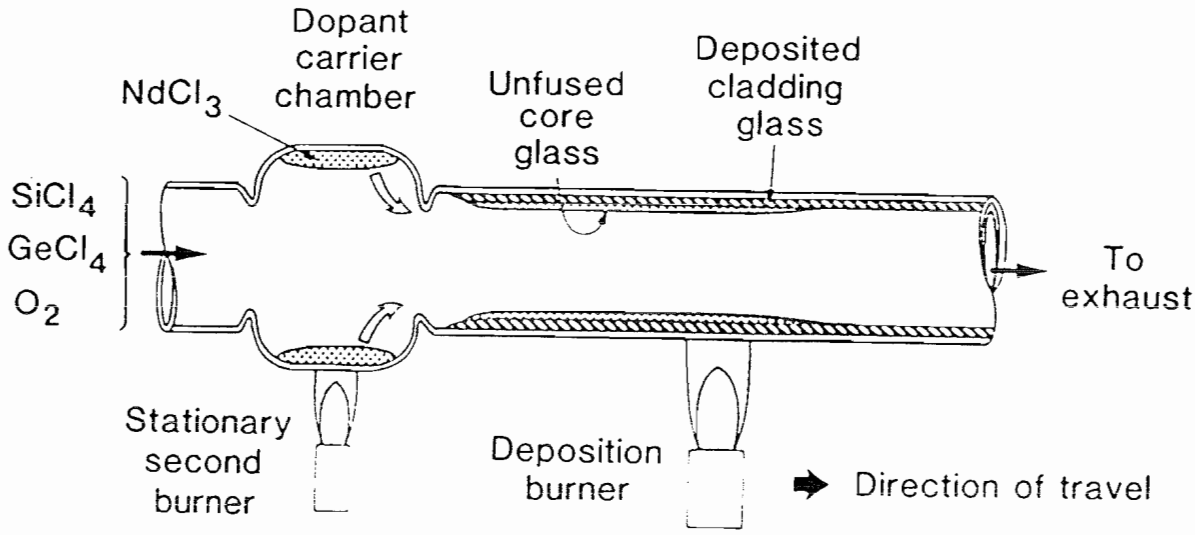

Figure 3.2 Fabrication of doped-preform by M.C.V.D.

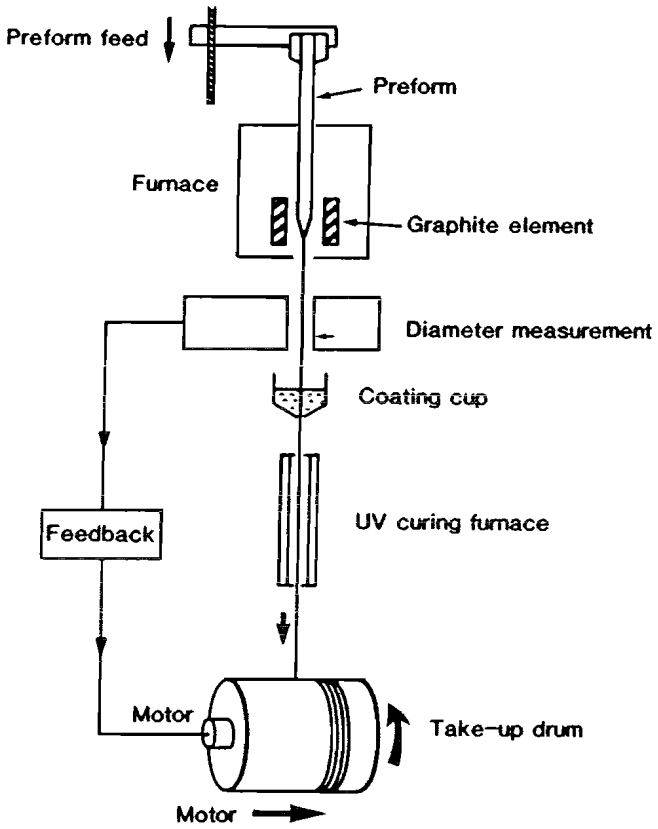

Figure 3.3 Fibre drawing process

The above method can introduce only a limited range of certain ions into a silica-based glass, the doping level is not well-controlled and it would appear to be very difficult to produce high dopant concentrations. The deposition rate is proportional to the partial pressures of the reagents, which for the rare-earth halides is considerably less than for the usual MCVD gases. In order to overcome these problems a solution technique based on published work by Stone and Burrus[4] has recently been developed[9].

3.1.3 Solution technique

In the second technique the dopant is introduced via an aqueous solution of the rare-earth halide. Fabrication of the preform proceeds in the usual manner, and the core is deposited as an unfused soot. The tube is then removed from the lathe, filled with a solution of the rare-earth halide, and left to stand for several hours. During this time, diffusion of the rare-earth ions into the soot occurs. The tube is dried with acetone and replaced in the lathe. The core is then thoroughly dried by the passage of chlorine before the preform is collapsed. The advantage of this technique is that it is not limited by the low vapour pressure of rare-earth halides, and high dopant concentrations can be readily achieved. The doping level is closely related to the concentration of the solution and hence can be well controlled. The technique is also suited to the incorporation of transition metal ions, which should lead to a new class of tunable fibre lasers. These fibres have yet to be fully characterised and are not discussed in this thesis.

3.2 Doped-Fibre Characterisation

A knowledge of the absorption and fluorescence characteristics of the active medium is essential to good laser design. Measurements of these properties for fibres containing Nd^{3+} and Er^{3+} ions are now presented.

3.2.1 Absorption spectra

An introduction to the properties of rare-earth ions in glass is given in Section 2.1, and an energy-level diagram for free rare-earth ions is shown in Figure 2.1.

The large variation in spectral attenuation poses a number of problems for the measurement of absorption spectra. Multiple cut-back measurements were made on two different systems; a York Technology FCm having a 5nm spectral resolution and 30dB dynamic range, and attenuation equipment optimised to provide a dynamic range in excess of 45dB with a 2nm spectral resolution. The latter system is described in detail in reference 10. The large dynamic range is achieved by the use of a double monochromator to reduce stray light, and a liquid-nitrogen-cooled Ge photodiode. A schematic of the system is shown in Figure 3.4. The advantages of the FCm lie in its ease of use and, more importantly, the repeatability of measurements (better than 5%) which is due to well-designed fibre holders and an automatic launch and detection system. In order to be able to compare and combine measurements made on the two systems, both monochromators were carefully calibrated with a HeNe laser at 633nm and a doped fibre with a narrow absorption at 1536nm. In general, measurements of low attenuation, away from absorption bands, were made on long lengths of fibre (typically 500m - 1km) with the FCm, whereas the absorption bands were characterised by short length cut-backs on the system having high dynamic range. The measurement limit of this technique is ~80dB/m. Thus, fibres with

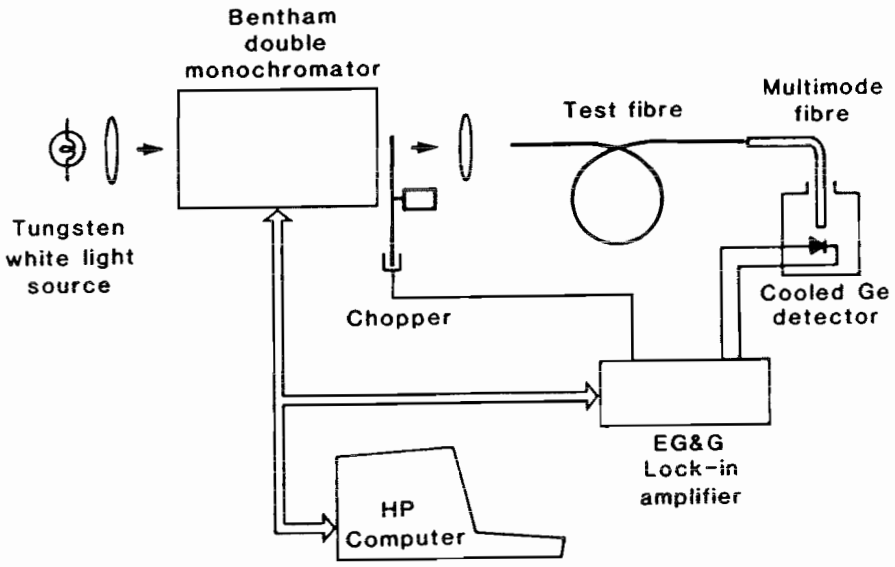

Figure 3.4 Attenuation measurement system.

dopant concentrations in excess of approximately 500ppm cannot be measured by this method which, nevertheless, is sufficient for all of the fibres described in this thesis.

3.2.1.1 Reduction of water content

The primary contaminant affecting infra-red propagation in optical fibres is water. The major absorption bands occur beyond 2μm, but there are significant harmonics at 1.38μm and 0.95μm. The preform "drying" stages developed by S.B. Poole have been very successful, and have resulted in losses at 1.38μm of less than 10dB/km.

3.2.1.2 Dopant concentration

As discussed in Section 3.1.2, the dopant concentration is primarily a function of the vapour pressure of the rare-earth halide, and hence of the temperature in the dopant chamber. The difference in the vapour pressures of the rare-earth halides and the usual MCVD reagents limits the dopant concentration to less than 1000 ppm.

In order to associate dopant concentrations with the fibre measurements it is necessary to make an assumption about the dopant ion cross-section. Although many studies have been made of the properties of rare-earth ions in glasses, no published measurements have been made in typical optical fibre core glass i.e. ~ 10% GeO_2, 90% SiO_2. It is well known that the ionic cross-sections are modified by the local Stark field, and hence vary from one glass host to another[6]. The calculation of dopant concentration from absorption measurements is discussed in Appendix A, and the characteristics of the doped fibres are given in Tables 3.1 and 3.2.

3.2.1.3 Neodymium absorption bands

The absorption spectrum of fibre ND199, which has an approximate Nd^{3+}-concentration of 100ppm, is shown in Figure 3.5. The strong absorption bands throughout the visible and near infra-red regions of the spectrum permit optical pumping of the ions with a wide variety of sources e.g. Ar^{+}- lasers (514.5nm), Rh6G dye lasers (550-630nm) and GaAlAs solid-state lasers (750-850nm). In contrast to these absorptions, the loss in the wavelength region 950-1300nm is less than 0.01dB/m. Many metres of fibre can therefore be deployed in optical devices before the loss at the lasing wavelength (1.088μm) is significant.

The absorption bands have typical half-widths ranging from 15nm-40nm. The origins of this broadening are discussed in Chapter 2. At low-temperatures (e.g. 77K) the effect of homogenous broadening is negligible and the dominant broadening mechanisms are

(i) inhomogenous broadening due to site-to-site variations in the crystal-field

(ii) crystal-field splitting of the individual energy levels (Stark splitting).

Figure 3.6 shows the absorption band at 900nm (the $^4I_{9/2}$ - $^4F_{3/2}$ transition) measured at 77K. As a result of the low temperature only the lowest Stark component of the $^4I_{9/2}$ multiplet is significantly populated, so that two lines are anticipated, corresponding to transitions to the upper and lower components of the $^4F_{3/2}$ level. The two components are visible in the figure, though poorly resolved due to the considerable inhomogenous broadening in the glass matrix. The Stark splitting and inhomogenous broadening are estimated to be $250cm^{-1}$ and $125cm^{-1}$ respec-

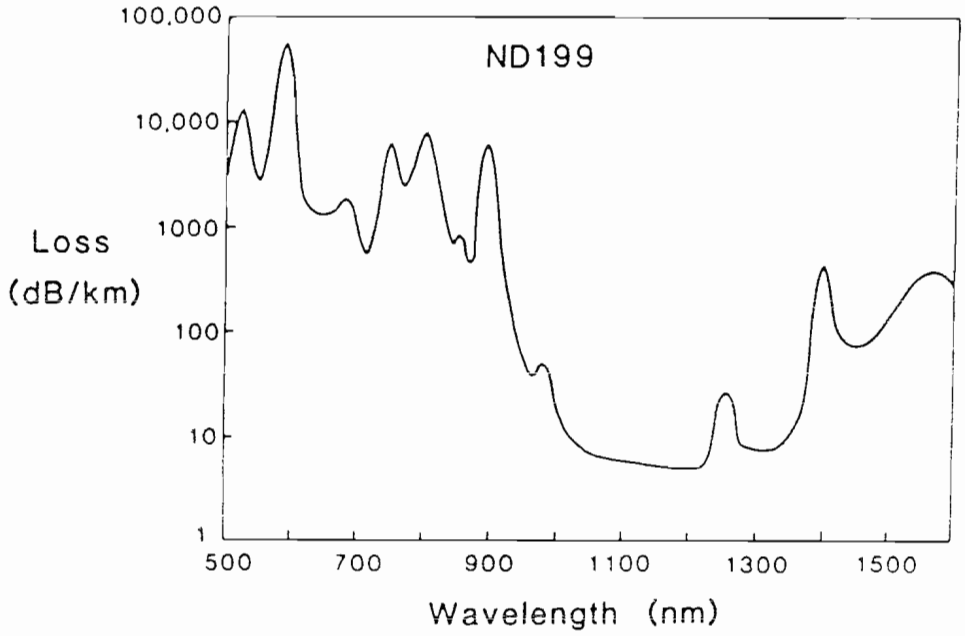

Figure 3.5 Absorption spectrum of neodymium-doped fibre (ND199).

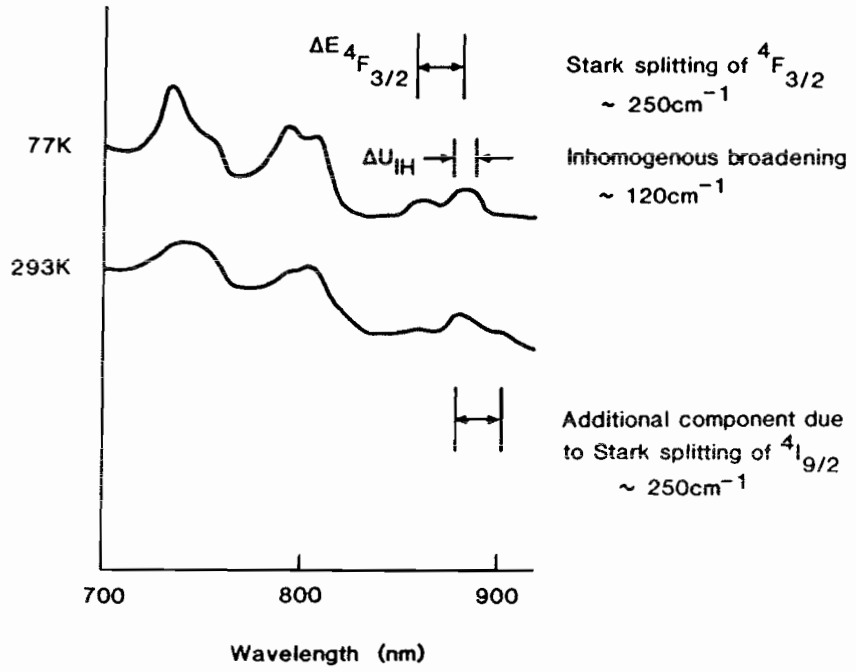

Figure 3.6 Temperature dependence of neodymium absorption spectrum, illustrating the Stark shift and broadening mechanisms.

tively (20nm and 10nm). A comprehensive study of the effects of Stark splitting, inhomogenous broadening and homogenous broadening is given in reference 11.

3.2.1.4 Erbium absorption bands

The absorption spectra of fibre ND263 is shown in Figure 3.7. The fibre has an approximate Er^{3+}-concentration of 350ppm. As discussed in Chapter Two, the lasing transition at 1.536μm is a three-level one, and hence a strong absorption band at this wavelength is visible in the Figure.

The major pump absorption bands occur at 520nm (accessible to an Ar^{+}-laser), 650nm (accessible to a DCM-dye laser), 800nm (accessible to a GaAlAs diode laser or Styryl-9 dye laser) and 980nm (potentially accessible to a InGaAsP or Yb^{3+}-laser). The fibre loss is not directly measurable at the lasing wavelength due to the three-level absorption, but measurements at 1.3μm indicate a loss as low as 10dB/km. The intrinsic absorption of the fibre is thus negligible for typical device lengths (1-3 metres).

The absorption bands show little resolvable structure (except at 1.536μm and 1.552μm above a broad background absorption) and are broadened typically by 15nm-30nm. Whilst the broad bands are advantageous to optical pumping, since they offer immunity to changes in the pump spectrum, the likelihood of excited-state absorption of the pump under intense excitation is also increased. A striking example occurs when the Er^{3+}-doped fibre is excited by a 650nm, or 800nm, pump source. Under intense excitation the $^4I_{13/2}$ level responsible for the 1.5μm absorption becomes significantly populated. Electrons in this level can also absorb pump photons, resulting in excitation to the $^4S_{3/2}$ level (see Figure 2.1). The latter is sufficiently long-lived for it to give rise to characteristic fluorescence in the region of

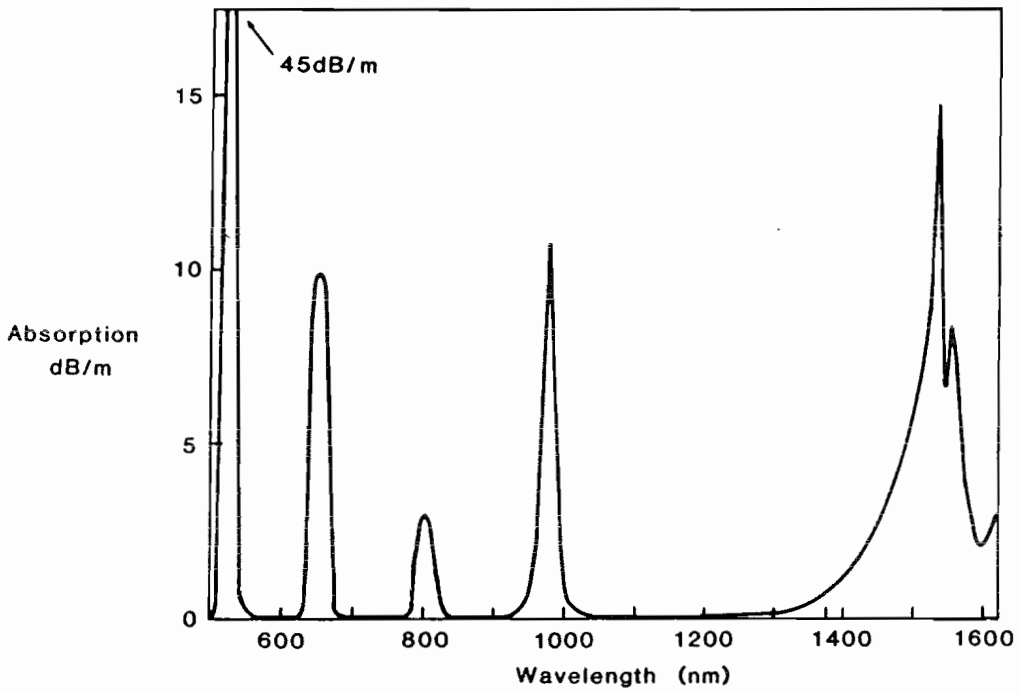

Figure 3.7 Absorption spectrum of erbium-doped fibre (ND263).

540nm i.e. green. The use of Er^{3+} in infra-red-to-visible convertors has been well characterised[12]. Usually, the process responsible is energy transfer from adjacent ions (e.g. Yb^{3+}), but the fibre fluorescence is clearly a single-ion phenomena, since the doping level is low. It is described further in Section 3.3.

3.2.2 Spectral measurements of fluorescence

A schematic of the fluorescence measurement apparatus is provided in Figure 3.8. In order to obtain representative fluorescence spectra, effects such as self-absorption and amplified spontaneous emission must be carefully avoided. Short specimen lengths are therefore investigated under low-power excitation. The detector for the majority of the measurements is an InGaAs p.i.n. diode which has a broad response and high quantum efficiency over the majority of the spectrum of interest. The response of the detector has been corrected for in the fluorescence spectra that follow. The monochromator used for all the measurements is a 0.5m SPEX with a resolution of 1nm.

3.2.2.1 Nd^{3+} fluorescence

The fluorescence spectrum of fibre ND199 doped with 100ppm of neodymium ions is shown in Figure 3.9 . The fibre specimen was approximately 40cm long and the pump source was a low-power air-cooled argon ion laser (Spectra Physics model). The fluorescence structure is mainly caused by Stark splitting of the terminal fluorescence levels ($^4I_{13/2}$, $^4I_{11/2}$ $^4I_{9/2}$). The broad fluorescent bands at 0.94μm, 1.08μm and 1.37μm have FWHM's (full width half maxima) of 65nm, 42nm and 70nm respectively. The prominent double peak at 1.08μm is characteristic of Nd^{3+} in a high silicate glass[4,13]. It is believed to be due to the large Stark splitting between the first two components

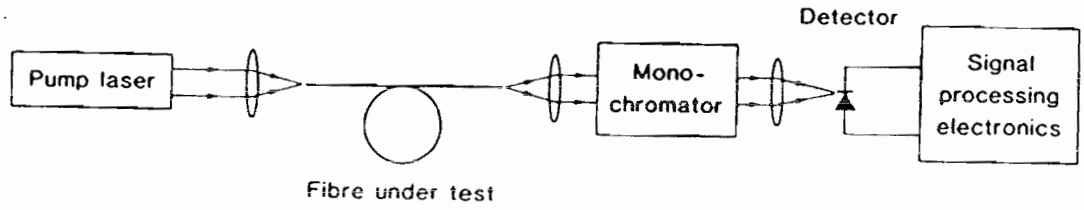

Figure 3.8 Schematic of fluorescence measurement equipment.

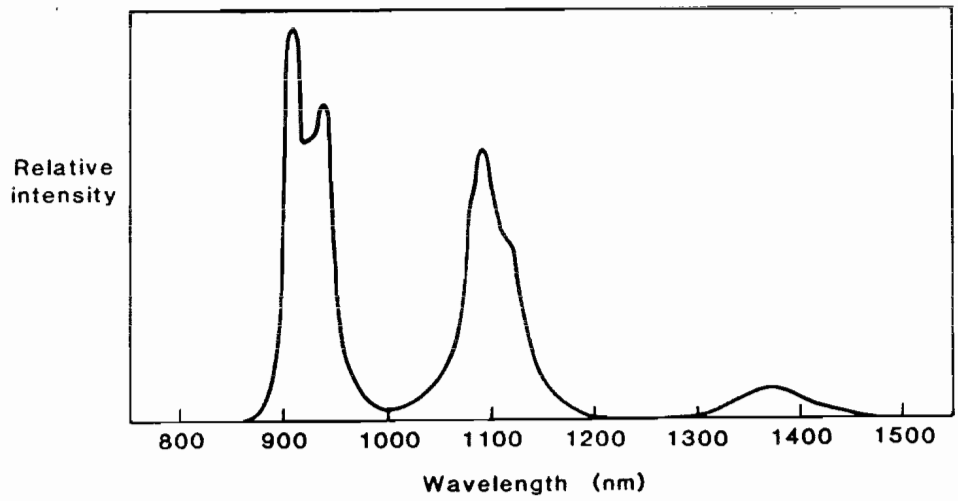

Figure 3.9 Spectral fluorescence of neodymium in fused silica.

of the $^4I_{11/2}$ level[14]. Fibre lasers have been demonstrated to operate over both the 900nm and 1.1μm fluorescent bands.

3.2.2.2 Er^{3+} fluorescence

The Er^{3+}-ion fluorescence of interest here consists of a single band at 1.54μm, and arises from the $^4I_{13/2}$ - $^4I_{15/2}$ transition. Considerably weaker fluorescence centred on 540nm can also be observed if the pump is tuned to an absorption from the metastable $^4I_{13/2}$ level to above the $^4S_{3/2}$ level. The 1.54μm fluorescence, Figure 3.10, was measured from a 9cm length of ND263 in order to minimise any self-absorption or amplified spontaneous emission of the fluorescence captured by the fibre. The pump was a DCM dye laser (Ar^+-ion laser pumped) at low power and tuned away from the excited state absorption (650nm).

According to the theory of rare-earth ions in glass (ref Chapter Two), the $^4I_{13/2}$ level is split into 7 components and the $^4I_{15/2}$ metastable level is split into 8 components. The anticipated 56 different transitions cannot be resolved because of the combined homogenous and inhomogenous broadening, and contribute to a broad band (FWHM 50nm) centred on 1.545μm. A striking feature of the Er^{3+} fluorescence spectrum, however, is the two narrow lines at 1.536μm and 1.552μm with FWHM's of 6nm and 8nm respectively. It is believed that these are due to the reinforcement of certain energy differences between the components of the two levels because the Stark splittings are of similar magnitude for each level. Tunable laser action has been demonstrated over a large portion of the available gain curve at 1.54μm, and is described in Chapter 4.

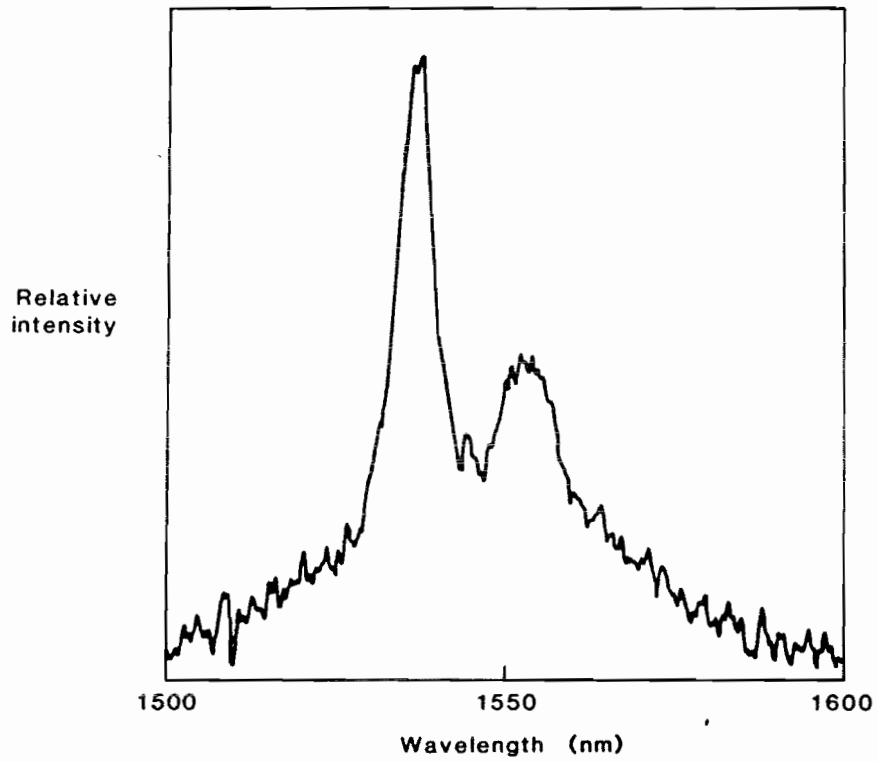

Figure 3.10 Spectral fluorescence of erbium in fused silica.

3.2.3 Temporal fluorescence measurements

The requirements for temporal fluorescence measurements are (i) a pump pulse with a fall time much shorter than the fluorescence lifetime; (ii) negligible gain (or absorption for three-level systems) in the excited medium, and (iii) sufficient signal for an analysis of the decay to be made. Conditions (ii) and (iii) are frequently contradictory, and a suitable compromise must be found. It is helpful to use short lengths of large-cored fibre in order to reduce gain for a given excited population.

3.2.3.1 Measurement of fluorescence decay in Nd^{3+}-doped fibres

The system for measurement of the fluorescence lifetime in Nd^{3+}-doped fibres is shown in Figure 3.11. In order to obtain a good discrimination between the pump decay and the fluorescence, the doped-fibre was excited with a Q-switched, frequency-doubled, Nd:YAG laser operating at 532nm. The pump was suitably attenuated so that the maximum inversion attainable was 0.1μJ, which corresponds to a gain of less than 1%. The fibre output was filtered by a monochromator and the fluorescence decay was analysed for both the 900nm and 1088nm fluorescent bands. The detector was an extended range silicon APD and the signal could be analysed, either on an analogue oscilloscope (Tektronix), or a digitising oscilloscope (Tracor Northern) which averaged successive fluorescence traces with a 4μs sampling time. The digitising oscilloscope was controlled by a Tektronix 4052 minicomputer and the typical number of averages was 65,000. In Chapter 2 (Section 2.2) it is stated that the decay time from the pump level (N_4) to the upper lasing level is so small that the population of N_4 and intermediate levels can be neglected. Measurement of the delay between the pump pulse and the peak fluorescence is an indication of the total decay time. The Q-switched pulse width for these

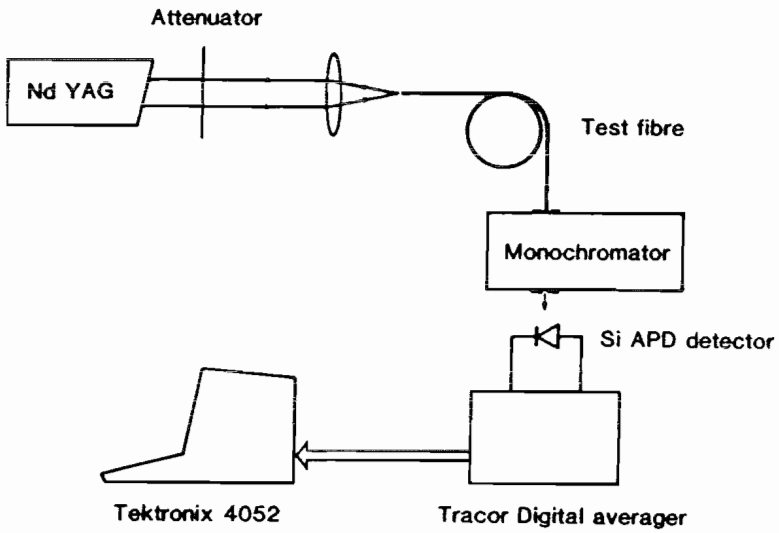

Figure 3.11 Measurement of neodymium fluorescence decay time.

experiments was 90ns and the delay between the pump pulse and peak fluorescence was less than 10ns. This is in good agreement with measurements by other authors[13].

The fluorescence decay at 1.08μm is shown in Figure 3.12. The 1/e decay time, $t_{1/e}$, is 450 ± 10μs. At 940nm the value is the same. It was decided to analyse the fluorescence by fitting the instantaneous decay rate to an exponential exp[-t/a(t)]. For a pure exponential decay a(t) is a constant (= $t_{1/e}$). The results at 1.08μm are shown in Figure 3.13. The observed time dependence of a is approximated by

$$a = T_O + \alpha t$$

where

T_O = 390μs

α = 0.125

Departures from an exponential decay of Nd^{3+}-ions in glass have been observed previously[6] and are believed to result from the inhomogenous broadening in the glass host. Since the energy levels vary from site to site it is reasonable to expect the decay rate to vary also. Using the model for inhomogenous broadening described in Chapter 2, the fluorescence amplitude at time t can be written

$$P(t) = P_0 \int_f p(f) \exp\left[\frac{-t}{a(f)}\right] df$$

where

p(f) is defined in Section 2.2.

a(f) is the dependence of the decay time on f

f is the inhomogenous parameter

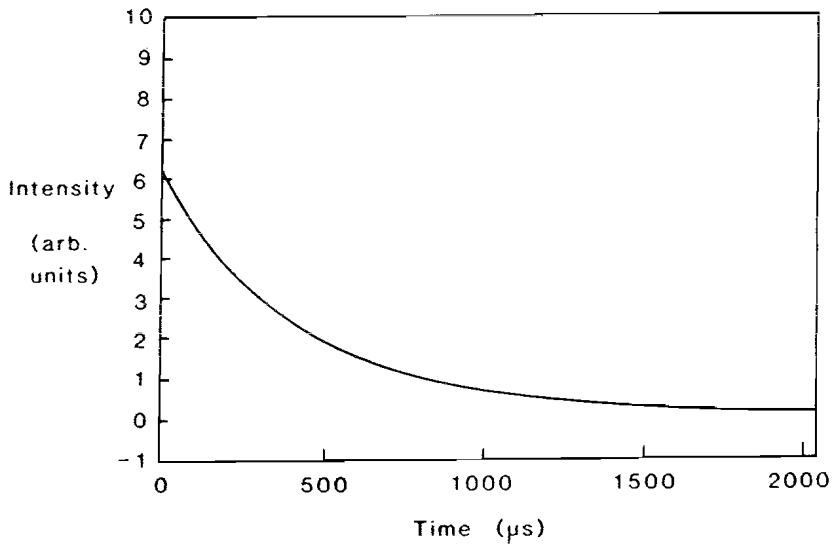

Figure 3.12 Fluorescence decay of neodymium in fused silica.

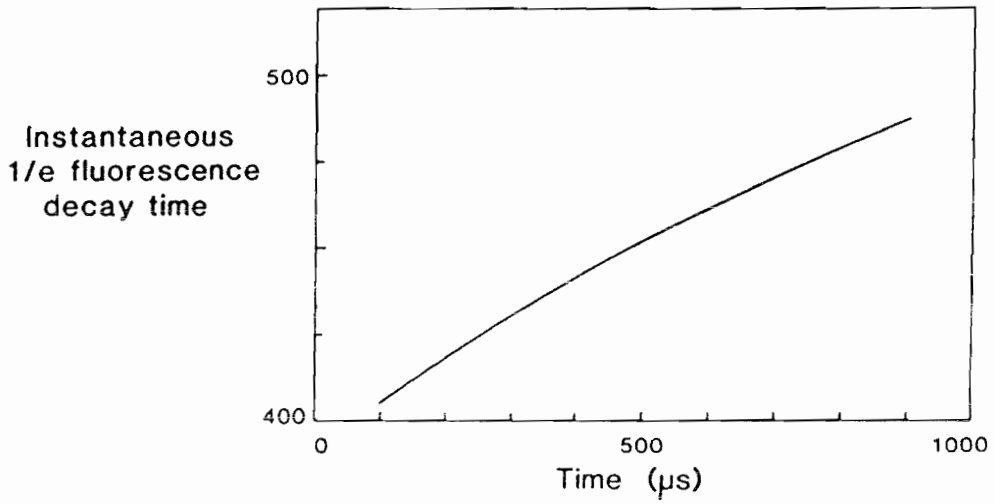

Figure 3.13 Temporal dependence of instantaneous decay rate of neodymium in fused silica.

A reasonable form for a(f) is given by

$$a(f) = \tau \left[1 + 4\alpha \frac{(f-\nu_o)^2}{\Delta\nu^2_{IH}} \right]$$

where

ν_o is the line centre frequency

$\Delta\nu_{IH}$ is the inhomogenous broadening

Thus the decay time is τ at the line centre and is greater by a factor of $(1+\alpha)$ at the FWHM points of the Gaussian distribution p(f). The best fit values of τ and α are

$$\tau = 270\mu s \pm 30\mu s$$
$$\alpha = 1.05 \pm 0.05$$

The results indicate a considerable variation in the decay time constant for ions in different sites in the SiO_2-GeO_2 matrix (a factor of 2 over the full width of the distribution). Although a previous study has indicated the presence of a fast (4μs) and a slow (450μs) decay process[7], to the author's knowledge this is the first analysis of the non-exponential decay in silica. The results have an important bearing on the analysis of rare-earth glass lasers, since the fluorescence lifetime cannot be taken to be a constant of the material. In equation (2.20), for example, the dependence of T_{32} on f should be included in the integration.

3.2.3.2 Measurement of fluorescence decay in Er^{3+}-doped fibres

The fluorescence lifetime of Er^{3+}-ions is 30 times greater than that of Nd^{3+}-ions. For this reason the decay rate was determined by a different measurement technique.

Light from the DCM dye laser at 665nm was chopped at a low frequency (typically 10Hz), the measured rise time of the chopped beam being less than 100μs (i.e. ~ 1% T_{21}). The pump was launched into a short length of Er^{3+}-doped fibre (10cm ND263, 120μm diameter) and the maximum gain in the fibre was estimated to be less than 2%. Because of the small fluorescence signal, no attempt to filter the output was made, and the results therefore represent an average over the fluorescence spectrum. The detector was an InGaAs p.i.n. diode and the fluorescence signal was stored on a digitising oscilloscope.

The fluorescence trace is shown in Figure 3.14. The 1/e decay time is 12.0 (± 0.2)ms. An analysis of the decay rate similar to that described in the previous section yielded values of

$$\tau = 6.4\text{ms}$$
$$\alpha = 1.3$$

The broadening factor α is close to the value for Nd^{3+} ions, indicating a similar variation in decay time across the inhomogenous profile. The delay between the pump and fluorescence was measurement-limited at less than 100μs. Further measurements by M.E. Fermann indicate that the delay between the upper pump level and the metastable level is ~10μs (i.e. $\ll$ 1% T_{21}). Thus the assumption of Section 2.2 is well-justified.

3.3 Excited-State Absorption Measurements

The absorption spectra of the rare-earth ions in glass consist of broad bands, typically 30nm wide. The spectra arise because of absorptive transitions from the ground-state, and have been well characterised in a variety of host glasses. In doped glass lasers or amplifiers a significant portion of the ionic population is excited to the metastable level. Additional

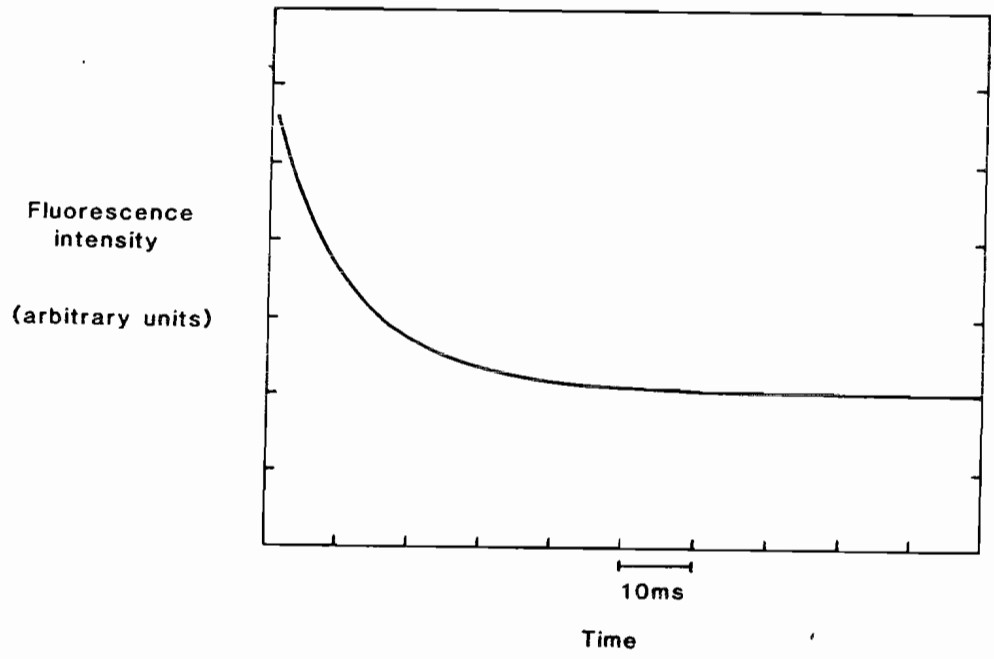

Figure 3.14 Fluorescence decay of erbium in fused silica.

absorptions from this level can degrade laser performance if there is a significant overlap with the pumping or lasing transition[15].

One of the reasons that neodymium-based lasers have been studied so extensively is that the Nd^{3+} ion is relatively free from troublesome excited-state absorptions, particularly for the $^4F_{3/2}$ - $^4I_{11/2}$ and $^4F_{3/2}$ - $^4I_{9/2}$ transitions. There is evidence, however, for excited-state absorption on the $^4F_{3/2}$ - $^4I_{13/2}$ transition[16], in the region of 1.32μm, and this is one of the contributory reasons that lasing has not yet been observed at this wavelength.

In four-level lasers, the fraction of the ground state excited to the metastable level is small, and the effect of additional absorption at the pump wavelength is negligible. This is not the case for three-level lasers, and excited state absorption of the pump radiation is an important consideration for the operation of Er^{3+}-doped fibre lasers.

3.3.1 Excited-state absorption at 1.3μm in Nd^{3+}-doped fibres

The experimental configuration for the measurement of excited-state absorption in Nd^{3+}-doped fibres is shown in Figure 3.15. The white-light source, computer-controlled double monochromator, and cooled germanium detector were the same as for the absorption measurements in Section 3.2. Light from an air-cooled Ar^+-ion laser was launched in the reverse direction via a polarising beamsplitter. It was found that fluorescence at 900nm and 1.08μm was sufficient to saturate the detector, and so a further filter with a 50% pass band above 1300nm was inserted in the output beam. The analysing signal from the monochromator was chopped at approximately 70Hz (higher chopper rates are not possible because of the slow response of the detector) and the signal analysed using an

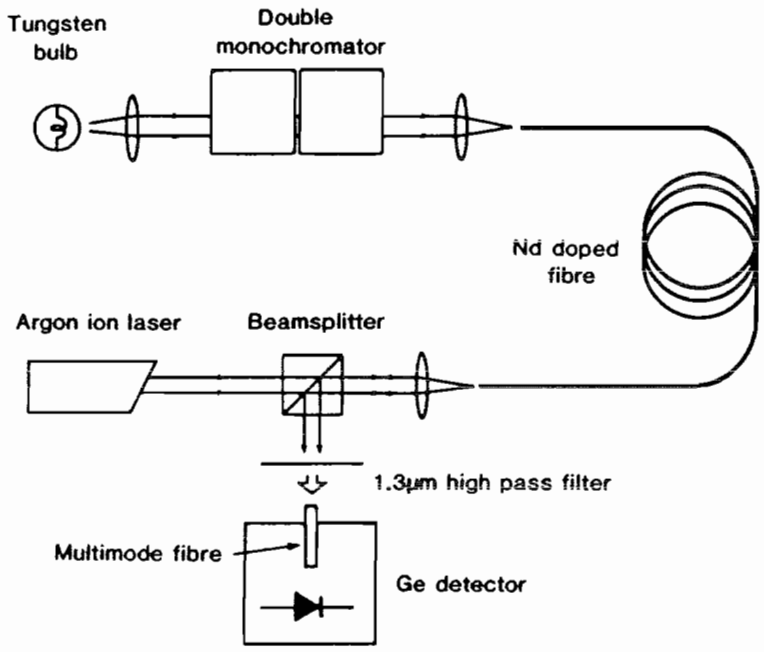

Figure 3.15 Measurement of excited-state absorption of neodymium in fused silica in the wavelength region of 1.3um.

EG & G lock-in amplifier, with a 3s time constant. In spite of the long time constant, the accuracy of the measurement was limited to ± 5%.

The signal was measured with, and without, the argon laser. A small reduction in signal (~ 10%) was observed at 1.32μm, compared to a small gain (~ 10%) at 1.37μm.

The launched power from the laser was 12.2mW and these values therefore correspond, respectively, to absorption and emission cross-sections of $8(\pm 4) \times 10^{-26} m^2$. At 1.37μm the cross-section is a factor of 25 smaller than at 1.08μm, in reasonable agreement with the ratio of the measured fluorescence amplitudes given in Section 3.2. The excited-state absorption at 1.32μm eliminates the possibility of lasing in the silica-based fibre. Laser action should be possible at 1.37μm, however, if feedback at 900nm and 1.1μm can be suppressed.

In view of the experimental uncertainty of these measurements an improved configuration consisting of a Rh6G dye laser as the pump source, and a monochromator following the fibre is now under investigation at Southampton.

3.3.2 Excited-state pump absorption in Er^{3+}-doped fibres

The erbium ion has ground-state absorption bands at 520nm, 650nm, 800nm and 980nm, all of which can pump the ion to the metastable $^4I_{13/2}$ level. In order to pump the ion efficiently a number of conditions must be fulfilled. Thus the band must be accessible to commonly-available lasers (this rules out 980nm); the absorption must be sufficiently strong to require only a small value of the threshold power (equation (2.46) of Chapter 2); and the absorption from the metastable $^4I_{13/2}$ level at the pump wavelength must be smaller than the ground-state absorption.

The pump source in the original experiments on Er^{3+}-doped fibres was an argon ion laser operating at 514.4nm, for which the absorption cross-section has been measured to be $1.4(\pm 0.2) \times 10^{-25} m^2$ (see Table 3.2). Although the value agrees well with the measured threshold of low-loss laser cavities, gain measurements at high powers (see Chapter 5) indicate much lower gains than would be expected from theory. Normally, in a three-level system, the absorption of the pump is expected to decrease as the ground-state is depleted. Measurement of the fibre attenuation by a series of cut-back measurements at high pump powers should reveal any residual absorption. The relative populations in the excited, and ground, levels can be estimated from the ratio of the pump power P to the saturation power P_s ($\simeq$ the threshold power for a low-loss cavity) and also from gain measurements; it is relatively easy to achieve a ratio $P/P_s = 10 \simeq 50mW$ throughout the fibre length so that absorption from the metastable level predominates.

Measurements on fibre ND263 indicated an excited-state cross-section at 514.5nm of $1.6 (\pm 0.2) \times 10^{25} m^2$, which is greater than the ground-state cross-section, i.e. the attenuation was observed to increase slightly as the pump power was increased. It is evident that 514.5nm is not an ideal pump wavelength. The excited-state absorption severely restricts the use of an Ar^+-ion laser as a pump for Er^{3+}-doped fibre amplifiers or more lossy laser cavities. The pump band most closely characterised is the $^4I_{15/2} - {}^4I_{7/2}$ transition at 650nm, and is the band used for the majority of the Er^{3+}-doped devices described here.

The full wavelength range of the absorption, 640nm-680nm, is easily spanned by a DCM dye laser. When the laser excites the short-wavelength side of the absorption, a striking green fluorescence is observed. The fluorescence is believed to result from the $^4S_{3/2} - {}^4I_{15/2}$

transition responsible for the 520nm absorption band, but appears to be shifted to ~540nm, because of self-absorption. The frequency up-conversion is the basis of a number of the commerial infra-red detectors, and is usually accounted for by a two-step resonant transfer of energy from adjacent ions . The low dopant concentration here rules out such effects (see Chapter 2) and the most probable cause is an excited-state pump absorption from the metastable $^4I_{15/2}$ level to above the $^4S_{3/2}$ level.

As discussed in the previous section, the excited state absorption is accompanied by a change in the fibre absorption. It was noted in Section 3.2 that the time taken to populate the metastable level for typical pumping conditions is of the order of 10μs. Thus it is relatively easy to monitor the change in absorption by observing the distortion of a pump pulse of duration greater than 10μs. Two typical pulses at 648nm and 665nm respectively are shown in Figure 3.16. For the first, the throughput power is seen to decrease as the metastable level is populated (the metastable population is indicated by the amplitude of the fluorescence). At this wavelength the excited-state absorption cross-section is evidently larger than the ground-state absorption. The behaviour at 665nm is much closer to the ideal theoretical response, with the throughput power increasing as the ground-state is depleted.

In order to quantify these effects the attenuation was measured at different wavelengths for pump powers well into the saturation regime (~100mW). At this pumping level, see Chapter 5, the gain of the fibre at 1.5μm tends towards the value of the unpumped absorption i.e. it is possible to achieve an almost complete inversion. Residual absorption from the ground-state was estimated to be less than 10% of its unpumped level.

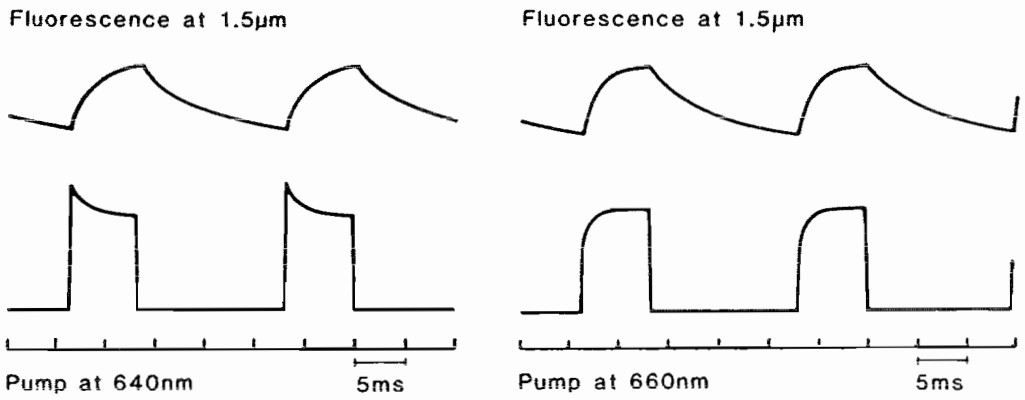

Figure 3.16 Excited-state pump absorption of erbium in fused silica.

The dependence of the excited-state cross-section and ground-state cross-section on pump wavelength is shown in Figure 3.17. Although measurements of excited state absorption in Er^{3+} ions have been made previously[17], the values here are almost certainly the most accurate because of the ease with which it is possible to saturate the absorption in a single-mode fibre.

The $^4I_{15/2}$ - $^4I_{9/2}$ pump absorption at 805nm suffers from two disadvantages. The first is that the absorption cross-section is approximately four times smaller than for the 650nm band. Thus the launched pump power required, even for low-loss cavities, is of the order of 30mW, which rules out laser-diode pumping. The second problem is that there is a further excited-state absorption from the metastable level (resulting in green fluorescence). This has yet to be characterised, but is anticipated to be at least as strong as in the 650nm band.

It should be noted that the one absorption band expected to be free of excited-state absorption is the $^4I_{15/2}$ - $^4I_{11/2}$ transition at 980nm, since the $^4S_{3/2}$ level is not accessible at this wavelength from the metastable level. Bulk-glass erbium lasers have been pumped indirectly at 980nm by resonant transfer from Yb^{3+} ions. The Yb^{3+} ion itself can be pumped at 1.06μm by a YAG laser[19]. It is hoped that by co-doping Er^{3+}-fibre lasers with Yb^{3+} ions a similar pumping scheme might be realised, possibly incorporating a diode-pumped Nd^{3+}-fibre laser.

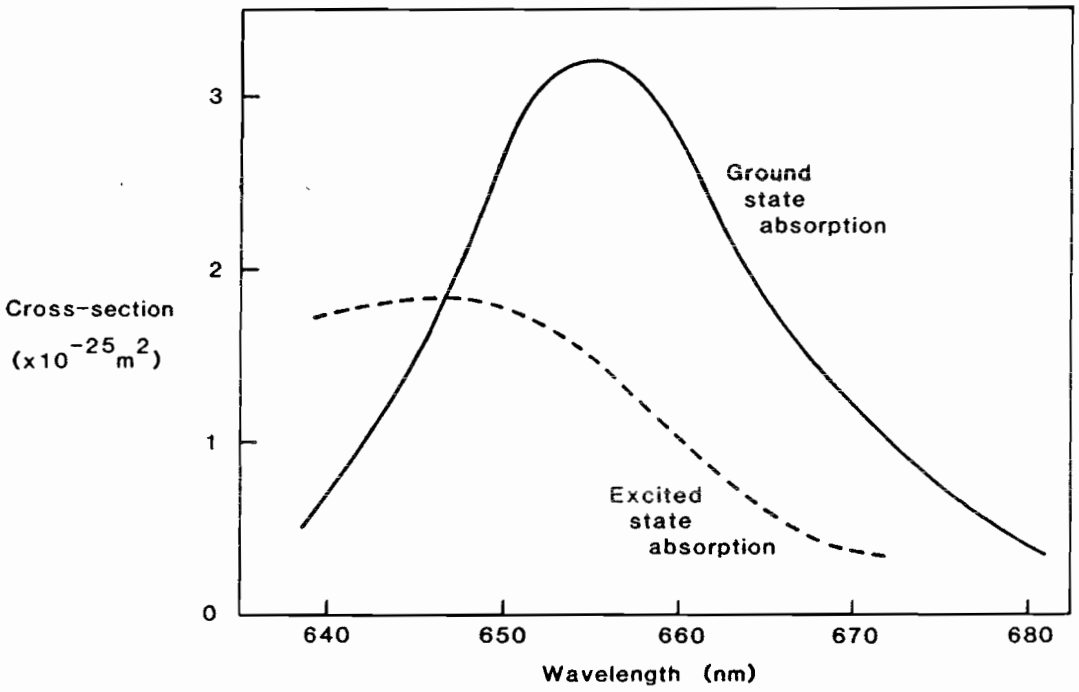

Figure 3.17 Excited-state and ground-state absorption cross-sections of erbium ions in the region of 650 nm.

APPENDIX 3A : CROSS-SECTIONS AND ABSORPTION MEASUREMENTS

Theoretical modelling of fibre lasers and amplifiers demands a detailed knowledge of both the emission, and absorption, cross-sections of the rare-earth dopants as a function of wavelength. They can be calculated from absorption and fluorescence measurements on the doped fibres provided the dopant concentration and distribution is known.

Throughout the work described here it is assumed that the dopant concentration is uniform over the fibre core cross-section so that equation (2.6) can be written as

$$\frac{dP(\nu)}{dz} = P(\nu) n_{TOT} \sigma(\nu) \int_{core} \hat{S} dA \qquad (3A.1)$$

where $\int_{core} \hat{S} dA \rightarrow 1$ for large V

The dopant concentration has been calculated by comparison of the fibre absorption with the absorption of bulk-doped silica of previously-determined composition[7]. The absorption cross-sections depend on glass composition but were assumed to be the same for the core glass (90% SiO_2; 10% GeO_2) and the reference (SiO_2). The emission cross-section can be calculated from integration of the fluorescence spectrum and from the average decay lifetime $t_{1/e}$. It follows from equation (2.16) that

$$\sigma_{peak} = \frac{\lambda^4}{8\pi \Delta\lambda_{eff} n^2 c t_{spont}} \qquad (3A.2)$$

The effective linewidth $\Delta\lambda_{eff}$ is calculated by integrating the fluorescence over the laser transition and dividing by the peak value. In Nd^{3+} ions, the spontaneous lifetime t_{spont} is twice the measured lifetime, since the fluore-

scence is divided into two approximately equal decays to the $^4I_{11/2}$ and $^4I_{9/2}$ levels. Taking t_{spont} = 900μs and $\Delta\lambda_{eff}$ = 64nm, the stimulated cross-section is calculated to be 1.5 x $10^{-24}m^2$. This value is identical to that quoted for silicate glass in Reisfeld and Jorgensen[20], although slightly less than the value calculated by Jacobs and Weber[6] (1.9 x $10^{-24}m^2$).

The calculated dopant concentration, and other important parameters, for the doped fibres studied in the laser and amplifier work are given in Table 3.1. The fibres have comparable numerical apertures and core dimensions so that the variations in performance are due solely to the differences in the rare-earth ions. Values for the absorption and emission cross-sections at various wavelengths are provided in Table 3.2.

Table 3.1

Parameters of fibres used in laser and amplifier experiments

Fibre No.	Dopant	Approximate Concentration	NA	Fibre diameter	Cut-off wavelength
ND199	Nd^{3+}	100ppm	0.21	110μm	950nm
ND263	Er^{3+}	350ppm	0.21	90μm	1050nm
ND263	Er^{3+}	350ppm	0.21	120μm	1100nm (resleeved)
ND281	undoped	-	0.21	105μm	950nm
ND281	undoped	-	0.21	125μm	1100nm (resleeved)

Table 3.2

Nd^{3+} and Er^{3+} Cross-sections at Selected Wavelengths

Neodymium

Wavelength (nm)	585	825	904	1088
Cross-section ($x10^{-24} m^2$)	6.2	0.8	1.0	1.5

Erbium*

Wavelength (nm)	514.5	650	1536	1552
Cross-section (m^2) ($x10^{-25} m^2$)	1.6	3.2	6.5	3.8

* Calculated from absorption and fluorescence data with reference to the peak cross-section at 1.536μm[19].

References Chapter 3

1. D.N. Payne and W.A. Gambling:
"New silica-based low-loss optical fibre",
Electron. Lett., 1974, 10, pp. 289-290.

2. J.B. MacChesney, P.B. O'Connor and H.M. Presby:
"A new technique for the preparation of low-loss and graded index optical fibres",
Proc. IEEE, 1974, 62, pp. 1280-1281.

3. D.B. Keck, P.C. Schultz, F. Zimmer:
US Patent No. 3,373,292, 1975.

4. J. Stone and C.A. Burrus:
"Neodymium-doped silica lasers in end-pumped fiber geometry",
Appl. Phys. Lett., 1973, 23, pp. 388-389.

5. E.I. Galant, Y.N. Kondrat'ev, A.K. Przhevuskii, M.N. Tolstoi and V.N. Shapovalov:
"Stimulated emission of neodymium ions in quartz glass",
JETP Lett., 1974, 18, pp. 372-373.

6. R.R. Jacobs and M.J. Weber:
"Dependence of the $^4F_{3/2}$ - $^4I_{11/2}$ induced emission cross-section for Nd^{3+} on glass composition",
IEEE J. Quant. Electron., 1976, QE-12,
pp. 102-111.

7. H. Namikawa, K. Arai, K. Kumata, Y. Ishii and H. Tanaka:
"Preparation of Nd-doped SiO_2 glass by plasma torch CVD,
Jap. J. Appl. Phys., 1982, 21, pp. 360-362.

8. S.B. Poole, D.N. Payne and M.E. Fermann:
"Fabrication of low-loss optical fibres containing rare-earth ions",
Electron. Lett., 1985, 21, pp. 737-738.

9. J.E. Townsend, S.B. Poole and D.N. Payne:
"Solution-doping technique for fabrication of rare-earth-doped optical fibres",
Electron. Lett., 1987, 23, pp. 329-331.

10. S.B. Poole:
Minithesis,
University of Southampton, 1985.

11. J.M. Pellegrino, W.M. Yen and M.J. Weber:
"Composition dependence of Nd^{3+}-homogenous linewidths in glasses",
J. Appl. Phys., 1980, 51, pp. 6332-6336.

12. T. Kushida:
"Energy transfer and cooperative optical transitions in rare-earth-doped inorganic materials",
J. Phys. Soc. Japan, 1973, 34, pp. 1318-1337.

13. E. Snitzer and C.G. Young:
"Glass Lasers",
Advances in Lasers, Vol. 2, A. Levine Ed.,
New York : Dekker, 1968, pp. 191-256.

14. K. Patek:
"Glass Lasers",
London Iliffe ISBN 0592 02778 3.

15. C.G. Young:
"Glass Lasers",
Proc. IEEE, 1969, 57, pp. 1267-1289.

16. I.P. Alcock:
Private communication.

17. C.C. Robinson:
"Excited state absorption in fluorescent uranium, erbium and copper-tin glasses",
Journal of the Optical Society of America, 1967, 57, pp. 4-7.

18. E. Snitzer and R. Woodcock:
"Yb^{3+}-Er^{3+} glass laser",
Appl. Phys. Lett., 1965, 6, pp. 45-46.

19. V.P. Gapontsev, S.M. Matitsin, A.A. Isineev and V.B. Kravchenko:
"Erbium glass lasers and their applications",
Optics and Laser Technology, 1982, pp. 189-196.

20. R. Reisfeld and C.K. Jorgensen:
"Lasers and Excited States of Rare Earths",
Springer-Verlag ISBN 3-540-08324-3.

CHAPTER 4 : OPTICAL FIBRE LASERS : CW OPERATION AND SPECTRAL CHARACTERISTICS

Chapter 2 shows that the laser threshold is predominantly a function of the active area. By virtue of their small cores, fibre lasers have thresholds which are orders of magnitude less than their bulk counterparts. Thus low-power pump sources, such as GaAs laser diodes, can be used. In addition, and for the first time, efficient CW operation has been achieved for three-level transitions in glass. The variety of wavelengths available for lasers and amplifiers in the fibre configuration is thereby significantly increased.

This chapter describes the CW operation and spectral characteristics of neodymium-doped, and erbium-doped, fibre lasers. The lowest reported thresholds of these lasers have been achieved, and the performance has been optimised for high slope efficiency. The results indicate the validity of the theory developed in Chapter 2, and enable further design to be carried out.

4.1 CW Operation of Fibre Lasers

A large number of rare-earth lasers have been demonstrated, using both crystal and glass hosts[1-10]. Of these, probably the best understood are the Nd:YAG and Nd-glass lasers, which have found widespread experimental and commercial use. Recently there has been considerable interest in waveguide lasers because of their lower thresholds an the increasing availability of low-cost, high-power, diode lasers as potential pump sources[11-14]. The mini-YAG is the most advanced of these, and is now a commercial product.

The single-mode optical fibre laser offers the ultimate in low threshold/high gain operation. This thesis concentrates on two dopants, neodymium and erbium,

as examples of a four-level and a three-level laser. The potential for rare-earth-doped fibre lasers, however, extends far beyond these two ions.

4.1.1 Experimental configuration

The simplest configuration for a fibre laser is a Fabry-Perot resonator formed by butting each end of the doped-fibre to dielectric mirrors, as shown in Figure 4.1. The pump radiation is launched into the fibre through one mirror, which is chosen to have a high transmission T at the pump wavelength, and a high reflectivity R at the laser wavelength. The reflectivity of the second mirror then determines the threshold and output power of the fibre laser. Typically the dielectric input mirror provides a pump transmission greater than 85% and a reflectivity greater than 99% over a 50-100nm band at the laser wavelength. Because the pump laser is focussed through the input mirror onto a small spot (~2μm radius) at the fibre/mirror interface, it is essential that the dielectric coating has a reasonable damage threshold ($> 10MW/cm^2$). In order to prevent damage from mechanical contact, the coatings should be protected by a final SiO_2 layer.

The need to maintain precise alignment of the mirror and fibre end determines a particular launching procedure. The input mirror is first aligned perpendicular to the pump-beam by monitoring the back-reflection. The fibre is cleaved, brought close to the mirror and aligned to the optical system by the usual micromanipulator (Micro-Controle differential x,y,z or Martok leaf-spring x,y,z mounted on a single micrometer stage for z motion). Index-matching fluid is applied to the fibre end, which is then carefully butted to the mirror. Since the fibre is now fixed in position, launching is effected by small movements of a further micromanipulator holding the launch objective.

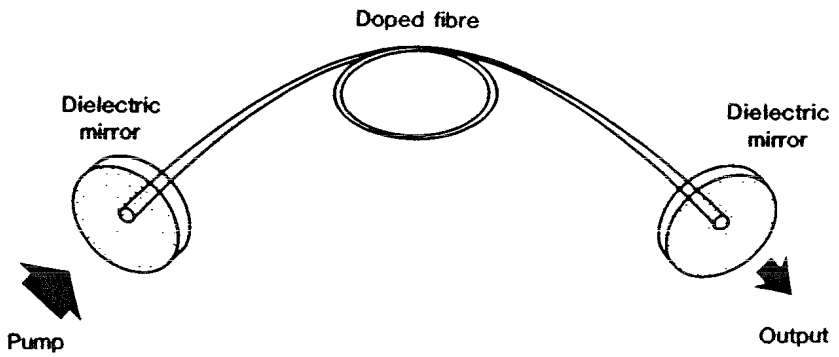

Figure 4.1 Fabry-Perot laser

By maintaining a small positive pressure on the butt joint, the angle the fibre core makes with the mirror is determined by the end-angle produced when the fibre is cleaved. The cavity loss is expected to follow the formula for the splice loss in identical fibres[15]. Whilst the loss is insensitive to changes in the relative displacement of the mirror and fibre, it is critically dependent on the angle between the two. An angle of 1^{o} is sufficient to induce a 2% power loss. Accordingly the fibre was cleaved with a precision fibre cleaver (York C007 or FK-11) to ensure that the fibre end angle was less than 1^{o}.

For the majority of the experimental work it was not necessary to permanently align the laser cavity. In some instances, however, a transportable laser is required. Instead of index-matching fluid, u-v adhesive (Electrolite Corp.) was inserted between the fibre end and the mirror, and once the laser had been aligned, the glue was cured. It was found that further application of epoxy around the fibre was necessary to strengthen the joint. Although this approach is sufficient for brass-boarding fibre lasers, it would be desirable to apply the dielectric coating directly to the fibre end. The majority of commercial dielectric coatings having a high damage threshold require a moderate deposition temperature ($400^{o}C$) which is above the melting point of the acrylate protective coating on the fibre. For this reason, and because of the high cost of coating runs, dielectric coating of fibre ends has not been pursued. It should be noted, however, that a high-temperature protective polyimide coating for optical fibres has been developed (e.g. Dupont "Pyralin"), and that commercial exploitation of the fibre laser would benefit from its use.

Chapter 3 shows that neodymium and erbium ions have a large number of absorption bands in the visible and near infra-red regions of the spectrum. A variety of pump sources have been employed, including a Spectra-Physics

model 2020 argon ion laser (maximum output > 2.5W at 514.5nm) and a Spectra-Physics model 375B dye laser (pumped by the Ar^+-laser). More than 1W output was available at 580nm with Rhodamine 6G dye, and the laser was tunable from 550nm to 620nm. The most efficient pump wavelength for erbium has been 660nm, which was obtained with DCM dye (tunable from 620nm-690nm). Neodymium-glass lasers can also be pumped in the wavelength range 780nm-830nm, permitting the use of GaAlAs laser diodes. A Hitachi HLP 1400 diode operating at 826nm, with a maximum output of 15mW, and a Sharp LT015 emitting at 826nm, with a maximum output of 40mW have successfully pumped fibre lasers. Although the diode wavelength lies in the wings of the $^4I_{9/2}$ - $^4F_{5/2}$ transition, efficient pumping is still possible, and the fibre length can be adjusted to permit complete pump absorption.

Light from the ion and dye lasers was launched into the doped fibre through a single microscope objective (x5, x10 or x20, depending on the spot-size of the fibre) at launch efficiencies of up to 75%. The best launching arrangement with the GaAlAs diode has been to collect the light with a x20 microscope objective, focus and then expand the beam as shown in Figure 4.2, and to launch into the fibre with a x10 objective. A launch efficiency of 30% was achieved, limited by the highly asymmetric spot (3:1) of the laser diode. Recent experiments incorporating an anomorphic prism pair to compensate the asymmetry have increased the launch efficiency to greater than 40%[16].

4.1.2 Neodymium-doped fibre lasers

The neodymium pump band which has been most fully characterised is the $^4I_{9/2}$ - $^4F_{5/2}$ transition at 826nm. The original experiments on low-threshold, and efficient, operation were performed with the Hitachi laser diode.

During this work the more powerful Sharp diode became available, and has resulted in the highest output powers yet attained in diode-pumped fibre lasers.

4.1.2.1 Low threshold operation

An expression for the laser threshold was derived in Chapter 2, and is given by

$$P_{abs} = \frac{A_{eff}}{\eta} \frac{h\nu_p}{\sigma\tau} \left[\alpha\ell - \ln \sqrt{R_1 R_2}(1-L)\right] \quad (4.1)$$

(see Chapter 2 for a definition of the symbols).

The threshold may be minimised by reducing the effective area, A_{eff}, and the cavity losses. The doped fibre studied in the experiments was ND199, 110μm diameter (see Chapter 3). This fibre has a high numerical aperture (0.21) and is operated at a signal V-value of 2.1 (1.09μm). The effective area, calculated to be $1.1 \times 10^{-11} m^2$ (see Figure 2.5), is within 10% of its maximum value. It was found that the launch efficiency into lower V fibres was reduced. The properties of the doped fibre are thus close to optimum for low-threshold, diode-pumped, operation.

The intrinsic loss of the fibre at wavelengths near 1μm is calculated from absorption measurements (see Chapter 3) to be approximately 0.3%/metre. The 1/e absorption length at the pump wavelength is 1.1m, so that for the majority of laser cavities the effect of fibre absorption is small, though not negligible.

The limit set by losses at the fibre/mirror interfaces is determined by setting up a laser cavity with high-reflectivity mirrors. A 70cm length of doped fibre (ND199) was cleaved and butted to mirrors with reflectivities of 99.8% and 99.5% at the laser wavelength of 1.088μm. The experimental arrangement is shown in

Figure 4.2. The output light was filtered by a 1090nm bandpass filter with a FWHM of 10nm, and detected with the InGaAs p.i.n. diode.

Lasing was indicated by a marked increase in the output power. When a small square-wave current modulation was applied to the pumping laser diode decaying relaxation oscillations were clearly observed (Figure 4.3). The semiconductor laser output power was measured on a Coherent power meter and the absorbed pump power was calculated by a multiple cut back technique. The laser threshold corresponded to an absorbed power of 320μW.

No saturation of the fibre laser output was observed at pump powers up to the maximum available. Operation of the laser at a reduced duty cycle gave no further decrease in laser threshold, indicating that thermal effects are negligible. Thus the fibre laser can be operated continuously without auxiliary cooling, unlike conventional neodymium-doped glass lasers.

The cavity loss has been determined by measurement of the natural relaxation frequency of the laser as a function of the pumping rate[17].

The relaxation frequency, ω, is given by

$$\omega^2 = \frac{(r-1)}{t_c \tau} \qquad (4.2)$$

where

$r = P_{abs}/P_{abs_{TH}}$

$t_c = \frac{n\ell}{cG_T}$ = cavity decay time

ℓ = cavity length

$G_T = \alpha\ell - \ln \sqrt{R_1 R_2}(1-L)$, as defined in Chapter 2.

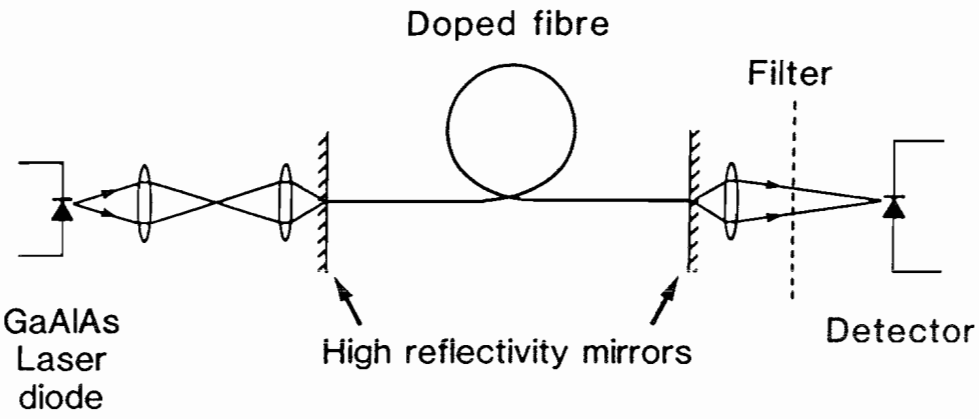

Figure 4.2 Diode-pumped neodymium-doped fibre laser.

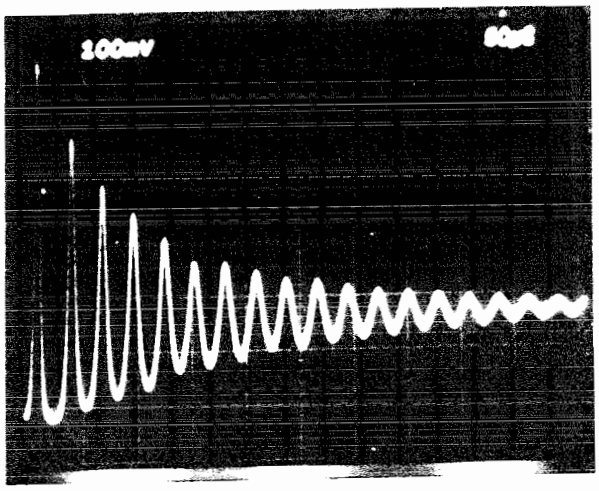

Figure 4.3. Relaxation oscillations of Nd^{3+} doped fibre laser (r=2.7; T_{osc}=28μs)

For the laser cavity described above, the loss was calculated to be 4.5% per mirror interface. Since this value was considered to be unacceptably large, the experiment was repeated a number of times, taking greater care over the end preparation. In particular, the fibre cleaver was optimised for the 110μm diameter fibre, and the ends were inspected with an interference microscope to ensure that the angle was less than 1^{o}. In this way the threshold was reduced to 100μW absorbed, corresponding to a mirror loss of a mere 1%. The lasing characteristic is shown in Figure 4.4. (Note that the cavity length in this case was 2m, so that the fibre absorption and mirror losses contributed an extra 1% to the cavity loss). Although a coherent source at 1.1μm was not available to measure the cavity finesse, it is calculated to be greater than 300. The laser threshold is the lowest reported for a Nd^{3+}-doped glass laser[18].

In order to compare the laser threshold with the theoretical expression of equation (4.1), a series of measurements were made, applying different dielectric mirrors to the output end of the fibre. The value of G_T was determined from the relaxation oscillation period (equation (4.2)). Figure 4.5 shows the variation of absorbed power at threshold for the various values of G_T. According to equation (4.1), the gradient is given by

$$\frac{A_{eff}}{\eta}\,\frac{h\nu_p}{\sigma\tau} = 7.0\text{mW} \qquad (4.3)$$

Substitution of A_{eff} ($1.1 \times 10^{-11}m^2$), $h\nu_p$ ($2.4 \times 10^{-19}J$) and $\sigma\tau$ ($6.8 \times 10^{-28}m^2s$ see Chapter 3), yields a value for the relative quantum efficiency of $\eta \simeq 0.56$. This compares favourably with the measurements of DeShazer and Komai on a barium crown glass (AO 3669), who obtained $\eta = 0.43$ [19]. Later measurements by Krupke on a

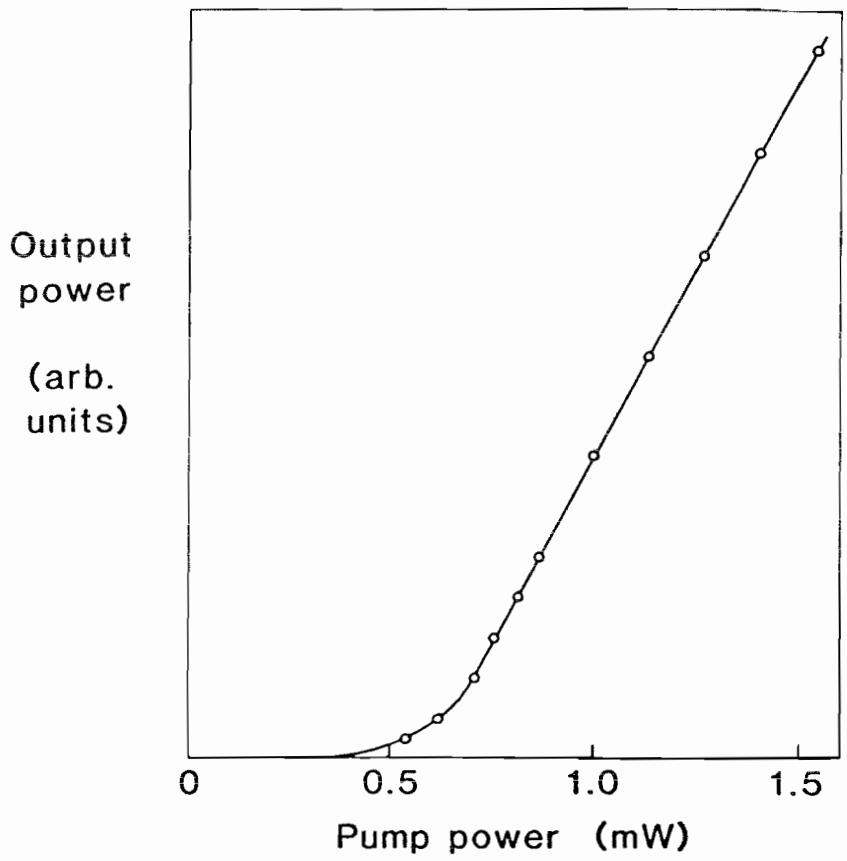

Figure 4.4 Lasing characteristic for low-threshold neodymium-doped fibre laser.

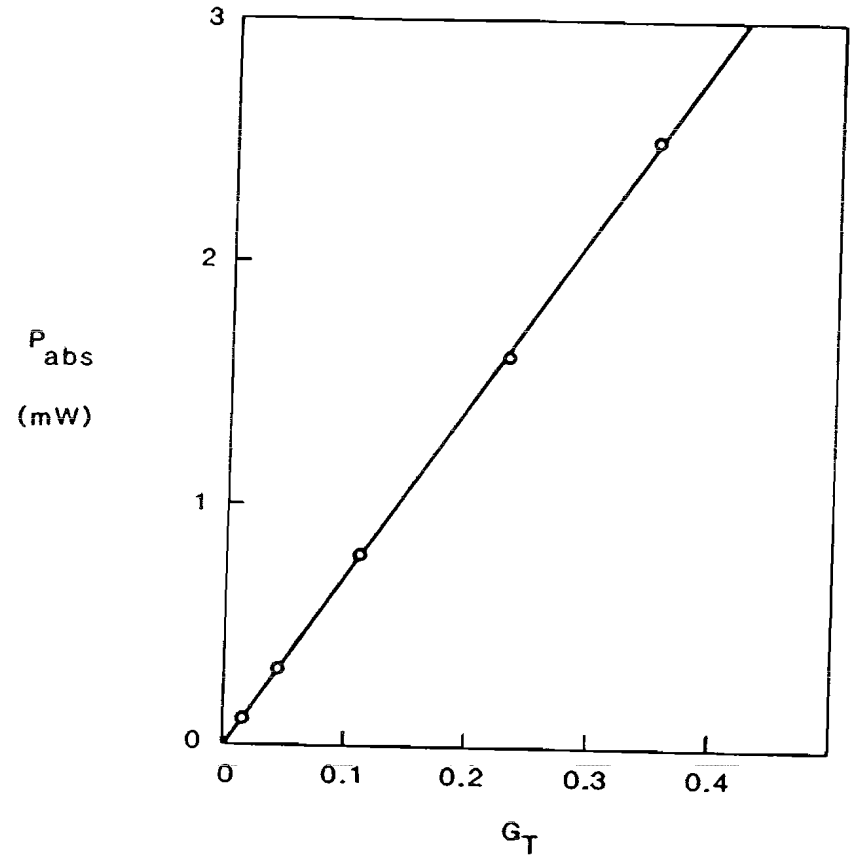

Figure 4.5. Comparison of experimental (o) and theoretical (-) values for the neodymium-doped fibre laser threshold

lithium-silicate glass (ED-2) indicated an efficiency as high as 0.83 [20]. It should be possible, therefore, to improve the efficiency of the neodymium-fibre laser by modifying the core glass composition.

4.1.2.2 Optimisation of output power

Although the high-reflectivity cavity has a low threshold, it also has a low output power (~ 20μW) and the reflectivity must be increased in order to operate the cavity efficiently. Various mirrors with 10%, 20%, 30% and 55% transmission at 1.088μm were therefore applied to the fibre output. The experimental configuration was as described previously, except that the fibre length was increased to 3.5m, giving a total absorption of 97% at the pump wavelength. The best results were obtained for the 55% transmission mirror, and the lasing characteristic is shown in Figure 4.6 [21].

The slope efficiency was measured to be 0.33. If the ratio of pump and laser frequencies, cavity loss and excitation quantum efficiency are taken into account, the factor η_s (the deterioration of the efficiency due to the inhomogonous broadening) is calculated to be 0.8 (±0.1). This is in good agreement with the value calculated in Chapter 2.

The change from the Hitachi laser diode to the Sharp laser diode has permitted pump powers in excess of 15mW to be launched into the doped fibre. The slope efficiency has been observed to increase from 0.33 to 0.40 at high powers[22], indicating that η_s tends towards unity as the laser linewidth broadens, as predicted in Section 2.4. It is evident that fibre lasers can be operated with high efficiency.

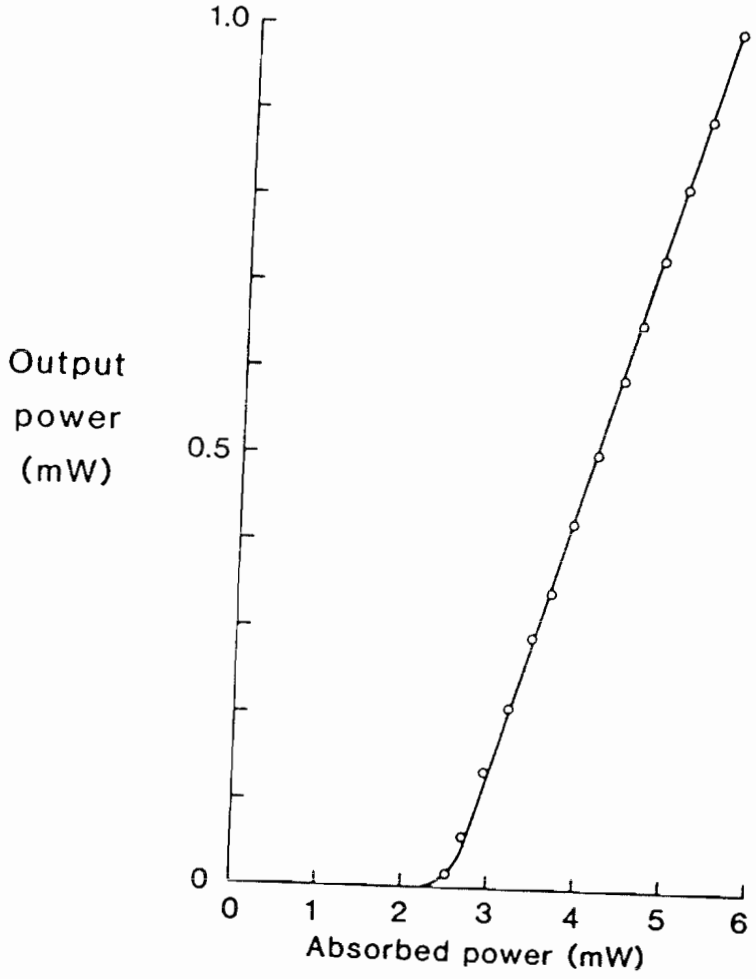

Figure 4.6. Lasing characteristic of efficient diode-pumped neodymium-doped fibre laser

4.1.2.3 Linewidth

The linewidth of the neodymium-doped fibre laser is typically of the order of a few nanometers. As the pump power is increased above threshold, more longitudinal modes reach the oscillation threshold, and the linewidth broadens substantially. The modes compete for gain as a result of the homogenous broadening in the glass, but gain saturation by a single longitudinal mode is prevented by the combined effects of the even larger inhomogenous broadening, and of spatial hole-burning in the standing-wave resonator. (Note that the linewidth is broad even in the travelling-wave ring cavity laser decribed in Chapter 6). The variation of the free-running linewidth with pump rate r, is shown in Figure 4.7. The results are in excellent agreement with the broadening predicted in Chapter 2.

The distribution of the longitudinal modes is extremely sensitive to the frequency dependence of the feedback. This is confirmed by the residual modulation on the output spectrum, which is due to the nominal Fabry-Perot cavity introduced by the collimating objective at the fibre output. The modulation period varied with the focal length of the objectives. By applying resonant end-reflectors, Zürn et al have observed both line-narrowing and line-broadening[23]. Analysis of the laser output with an electrical spectrum analyser (Marconi 2830/2) has revealed a significant, and time-varying, difference in amplitudes of the first five harmonics of the longitudinal mode-spacing. The strong presence of the first harmonic indicates that adjacent modes do oscillate, in spite of the strong competition between them. It should be noted that the mode-spacing is sufficiently small (~ 100MHz) that variations in the modal amplitudes are averaged out in most types of spectral measurement. Techniques to reduce the number of oscillating modes are discussed in Section 4.2.

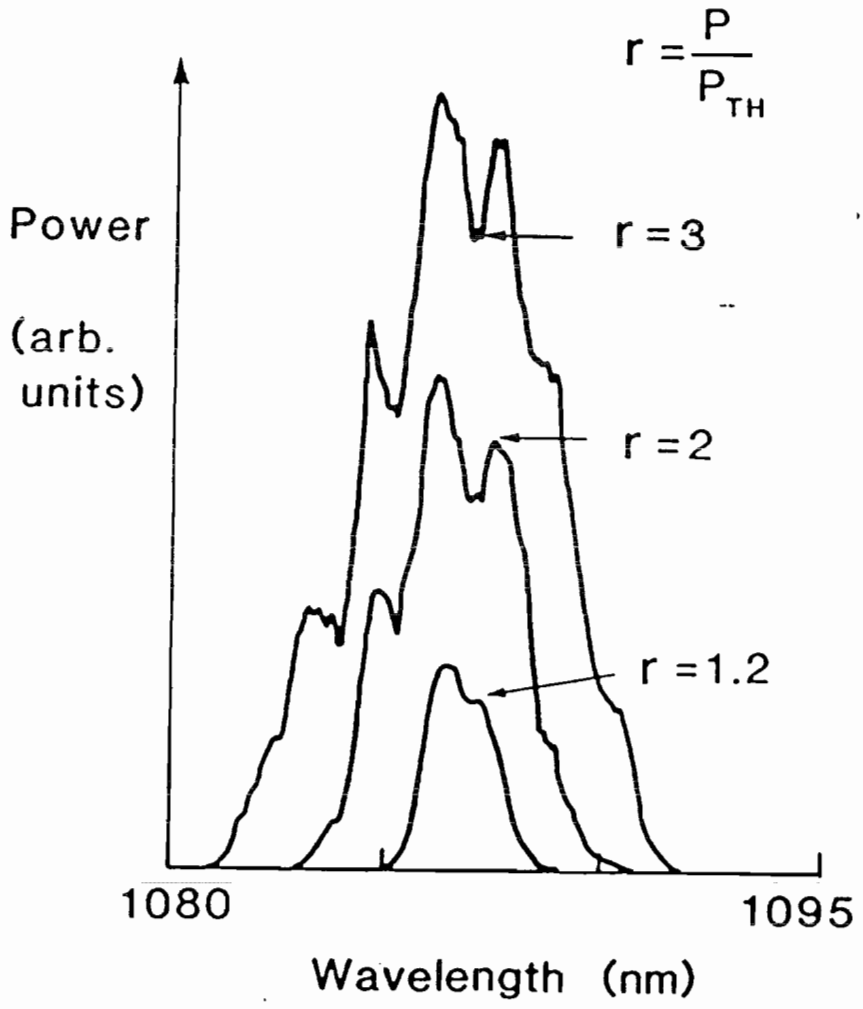

Figure 4.7. Power broadening of neodymium-doped fibre laser linewidth

4.1.2.4 Other pump sources

Although GaAlAs-diode lasers have been employed for the majority of the characterisation of the Nd^{3+}-doped fibre laser, two other pump sources have proved useful in this study; the Ar^{+}-ion laser at 514.5nm, and the Rh6G dye laser in the region of 580nm. The high powers available from these sources have enabled the operation of more lossy cavity configurations, such as those described in section 4.2 (tunable laser) and Chapter 5 (Q-switched laser). Comparison of the laser threshold and cavity loss for the 514nm and 580nm pump wavelengths indicate that the relative quantum efficiency is unchanged from its value for the 826nm pump (η = 0.56). This is consistent with the findings of DeShazer and Komai[19].

4.1.3 Erbium-doped fibre lasers

Erbium-doped fibre lasers are of interest because they operate in the wavelength region of 1.5μm, which coincides with the lowest loss window of silica-based optical fibres. However, the 3-level nature of the 1.5μm transition necessitates a high pump intensity in order to saturate the absorption and achieve a population inversion. The fibre configuration is well suited to low threshold, and efficient opertion of 3-level lasers. For example, the saturation intensity of $1GW/m^2$ required to saturate a typical Er^{3+} absorption (e.g. at 650nm) can be achieved in a single-mode fibre with a pump power of a few milliwatts. This is a practical power for a variety of systems, and makes the Er^{3+}-doped fibre laser an attractive source for 1.5μm operation.

4.1.3.1 Low threshold operation

The pump source for the early experiments on the Er^{3+}-doped fibre laser was the argon ion laser operating at 514.5nm. The reasons for this choice were that plenty of power was available (up to 2.5W for the Spectra Physics

2020 model) and that the wavelength was sufficiently close to the 520nm $^4I_{15/2}$ - $^4S_{3/2}$ transition for there to be an appreciable absorption cross-section. The laser cavity was similar to that of the Nd^{3+}-doped laser. The fibre was butted to two dielectric mirros having 82% and 99% reflectivity at 1.54μm. Because the laser wavelength is an odd harmonic of 514.5nm, multi-layer dielectric reflectors at 1.5μm are usually effective for the pump as well. Whilst this prohibited the placing of the 99% reflectivity mirror at the pump input, the coating of the 82% reflectivity mirror was sufficiently dispersive to permit 77% transmission of the pump. It should be possible to design a dispersive coating combining full reflectivity at 1.54μm with high transmission at 514nm, but attempts to obtain one commercially have not been successful.

The fibre chosen for the experiments was 90μm diameter ND263 (see Table 3.1), which had a core diameter of 3.8μm. After carefully optimising the cavity configuration, the threshold was reduced to a launched power of 5mW (corresponding to 4mW absorbed in the 70cm long fibre). The lasing characteristic is shown in Figure 4.8 . The slope efficiency was only 1%, but measurement of the power from the input end via a 50% beamsplitter indicated that up to 20 times more power was available. The laser was by far the lowest threshold 3-level glass laser demonstrated, and the results indicated that the Er^{3+}-doped fibre laser can be a practical source of 1.5μm radiation[24].

Modelling of the results according to the theory in Chapter 2 is made difficult by the lack of a value for σ in the wings of the $^4I_{15/2}$ - $^4S_{3/2}$ absorption. Assuming that the total ion population contributes to the small signal pump absorption, so that it can be written $\exp(-n_{TOT}\sigma\ell)$, the cross-section σ is evaluated to be 1.6×10^{-25} m^2. With this value, the threshold results indicate a high fluorescence efficiency, $\eta \simeq 0.9$.

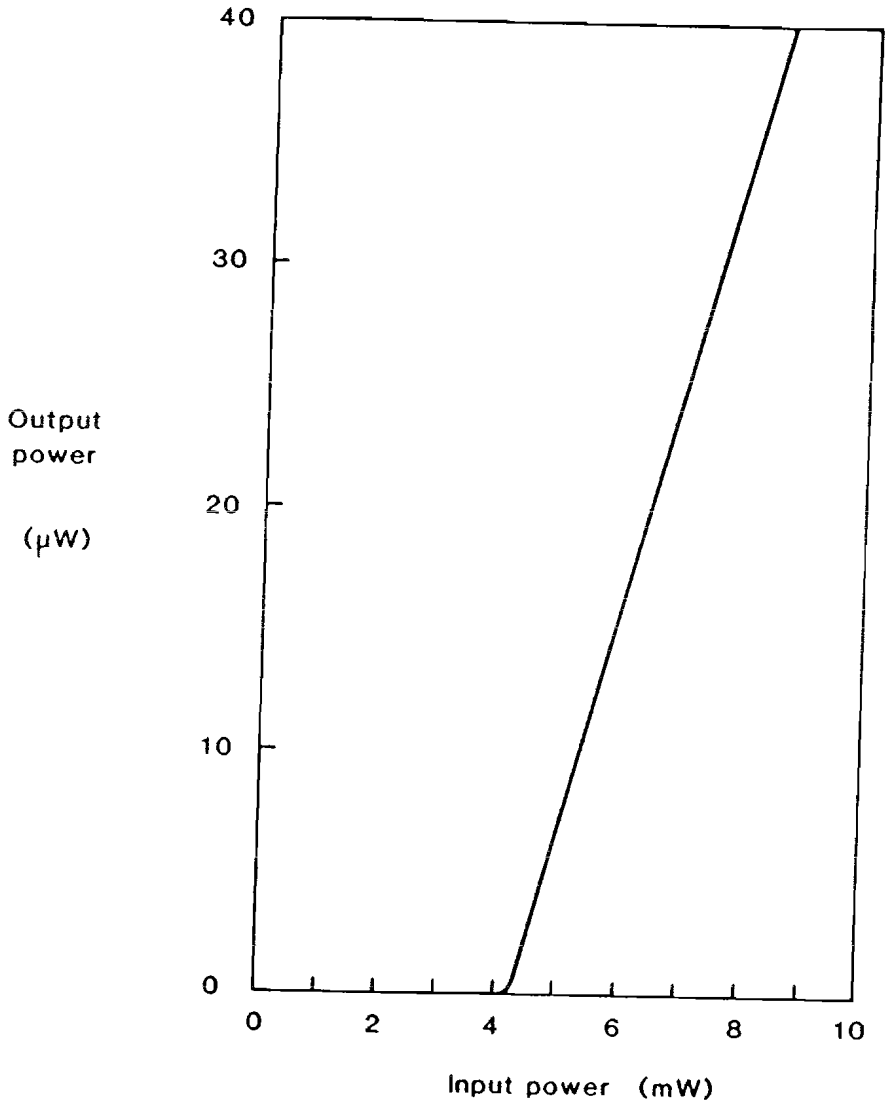

Figure 4.8. Lasing characteristic of low-threshold erbium-doped fibre laser

Further experiments on longer fibre cavities and with higher transmission output couplers indicated a significant discrepancy between the predicted and observed thresholds. For example, well over 1W of power was required to observe lasing in a 3m length of fibre, even though theory suggested a threshold of a few tens of milliwatts. Measurement of the fibre gain at 1.5μm (see Chapter 5) demonstrated that whilst the absorption was rapidly saturated at low power levels, it was difficult to achieve a large inversion. The results were reconciled by recognising the deleterious effect of excited state absorption of the 514.5nm pump (see Chapter 3). This spurred the author to investigate pumping on the $^4I_{15/2}$ - $^4I_{7/2}$ transition in the region of 650nm.

4.1.3.2 Efficient operation at 1.536μm and 1.55μm

When pumped with an Argon ion laser, DCM dye can be tuned over the range 620nm - 690nm, which spans the entire range of the $^4I_{15/2}$ - $^4I_{7/2}$ Er^{3+}-absorption. It is thus well suited to the characterisation of the doped fibre.

Light from the dye laser was launched into the doped fibre (ND263, 120μm diameter) through a dielectric mirror in the usual fashion. The mirror was designed to be a full reflector from 1.5μm - 1.6μm, and had a transmission of 85% for the pump. The doped fibre had a V-value of 4 at the pump wavelength, and could therefore support a number of modes. Nevertheless, a launch efficiency of 68% into the fundamental mode was obtained by careful adjustment of the launch objective.

In Chapter 3 it was noted that the fluorescence spectrum of Er^{3+}-ions in silica has two pronounced peaks at 1.536μm and 1.553μm. The maximum gain is observed at the shorter of the two wavelengths and can be as high as

28dB [25] (Chapter 5). The high gain makes possible efficient laser operation with feedback from Fresnel reflection (4%) at the output end of the fibre.

The slope efficiency and threshold were measured as the length of the fibre cavity was reduced from 3m to 0.7m. The variation of the threshold with length is shown in Figure 4.9. In sharp contrast to the argon-ion laser results, the threshold for the 3m fibre is less than 30mW. This value reduced to 11mW for the 1.3m cavity. The slope efficiency increases as the length is reduced, reaching a maximum value of 18% when the threshold is minimised. The laser characteristic for this length is given in Figure 4.10. The maximum output power obtained at 1.536μm was in excess of 25mW.

For certain applications it may be desirable to operate the Er^{3+}-doped fibre laser on the second line at 1.552μm, and suitable techniques involving bulk or fibre gratings are discussed later in the chapter. Operation at 1.552μm is also possible with a wavelength-selective dielectric mirror.

The mirror chosen had a reflectivity of 65% at 1.552μm, compared to 50% at 1.536μm. This difference was sufficient to switch the laser operation from one line to the other. For low-loss cavities, the three-level nature of the transition also favours 1.552μm operation, since the ratio of the gain to the absorption is higher (only the lower levels of the ground state are thermally populated, which shifts the absorption spectrum to shorter wavelengths relative to the fluorescence spectrum).

The variation of threshold power with cavity length is given in Figure 4.11. The minimum absorbed power is less than 4mW. Although the maximum slope efficiency was observed to be reduced to 10%, a useful 17mW of CW output at 1.552μm was obtained.

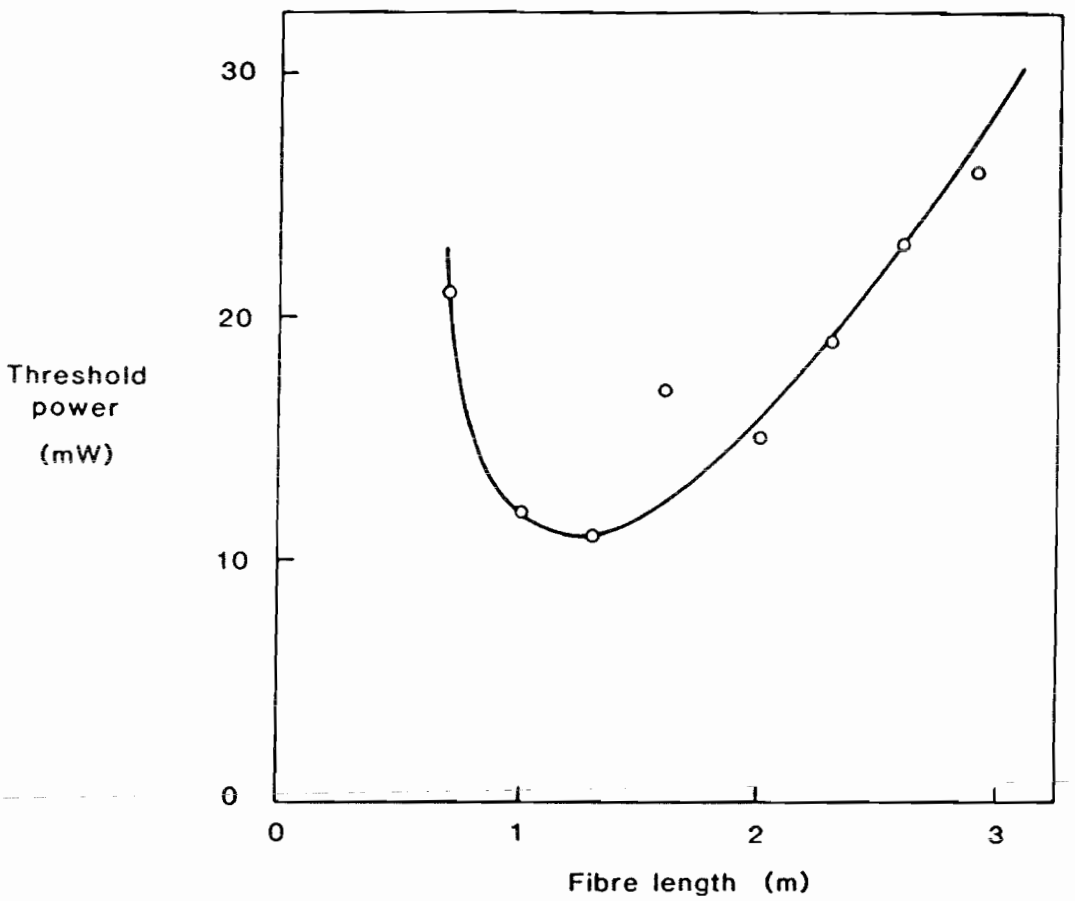

Figure 4.9. Length dependence for the threshold of the efficient erbium-doped fibre laser

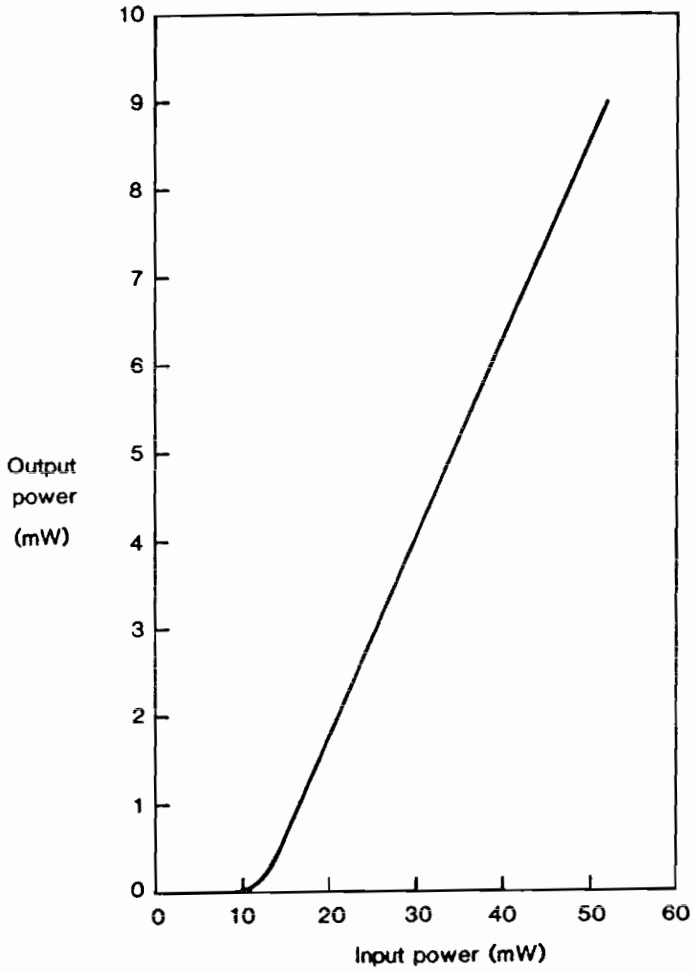

Figure 4.10. Lasing characteristic of efficient erbium-doped fibre laser

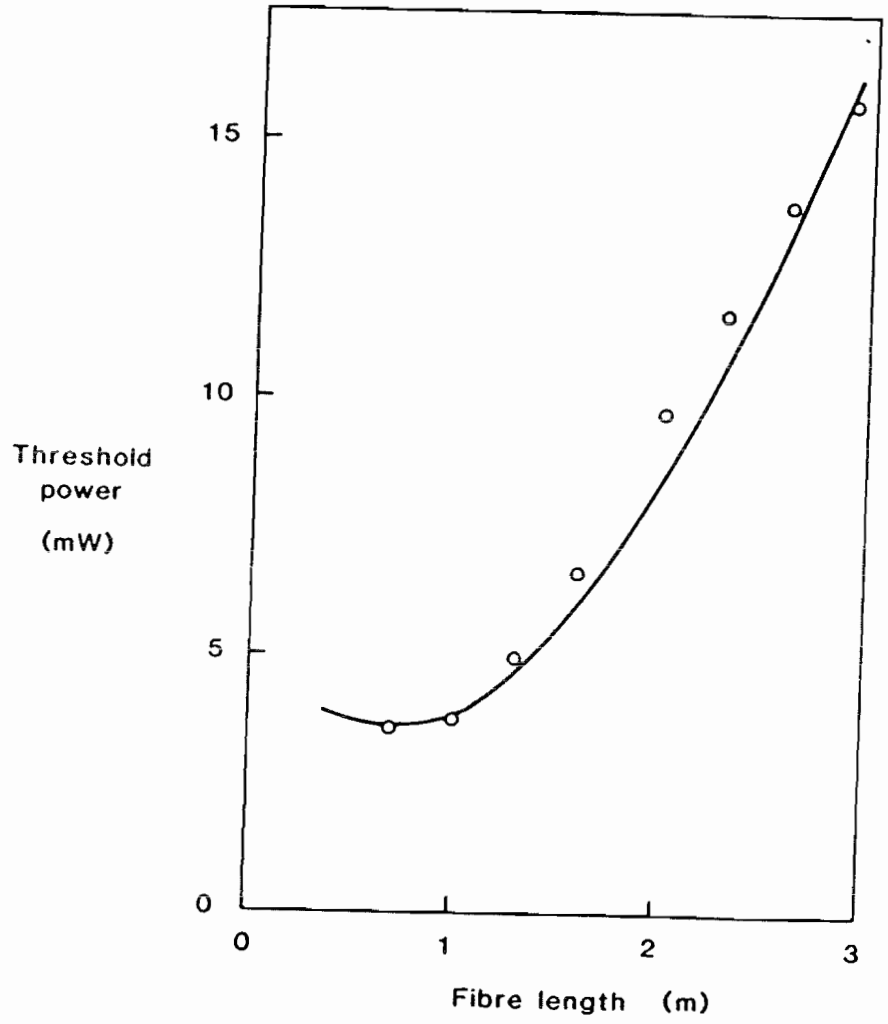

Figure 4.11. Length dependence for the threshold of the 1.55um erbium-doped fibre laser

4.1.3.3 Linewidth

The lindwidth of the erbium-doped fibre laser is observed to broaden as the pump power is increased, but the broadening is less pronounced than for the neodymium laser. The variation of linewidth with pump power is given in Figure 4.12. It can be seen that the linewidth is typically of the order of 2nm. The relatively small value of the power-dependent broadening suggests that effective homogenous linewidth resulting from the many transitions between the Stark multiplets is much larger than the inhomogenous broadening (i.e. the gain depletes uniformly).

4.2 Tunable and Line-Narrowed Fibre Lasers

As a result of the various broadening mechanisms in glass, the fluorescence spectra of rare-earth-doped fibres typically extend over some tens of nanometres. This is in marked contrast to the situation in crystal hosts, where the absorption and fluorescence lines have widths of only a few nanometres or less[2,3]. Narrow linewidths are desirable for single-line operation, since the gain cross-section varies inversely with the fluorescence bandwidth.

For many years the high-thresholds associated with glass lasers have hindered their efficient operation. The single-mode fibre laser configuration offers the opportunity to design efficient, low-threshold cavities. The broad linewidth can be be exploited to facilitate tunable operation. Because of the wide variety of ions that can be made to lase in glass, it is possible that a tunable fibre laser may replace the dye laser for certain applications in the infra-red.

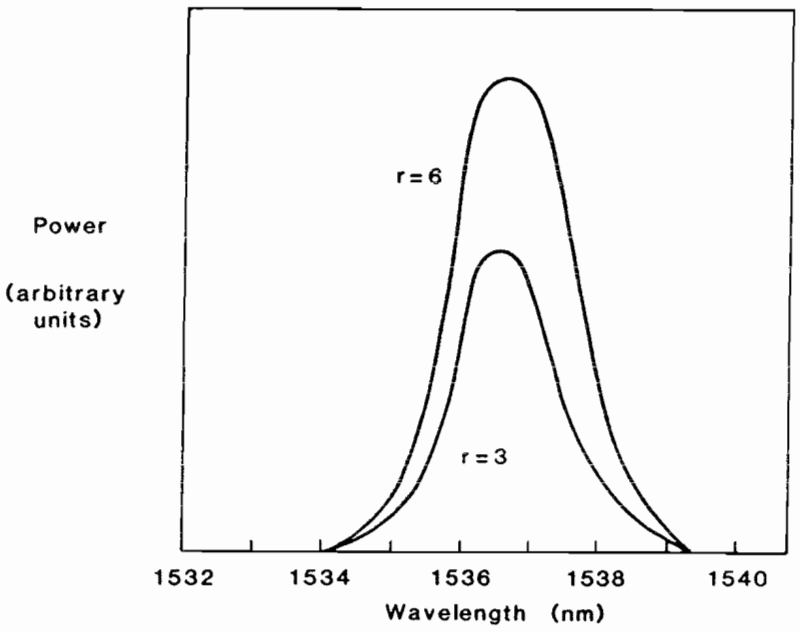

Figure 4.12. Power broadening of the erbium-doped fibre laser linewidth

The fibre laser linewidth is normally a few nanometres, permitting many longitudinal modes to oscillate. The incorporation into the cavity of a wavelength selective element, such as a grating, restricts the linewidth considerably. Bulk gratings and distributed fibre gratings have both been used to achieve line-narrowing.

4.2.1 Tunable operation

Limited tunaility of a Nd^{3+}-doped glass laser with a resonant end reflector was first demonstrated by Snitzer[26]. The technique was extended by Magnante, who replaced one of the end reflectors with a diffraction grating and observed a 30nm tuning range[27]. It is known that the fluorescence linewidth of neodymium in fused silica is considerably broader than in commercial silicate or phosphate laser glasses[28]. The silica fibre laser is thus well suited to tunable operation. The tuning ranges for Nd^{3+}- and Er^{3+}-ions reported here are the broadest recorded for a glass laser[29,30].

4.2.1.1 Experimental configuration

In order to introduce wavelength-selective elements into the fibre cavity, one of the mirrors must be separated from the end of the fibre. A typical experimental configuration for the tunable laser is given in Figure 4.13. The dielectric mirror at the fibre input was effective over a 100nm bandwidth, which exceeds the laser tuning range. At the fibre output, light was collimated by a low-power lens or objective onto a diffraction grating. The loss introduced by the intra-cavity objective was measured to be 1.2 (± 0.2)dB at both 1μm and 1.5μm. Although it would be preferable for the intra-cavity optical components to be anti-reflection coated at each laser wavelength, this was deemed to be unnecessary for the initial demonstration of a tunable fibre laser. The tuning element in the wavelength range 900nm to 1150nm was a holographically ruled grating (600

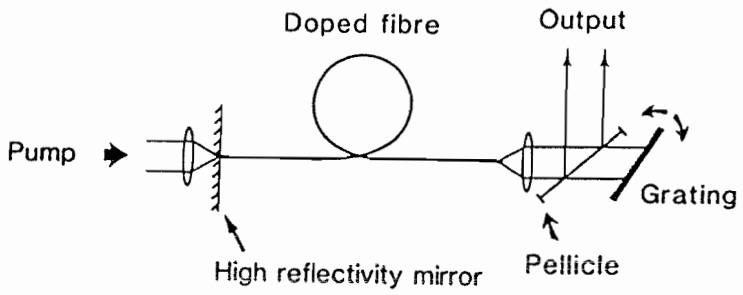

Figure 4.13. Experimental configuration for tunable fibre laser

lines/mm) with a blaze wavelength of 1μm. The Er^{3+}-doped fibre laser was tuned with a similar grating blazed at a wavelength of 1.6μm. The grating was mounted on a sine-bar driven turntable and tuning was accomplished by changing its angle to the incident light. Output coupling was via an intra-cavity pellicle.

4.2.1.2 Neodymium-doped laser

Initial experiments were performed with an argon ion laser source at an input pump power of 125mW, corresponding to an absorbed power of 50mW. The laser tuning curve is given in Figure 4.14, together with the fluorescence curve taken from Chapter 3. A full tuning range of 80nm was obtained in the region of 1.08μm, corresponding to the majority of the available gain profile. Over this broad tuning range it is evident that various components of the $^4F_{3/2}$ doublet and $^4I_{11/2}$ multiplet form the upper and terminal levels of the laser transition. Nevertheless, the tuning curve is smooth, as a result of the considerable inhomogenous broadening. The "knee" at 1120nm is mainly due to the large splitting ($\sim 200cm^{-1}$) between the two lowest components of the $^4I_{11/2}$ term. If the input mirror is replaced by one with a high reflectivity at 900nm (low reflectivity, R = 20%, at 1.1μm), the neodymium-doped fibre laser can also be tuned over the $^4F_{3/2}$ - $^4I_{9/2}$ transition, from 904nm to 954nm. For the shorter wavelengths around 900nm, Nd^{3+}-ions behave as a three-level system. Prior to this work, lasing at 900nm in neodymium had only been achieved in glass at reduced temperatures and in pulsed operation. The result illustrates the usefulness of the fibre laser configuration in permitting the CW operation of three level transitions.

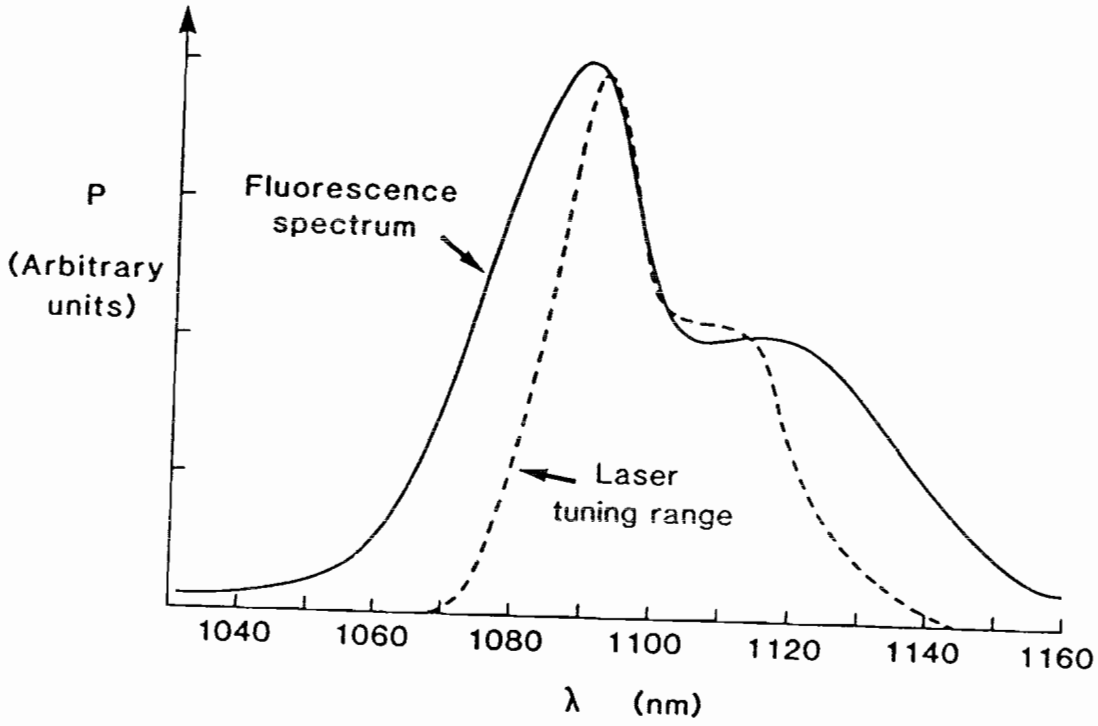

Figure 4.14. Tuning curve for neodymium-doped fibre laser

4.2.1.3 Tunable erbium-doped laser

The erbium-doped fibre has been tuned over both peaks of the fluorescence spectrum at 1.5μm. The pump source for the initial characterisation was the argon-ion laser and the doped fibre was a 90cm length of ND263 pulled to 120μm diameter. The results are published in reference 29.

As noted earlier in the Chapter, the performance of the erbium laser pumped by the argon laser is poor; the typical slope efficiency for the tunable cavity was less than 1%. In order to improve the efficiency, the experimental configuration was altered to that given in Figure 4.15. Tuning was accomplished by changing the angle of the high-reflectivity mirror. This configuration eliminates the need for a pellicle, since the output can be taken directly from the zeroth-order reflection. The fraction of the power in the zeroth order was measured to be 27%.

The tuning curve for the improved erbium-doped fibre laser is shown in Figure 4.16. A maximum output in excess of 4mW was obtained at a pump power of 80mW. The laser is thus a useful spectroscopic source in the region of 1.5μm[31]. The slope efficiency (~ 8%) is reduced from the optimised laser of Section 4.1 as a result of the cavity losses introduced by the intra-cavity lens and the diffraction grating.

4.2.2 Line-narrowing

The normal operating linewidth of the fibre laser is of the order of a few nanometres, and consists of a large number of longitudinal modes. A broad spectral width is useful in certain applications. The fibre-gyroscope, for example, requires a spectrally broad

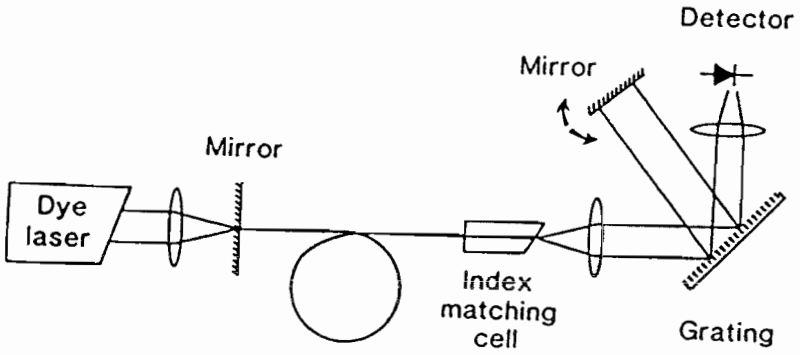

Figure 4.15. Improved configuration for tunable fibre laser

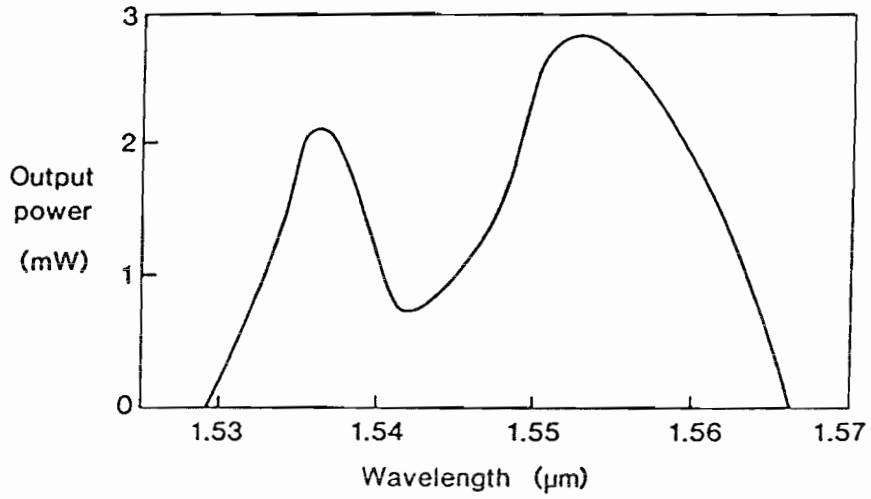

Figure 4.16. Tuning curve for erbium-doped fibre laser

source in order to average out interference effects caused by fibre birefringence[32]. In many instances, however, some control over the linewidth is required.

4.2.2.1 Experimental configuration

One of the simplest methods for narrowing the output spectrum is with an external grating, as described in section 4.2.1. An extension of this technique is to incorporate a Bragg grating integrally in the fibre[33].

Fibre Bragg gratings were made under a collaborative project with Plessey Research (Caswell). Optical fibres were embedded in fused silica substrates and polished to within a few microns of the core, as shown in Figure 4.17. The transverse grating was written in a deposited photoresist layer by two-beam interference lithography and transferred into the fibre by reactive ion-beam etching. In order to control the interaction of the optical field with the grating, a further high-index layer of Al_2O_3 was deposited, and overlaid in turn with a low-refractive-index oil. The work is described in more detail in Bennion et al[34]. The Bragg wavelength and peak reflectivity varied between gratings, and could be tuned by changing the index of the overlaying oil. The grating thus formed a variable reflector. The fibre curvature in the silica block limited the region of interaction with the grating to approximately 1cm. This gave a passive reflectivity of typically 1nm FWHM, the smallest measured bandwidth being 0.8nm.

The laser was configured in the usual manner except that the output end was spliced to the pigtail of the fibre grating (Figure 4.18). The early gratings were deposited on fibres having larger spot sizes (typically 4μm) than the doped fibre. The splice loss was 2 ± 1dB, resulting in a high threshold of the order of 4mW, and a poor slope efficiency. For this reason it was decided to

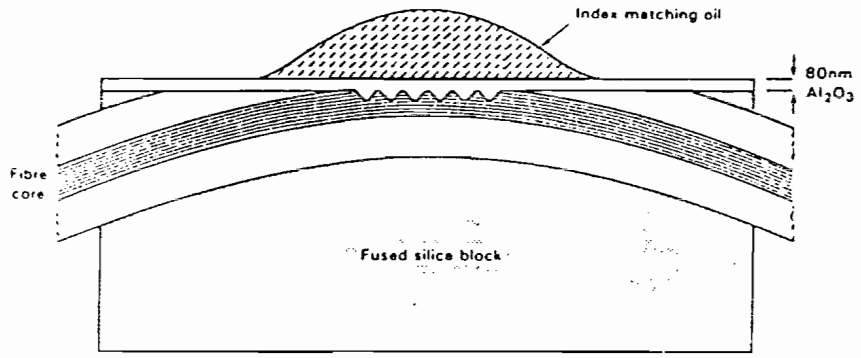

Figure 4.17. Fibre Bragg grating

fabricate gratings from a fibre which matched the doped fibre in cut-off wavelength and spot-size.

4.2.2.2 Line-narrowed Nd^{3+}-doped fibre laser

The original line-narrowing measurements were made with the external holographic grating in the first-order Littrow configuration described in Section 4.2.1. The beam size at the grating was 7mm, giving a resolving power of 4×10^3. Linewidth measurement was limited by the resolution of the monochromator at 0.25nm. The output power from the intra-cavity pellicle changes by less than 10% when the grating was replaced by a high-reflectivity dielectric mirror (99.5% R at 1.088μm). This important result indicates that the efficiency of the laser is approximately independent of the degree of line-broadening, as predicted in Chapter 2.

The availability of the fibre grating enabled a close comparison to be made between the threshold and efficiency of the line-narrowed, and free-running, neodymium-doped fibre laser. A series of experiments were made with fibre cavity shown in Figure 4.18. The reflectivity of the fibre-grating output coupler varies in a precise manner with the refractive index of the oil overlay. By varying this index, the dependence of the laser threshold and slope efficiency on the output reflectivity were examined without changing the internal cavity loss.

The splice loss between the grating fibre and the doped fibre (ND199) was measured to be 0.3 ± 0.1dB. In order to vary the output coupling, the grating was overlaid with various Cargylle standard refractive index oils, the grating being carefully cleaned with acetone and dry-air between each measurement.

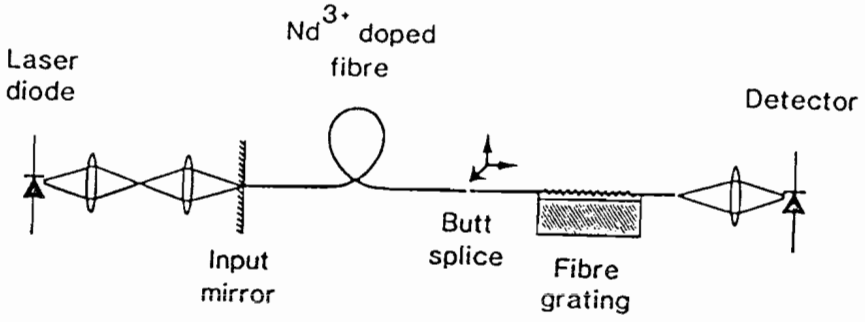

Figure 4.18. Experimental configuration for line-narrowed fibre laser

Figure 4.19 shows the variation of laser threshold with output transmission (calculated from refractive-index data for the grating, provided by Plessey) and Figure 4.20 gives the slope efficiency for each of these measurements. The results have been compared with the expression for the laser threshold (equation (4.1) and Figure 4.5) and the slope efficiency (predicted in Chapter 2 and supplemented by the values of η and η_s determined in Section 4.1). The line-narrowed laser threshold is unchanged from the line-broadened case, as would be expected since the grating reflectivity is centred on the gain maximum at 1.09μm. More importantly, the slope efficiency is also well modelled by the values of η and η_s determined for the line-broadened laser. Thus the line-narrowed laser can also be operated with high efficiency. The output spectrum of the line-narrowed laser was obtained initially at Plessey, using a Fourier-transform Michelson interferometer. The profile was approximately Gaussian, with a FWHM of 16GHz (0.06nm), ±10%. Later measurements at Southampton on a Burleigh scanning Fabry-Perot interferometer indicated a linewidth as small as 1GHz (4×10^{-3} nm), equivalent to approximately 20 longitudinal modes in the 2m cavity. If the cavity length can be reduced to a few centimetres (by using a higher-dopant concentration and fabricating the grating from the doped fibre itself), it should be possible to achieve single-longitudinal mode (SLM) operation[35]. The linewidth would then be considerably reduced. The typical linewidth of a SLM crystal laser is of the order of 100kHz. The great advantage of a SLM glass laser is the combination of a narrow-linewidth with broad tunability/wavelength selection. Such a laser has considerable potential for wavelength-multiplexed coherent communications systems.

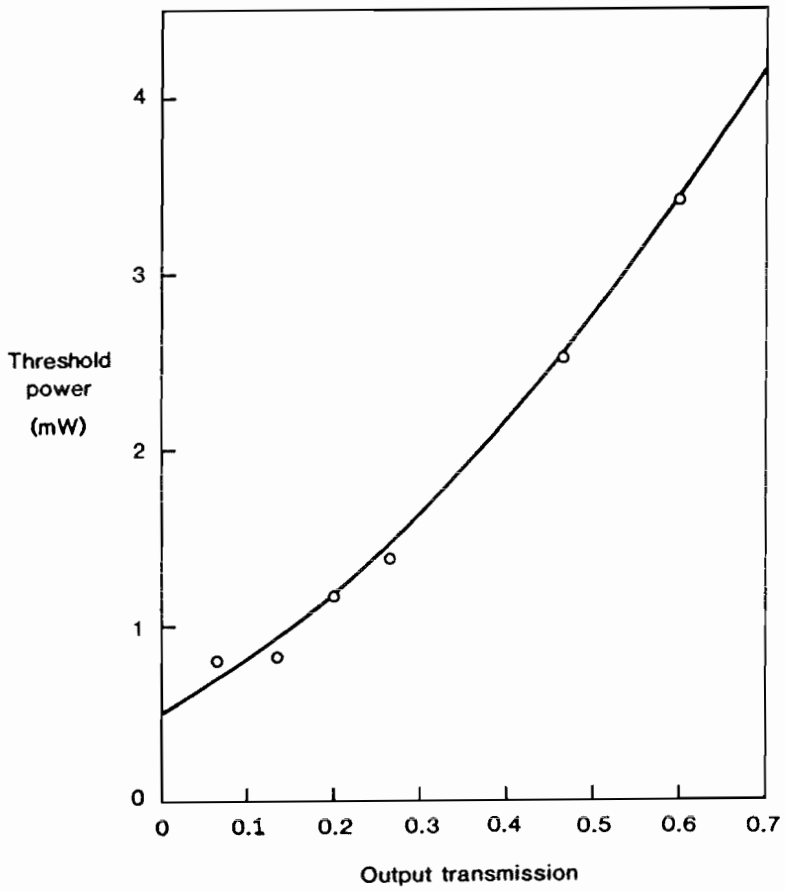

Figure 4.19. Threshold versus output transmission for line-narrowed neodymium-doped fibre laser

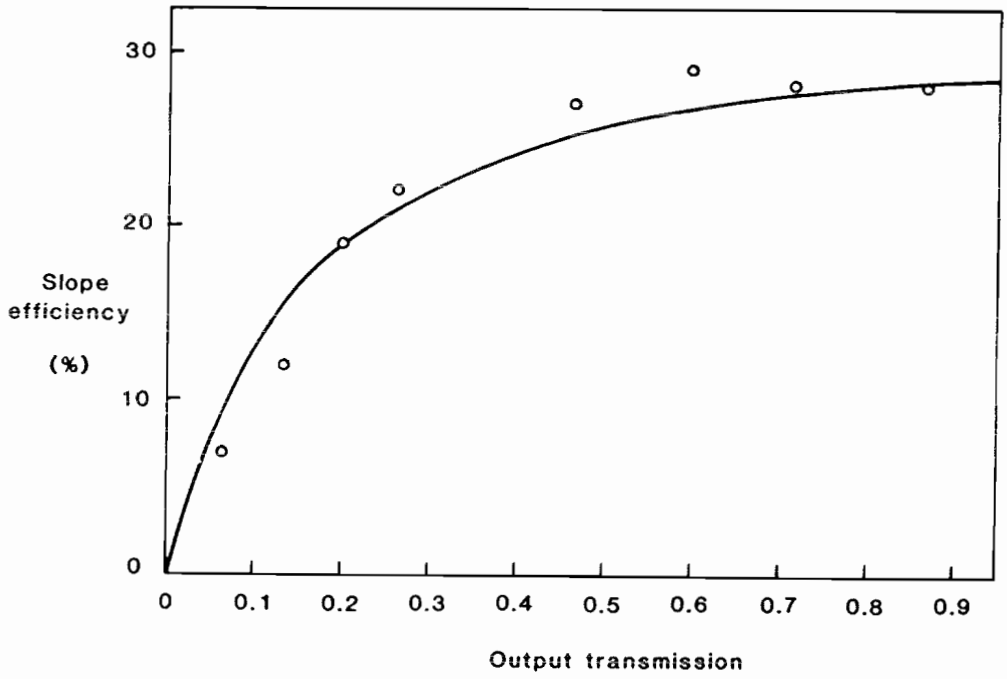

Figure 4.20. Efficiency versus output transmission for line-narrowed neodymium-doped fibre laser

4.2.2.3 Line-narrowed Er^{3+}-doped fibre laser

The linewidth of the erbium-doped fibre laser has been reduced by incorporting a 1.55μm Bragg grating into the fibre cavity[36]. The fibre gratings are fabricated routinely at Plessey from 1.55μm telecommunications fibre. The splice loss with the doped fibre ND263 was measured to be 3 ± 1dB. The maximum of the grating reflectivity coincided with the second peak of the fluorescence spectrum (see Chapter 3). The action of the grating is similar to that of the wavelength-selective dielectric mirror described in Section 4.1.3.2.

The threshold for the 2m cavity was 13mW, compared to 8.5mW for the line-broadened laser, but the difference is accounted for by the additional cavity loss. These figures are consistent with the measured slope efficiency of 5%, compared to 10% for the spectrally broad laser. Thus, once the additional cavity loss is taken into account, the threshold and efficiency of the line-narrowed erbium-doped fibre laser are identical to the corresponding values for the free-running laser.

The linewidth of the laser was measured on the Burleigh scanning Fabry-Perot interferometer, Figure 4.21. The spectrum had a FWHM of 4.9GHz (0.04nm). Once again mode competition makes the observed spectrum considerably narrower than the passive bandwidth of the grating (~ 1nm). Within the narrow band selected by the grating, the laser behaves more like a homogenously broadened system. It should be possible to achieve single-longitudinal mode operation if the fibre dopant concentration can be increased sufficiently to permit cavity lengths of the order of a few centimetres.

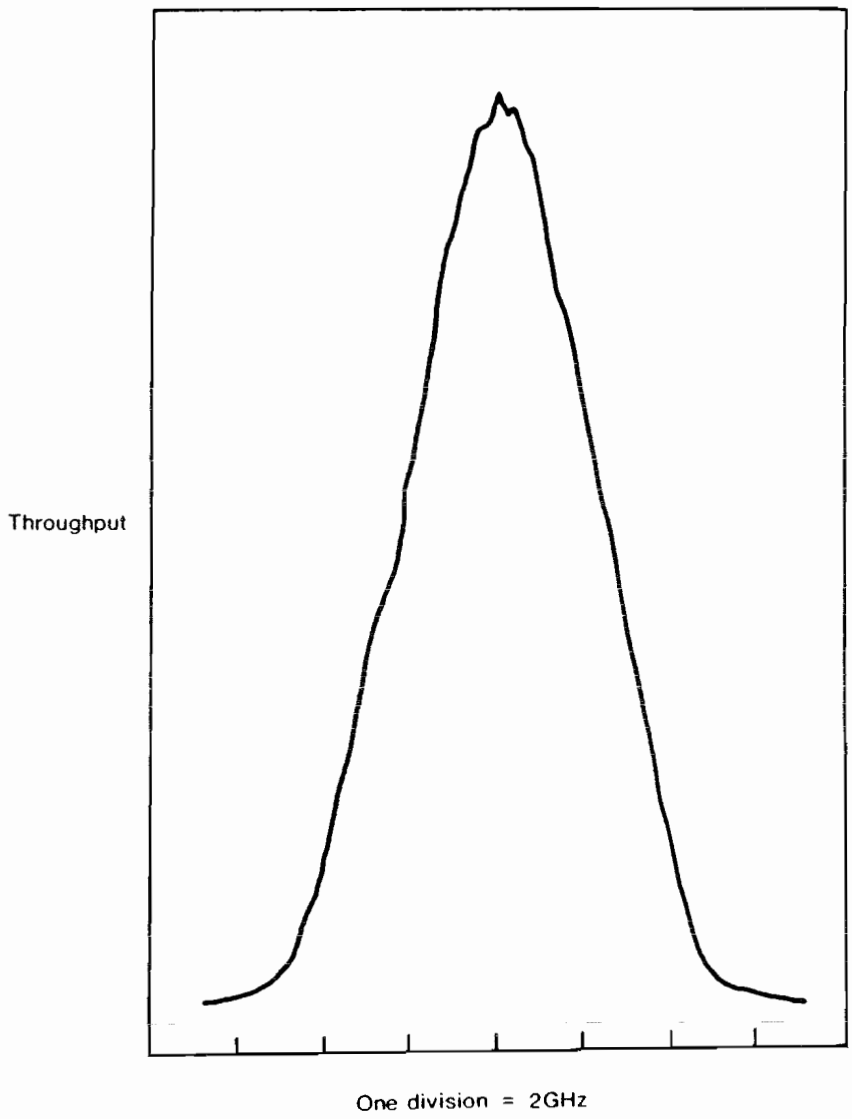

Figure 4.21. Linewidth of grating-narrowed erbium-doped fibre laser

4.3 Summary

The optical-fibre laser has given low-threshold operation of three and four-level neodymium- and erbium-doped lasers. The thresholds are the lowest reported for glass-laser systems, and are well-modelled by the theory developed in Chapter 2. Optimisation of the cavity parameters has resulted in highly-efficient operation, both at 1.088μm and 1.53μm.

The lasers have been tuned over the majority of their gain curves with an external diffraction grating. As a result of the broad linewidths in silica glass, and the low-thresholds of the fibre configuration, the tuning ranges are the widest yet reported for Nd^{3+}- and Er^{3+}-ions.

Under normal operating conditions the laser linewidth is a few nanometres, and the broadening with pump power is consistent with the combined homogenous and inhomogenous components of the transition. The linewidth has been narrowed with an external grating, and with the inclusion of a fibre Bragg grating. Linewidths down to 1GHz were recorded during this work.

References to Chapter 4

1. E. Snitzer:
"Optical maser action of Nd^{3+} in a barium crown glass",
Phys. Rev. Lett., 1961, 7, pp. 444-446.

2. L.F. Johnson, G.D. Boyd, K. Nassau and R.R. Soden:
"Continuous operation of a solid-state optical maser",
Phys. Rev. 1962, 126, pp. 1406-1409.

3. J.F. Geusic, H.M. Marcos and L.G. Van Uitert:
"Laser oscillations in Nd-doped yttrium aluminium, yttrium gallium and gadolinium garnets,
Appl. Phys. Lett., 1964, 4, pp. 182.

4. R.D. Maurer:
"Operation of a Nd^{3+} glass optical maser at 9180 Å",
Appl. Opt., 1963, 2, pp. 87-88.

5. P.B. Mauer:
"Laser action in neodymium-doped glass at 1.37 microns",
Appl. Opt., 1963, 2, pp. 153.

6. H.W. Etzel, H.W. Gandy and R.J. Ginther:
"Stimulated emission of infra-red radiation from ytterbium activated silicate glass",
Appl. Opt. 1962, 2, pp. 534-536.

7. H.W. Gandy and R.J. Ginther:
"Stimulated emission from holmium activated silicate glass",
Proc. IRE., 1962, 50, pp. 2113-2114.

8. E. Snitzer and R. Woodcock:
"Yb^{3+}-Er^{3+} glass laser",
Appl. Phys. Lett., 1965, 6, pp. 45-46.

9. H.W. Gandy, R.J. Ginther and J.F. Weller:
"Stimulated emission of Tm^{3+} radiation in silicate glass",
J. Appl. Phys., 1967, 38, pp. 3030-3031.

10. E. Snitzer and C.G. Young:
"Glass Lasers",
Advances in Lasers, Vol. 2, A. Levine Ed.
New York : Dekker, 1968, pp. 191-256.

11. R.B. Chesler and D.A. Draegert:
"Miniature diode-pumped Nd:YAℓG laser",
Appl. Phys. Lett., 1973, 23, pp. 235-236.

12. J. Stone and C.A. Burrus:
"Neodymium doped silica laser in end-pumped fiber geometry",
Appl. Phys. Lett., 1973, 23, pp. 388-389.

13. E.I. Galant, Y.N. Kondrat'ev, A.K. Przevuskii, M.N. Tolstoi and V.N. Shapovalov:
"Stimulated emission of neodymium ions in quartz glass",
JETP Lett., 1973, 18, pp. 372.

14. K. Kubodera and K. Otsuka:
"Single transverse mode $LiNdP_4O_{12}$ slab waveguide laser",
J. Appl. Phys, 1979, 50, p. 653.

15. A.W. Snyder and J.D. Love:
"Optical Waveguide Theory",
Chapman and Hall, ISBN 041209950 0.

16. I. Jauncey:
Private communication.

17. A. Yariv:
"Optical Electronics",
Holt Saunders ISBN 4-8337-0274-6.

18. R.J. Mears, L. Reekie, S.B. Poole and D.N. Payne:
"Neodymium-doped silica single-mode fibre lasers",
Electron. Lett., 1985, 21, pp. 738-740.

19. L.G. Deshazer and L.G. Komai:
"Fluorescence conversion efficiency of neodymium glass",
J. Opt. Soc. Am., 1965, 55, p. 940.

20. W.F. Krupke:
"Induced emission cross-sections in neodymium laser glasses",
IEEE J.Q.E., 1974, QE-10, pp. 450-457.

21. I.M. Jauncey, J.T. Lin, L. Reekie and R.J. Mears:
"An efficiency diode-pumped CW and Q-switched single-mode fibre laser",
Electron. Lett., 1986, 22, pp. 198-199.

22. L. Reekie:
Private communication.

23. M. Zürn, J. Voigt, E. Brinkmeyer and R. Ulrich:
"Line-narrowing and spectral hole-burning in single-mode Nd^{3+}-fibre lasers",
Opt. Lett., to be published.

24. R.J. Mears, L. Reekie, S.B. Poole and D.N. Payne:
"Rare-earth-doped fibre lasers",
Proc. OFC., 1986, Atlanta.

25. R.J. Mears, L. Reekie, S.B. Poole and D.N. Payne:
"High gain rare-earth-doped fibre amplifier at 1.5μm",
Proc. OFC., 1987, Reno, Nevada.

26. E. Snitzer:
"Frequency control of a Nd^{3+} glass laser",
Appl. Opt., 1966, 5, pp. 121-125.

27. P.C. Magnante:
"A high spectral radiance neodymium glass laser"
IEEE J.Q.E., 1968, QE-4, pp. 363-364.

28. R.R. Jacobs and M.J. Weber:
"Dependence of the $^4F_{3/2}$ - $^4I_{11/2}$ induced emission cross-section for Nd^{3+} on glass composition",
IEEE J.Q.E., 1976, QE-12, pp. 102-111.

29. R.J. Mears, L. Reekie, S.B. Poole and D.N. Payne:
"A low-threshold tunable CW and Q-switched fibre laser operating at 1.55μm",
Electron. Lett., 1986, 22, pp. 159-160.

30. L. Reekie, R.J. Mears, D.N. Payne and S.B. Poole:
"Tunable single-mode fibre lasers",
J. Lightwave Tech., 1986, LT-4, pp. 956-960.

31. R.J. Mears and L. Reekie:
"A high-power tunable erbium-doped fibre laser operating at 1.55μm",
Proc. C.L.E.O., 1987, Baltimore.

32. K. Bohm, P. Marten, K. Petermann, E. Weidel and R. Ulrich:
"Low drift fibre gyro using a superluminescent diode",
Electron. Lett., 1981, 17, pp. 352-353.

33. I.M. Jauncey, L. Reekie, R.J. Mears, D.N. Payne, C.J. Rowe, D.C.J. Reid, I. Bennion and C. Edge: "A narrow linewidth fibre laser with integral fibre grating", Electron. Lett., 1986, 22, pp. 987-988.

34. I. Bennion, D.C.J. Reid, C.J. Rowe and W.J. Stewart: "High-reflectivity monomode fibre grating filters", Electron. Lett., 1986, 22, pp. 341-343.

35 I.M. Jauncey, L. Reekie, J.E. Townsend, D.N. Payne and C.J. Rowe: "Single longitudinal mode operation of a Nd^{3+}-doped fibre laser", Submitted to Electronics Letters, 1987.

36. I.M. Jauncey, L. Reekie, R.J. Mears and C.J. Rowe: "A narrow linewidth fibre laser operating at 1.55μm", Optics Letters, to be published, 1987.

CHAPTER 5 : OPTICAL FIBRE LASERS : TEMPORAL CHARACTERISTICS AND AMPLIFICATION

The aim of this chapter is to outline experiments to characterise the potential of the fibre laser as a pulsed source. The standard techniques of Q-switching and mode-locking have been applied to the optical fibre laser configuration, and have resulted in the generation of short intense pulses with high efficiency. Furthermore, a bistable threshold has been demonstrated, enabling a three-level laser such as the Er^{3+}-doped fibre laser to be configured as a switch or logic gate.

Although the majority of the thesis is concerned with the operation of optical fibre lasers, the doped-fibre can also be used as an amplifier. The final section assesses the results achieved so far and the potential for the future.

5.1 Q-Switched and Mode-Locked Operation

The long fluorescent lifetimes of the rare-earth ions in glass make them ideal for storing energy provided by a CW or quasi-CW pump source. The technique of Q-switching enables the stored energy to be released in a single high-power pulse[1]. By means of some mechanical or optical device, feedback into the laser cavity is reduced whilst the ionic population is optically excited, until the gain in the cavity is as high as possible. At this point, feedback is restored; the gain far exceeds the round-trip losses; and the laser power increases until the majority of the excited population has been swept out. The resultant pulse is typically between 10ns and 100ns in duration.

An efficient source of high-power pulses is required for a number of applications. Sensor systems such as the distributed temperature monitor[2] require pulses of 1μJ energy and less than 1μs duration at repetition rates greater than 1kHz. It is difficult to achieve this specification with a single-stripe semiconductor laser because of the low damage threshold of the output facet. A more satisfactory approach is to use a CW semiconductor laser to pump a Q-switched fibre laser. The silica fibre has excellent power handling characteristics, and can be spliced with low-loss into optical fibre systems. The free-running optical fibre laser operates on a very large number of longitudinal modes. If the phases of these modes are locked coherently, the resultant output of the laser is a train of very short pulses spaced by the round-trip time of the cavity. The technique of mode locking is an extension to the optical domain of the microwave regenerative pulse amplifier described by Cutler[3]. Picosecond light sources have found a variety of applications ranging from materials science to communications[4,5].

5.1.1 Experimental configuration for Q-switching

The neodymium-doped and erbium-doped fibre lasers have been Q-switched with either an acousto-optic deflector, or a mechanical chopper, Figure 5.1. The introduction of bulk elements into the fibre cavity necessitates an intra-cavity lens, as described in Section 4.2. Although the lens can be arranged so as to collimate the light from the fibre, the most stable configuration is achieved with the beam focussed on the output mirror. The original Q-switching experiments were performed with the acousto-optic deflector belonging to the Quantronix YAG laser, although it was later replaced by a second acousto-optic deflector (Isomet 1205C). When a RF signal is applied to the device, a portion of the light passing through it is diffracted, and undergoes a frequency shift. The remaining light passes through unchanged. The lowest-

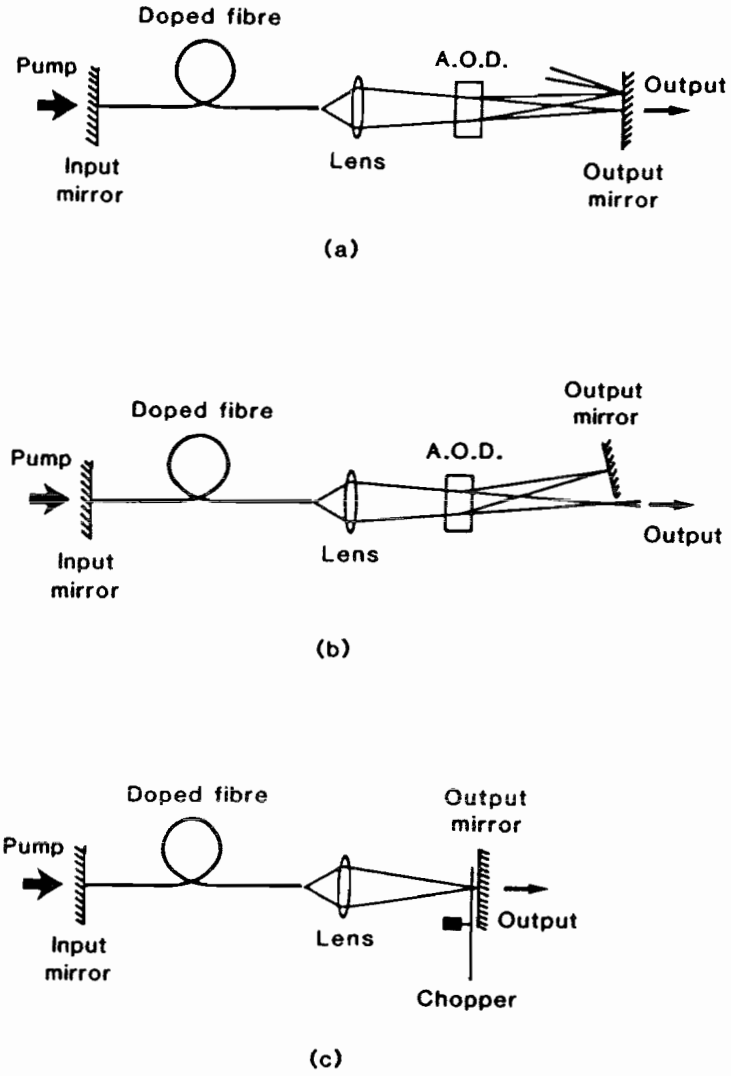

Figure 5.1. Q-switching configurations
a) Zeroth order
b) First order
c) Chopper

loss configuration for Q-switching is that which provides feedback on the zeroth order, as shown in Figure 5.1(a). Thus when the RF signal is applied, the cavity loss increases due to diffraction. It was necessary to employ the zeroth order configuration for the first diode-pumped Nd^{3+}-doped fibre laser because of the low-gain available. It is also the configuration most commonly used in commercial Q-switched lasers.

The limitation of the technique is the diffraction efficiency of the deflector; typically up to 50% of the power remains in the zeroth order when the RF signal is on. The geometry of the fibre laser permits high gains to be achieved at modest pump powers, and the gain is often sufficient to permit lasing even when the RF signal is applied. This obviously limits the maximum population inversion.

A different configuration is therefore employed for high-gain fibre lasers[6]. The deflector is adjusted to the Bragg condition, so that the majority of the diffraction occurs only into the first order. Feedback for the Bragg-diffracted spot is provided by a high-reflectivity mirror, and the detector is positioned to collect the remaining zeroth order, as shown in Figure 5.1(b). In this arrangement the deflector need only be activated during the build-up of the Q-switched pulse. No feedback is provided when the deflector is off. It was necessary to index-match one end of the fibre to prevent lasing from the 4% Fresnel reflection.

An alternative technique, which is quite effective for lasers with long fluorescent lifetimes, is to use a mechanical chopper[7,8], as shown in Figure 5.1(c). The chopper provides a high isolation during the build-up of the population inversion, and has zero-loss otherwise. Its limitations are a relatively slow switching time and poor pulse-to-pulse stability. The switching time is minimised by reducing the spot-size at the chopper and by

positioning the beam at the perimeter of a large-diameter wheel. Switching times of a few microseconds are relatively easy to obtain. It is usually necessary to reduce the "on" time by masking the chopper so as to prevent further relaxation oscillations.

5.1.2 Q-switched Nd^{3+}-doped fibre laser

The Nd^{3+}-doped fibre laser permits a comparison to be made between the alternative configurations of the acousto-optic deflector. Pump radiation was provided by the Rhodamine 6G dye laser and was attenuated to give a maximum absorbed power of 100mW. The Q-switch was activated by 1-2μs electrical pulses of variable repetition rate into the RF driver.

5.1.2.1 Zeroth-order configuration

The measured absorbed power threshold was 10mW for the 65% transmitting output mirror. Allowing for intra-cavity objective losses and a 10% loss for the transmission through the Q-switch, the threshold indicates a fluorescence efficiency of 0.5 for the 580nm pump. The predicted slope efficiency is given by

$$\frac{T}{T+L}\,\eta\,\frac{\nu_e}{\nu_p}\,f\left\{\frac{\Delta\nu_{IH}}{\Delta\nu_H}\right\} = 0.12$$

As the pump power was raised above threshold, the Q-switched pulses narrowed and increased in power. The pulse energy rapidly saturated, however, reaching a maximum value of 0.7μJ. This was the inversion required for lasing to occur whilst the acousto-optic deflector was activated. The average power of the Q-switched pulses could only be raised by increasing the repetition rate. At the maximum pump power, pulses of 4.5W and 160ns FWHM were obtained at a repetition rate of 14KHz. This corresponds to an average power of 10mW indicating that the Q-switching efficiency is approximately the same as for CW operation.

5.1.2.1 First-order configuration

Although the average power obtained for the zeroth order configurtion is high, the pulses are rather long (~ 200ns) and the peak power is poor. The first-order configuration offers the potential of higher energy pulses and higher peak powers.

Feedback was provided on first-order by a 1.09μm high-reflectivity mirror. It should be noted that the deflector contributes an extra loss in this configuration because of the second diffracted output on the return pass through the device. The diffraction efficiency into first-order was measured as 40%.

Figure 5.2 shows the variation in the average power at the maximum pump rate. The average power reaches its maximum at approximately 4kHz repetiton rate. The slope efficiency was reduced because of the increased cavity loss. Nevertheless, at the maximum average power, the pulses were 16W; 75ns FWHM, which is a significant improvement. At lower repetition rates, pulse energies of up to 2μJ were obtained.

5.1.3 Diode-pumped, Q-switched, fibre laser

The highest gain attainable with the Hitachi laser diode (HLP1400) was limited to 1-2dB. Although the gain was sufficient to permit insertion of an objective into the fibre laser cavity, threshold was close to the maximum output power of the diode.

The insertion of the acousto-optic deflector (AOD) increased the cavity loss further, and the maximum pump rate was only 10% above threshold. Because of the limited power, the output reflector in this experiment was chosen to have a 12% transmission at 1.09μm. A typical Q-switched

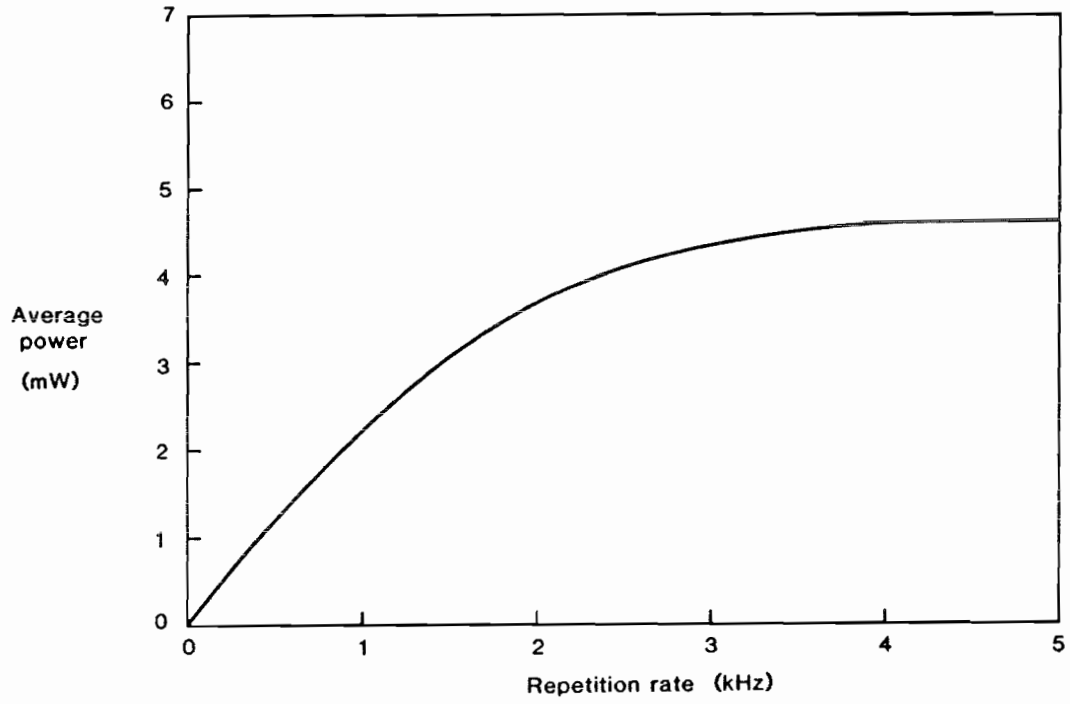

Figure 5.2. Pulse energy and average power versus repetition-rate for Q-switched neodymium-doped fibre laser

pulse is shown in Figure 5.3(a). The average power at 4kHz was a mere 20μW, but this value is in good agreement with the slope efficiency prediction.

In order to increase the peak and average power the AOD was replaced with a mechanical chopper[8]. The chopper was masked to give a mark/space ratio of 1 : 300 and the speed was adjusted to give a repetition rate of 400Hz. Typical pulses are given in Figure 5.3(b). The photograph is a multiple exposure indicating the limited pulse-to-pulse stability. It was possible to increase the output transmission up to 65%, thereby obtaining pulses of 300mW amplitude and 1μs FWHM. The pulse duration was limited by the slow switching speed of the chopper, but the pulse energy was a respectable 0.3μJ.

Further improvement in the performance was only possible with a more powerful laser diode. After extensive enquiries, an order was made for the Sharp LT015 40mW laser diode, which offered three times as much power as the Hitachi diode. Recent results indicate pulse energies in excess of 1μJ[9].

5.1.4 Q-switched, Er^{3+}-doped, fibre laser

The original experiments on Q-switching the Er^{3+}-doped fibre laser were performed in the zeroth-order configuration and with the argon-ion laser pump source. As already noted in Chapter 4, the ion laser appears to be far from ideal as a pump source and the maximum gain is limited to ~ 3dB. Since the typical losses introduced by the intra-cavity lens and acousto-optic deflector are of the same order of magnitude, the available inversion is rather small. Initial results indicated a maximum 2W pulse of 60ns duration[10].

(a)

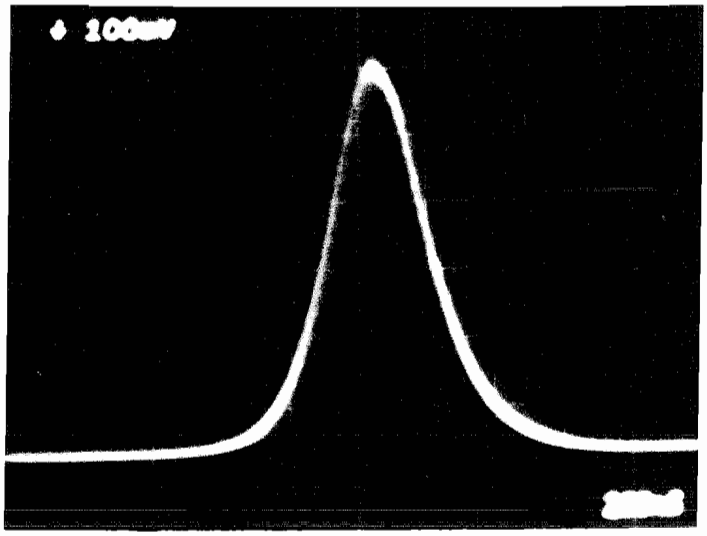

(b)

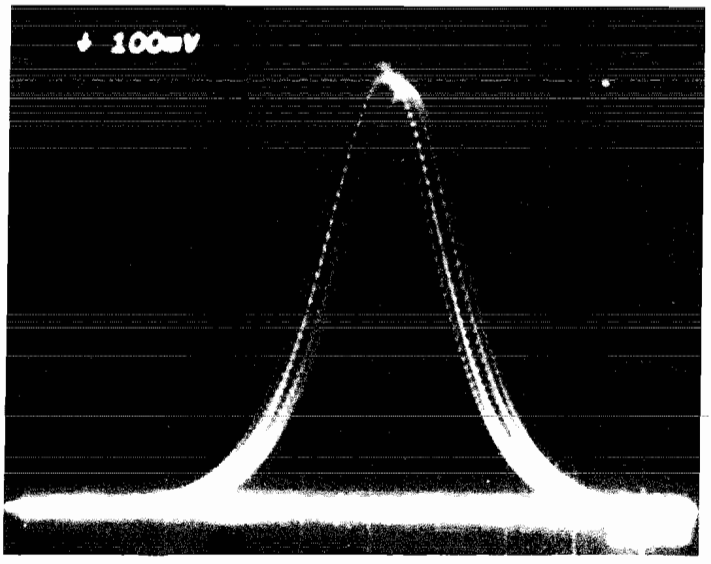

Figure 5.3. Q-switched pulses for diode-pumped Nd^{3+}- doped fibre laser
(a) using acousto-optic deflector (200ns/div.)
(b) using mechanical chopper (500ns/div.)

The higher gains attainable with the DCM dye laser at 660nm have greatly expanded the potential of the Er^{3+}-doped laser. In order to Q-switch the laser efficiently, it is essential to employ a technique which introduces a high extinction in the low-Q state. The gain is so high that it is also necessary to index-match one end of the fibre to prevent lasing from 4% Fresnel reflection. Insertion of a mechanical chopper into the cavity as described in the previous section, resulted in 6W, 150ns pulses, which is almost an order of magnitude increase in pulse energy. The slow switching time of the chopper Q-switch results in rather long pulses, however, and the laser was therefore configured with the acousto-optic deflector as described in section 5.1.1. The diffraction efficiency at 1.5μm was 30%.

5.1.4.1 High-power, Q-switched operation

The relatively low diffraction efficiency of the acousto-optic deflector results in the majority of the output power passing out of the cavity through the zeroth order diffracted beam. It is shown in Chapter 2 that high-gain lasers, such as the Er^{3+}-doped fibre laser, work efficiently with a high value for the output coupling. The slope efficiency anticipated for the overall cavity loss of 45% is approximately 0.05. The laser threshold is very similar to that observed for the fibre laser relying on Fresnel reflection at one end, described in Chapter 4. For the 3m fibre (ND263; 120μm diameter) the threshold at 660nm was 30mW. Measurements were made at a pump power of three times threshold.

Figure 5.4 shows the variation in pulse energy and average power as the repetition rate was varied from a 10Hz to 20kHz. The pulse energy was observed to decrease beyond 800Hz, although the average power reached its maximum value of 3.4mW at approximately 1.2KHz. The slope efficiency was therefore 0.057, in excellent agreement with the predicted value for CW operation. The

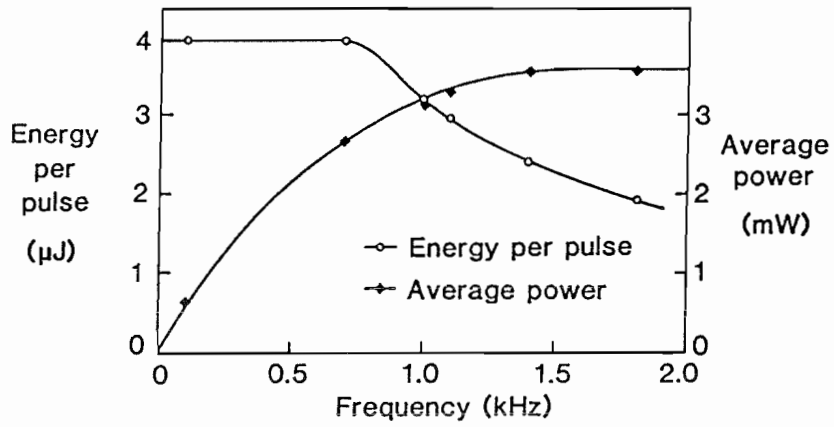

Figure 5.4. Pulse energy and average power versus repetition-rate for Q-switched erbium-doped fibre laser

efficiency observed for the erbium-doped fibre laser is unimpaired under Q-switched operation, as it is for the neodymium-doped laser.

The pulse energy (at 800Hz) and pulse duration were examined as the fibre length was varied from 4.5m to 0.8m. The optimum length was in the region of 2m, Figure 5.5. This value is greater than, for example, the low-threshold laser described in Chapter 4, because of the need to maintain a relatively high gain in order to overcome the losses in the optical system. The pulse energy reached its maximum value of 3.4μJ at 2.2m, whereas the pulse duration was minimised at 31ns for a 1.8m fibre length. The peak output power was in excess of 100W [6], and a typical pulse is shown in Figure 5.6. Although the output power is modest by comparison with conventional bulk lasers, it nevertheless indicates a very high intensity in the fibre core (> $1GW/cm^2$). The Q-switched fibre laser is thus a potential source for non-linear-optical devices.

5.1.5 Non-linear generation with a Q-switched erbium-doped fibre laser

Optical fibres provide an ideal geometry for the demonstration of a number of non-linear effects due to their small guiding cores and long-interaction lengths. The past fifteen years have seen a large number of non-linear experiments based on optical fibres, including the generation of stimulated Raman and Brillouin scattering, self-phase modulation, the optical Kerr effect, 3-wave mixing, and Second-Harmonic generation[11-17]. One of the limitations of the silica optical fibre for such work is its very small non-linear refractive index. Conventional experiments require large, high-power laser sources. If devices based on non-linear effects are ever to become practical, a means must be sought to use more compact, low-power sources.

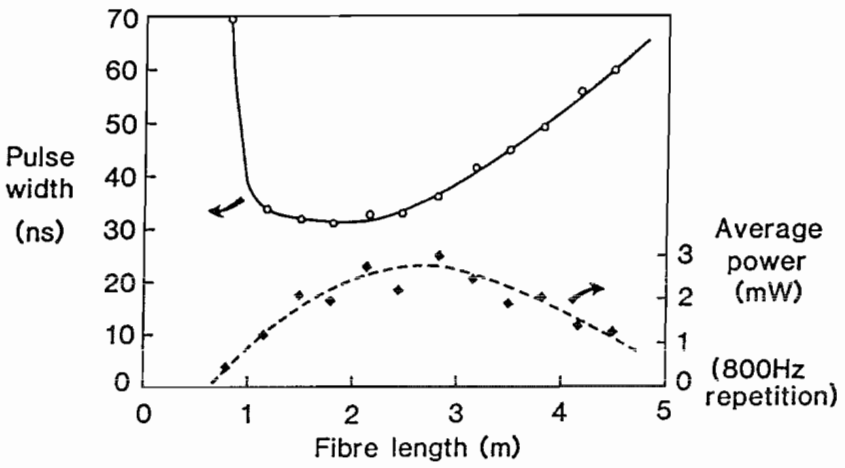

Figure 5.5. Pulse energy and duration versus length for Q-switched erbium-doped fibre laser

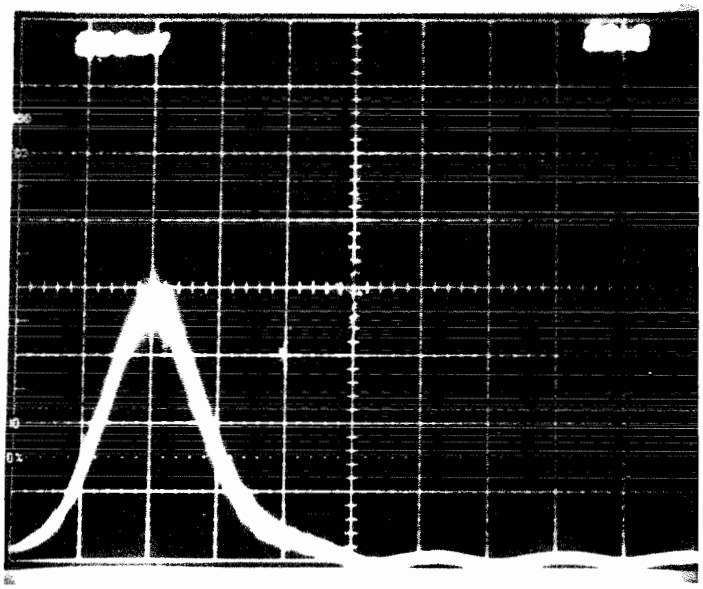

Figure 5.6. High-power Q-switched pulse for Er^{3+}- doped fibre laser (20ns/div.)

One approach has been to develop new fibre materials with higher non-linear coefficients. It is also useful to develop a means of reducing the source power requirements. In the light of recent technological advances, the junction diode laser is the most likely source for future non-linear devices since it uses direct electrical-optical conversion to achieve a high operating efficiency. The optical fibre laser offers a useful supplement to this source, since it expands the number of available wavelengths, and more importantly, it has a higher optical damage threshold. It is believed that a pulsed fibre laser, pumped by a CW diode laser, has considerable potential for the practical implementation of non-linear optics.

5.1.5.1 Experimental configuration

The experimental configuration is given in Figure 5.7. The zeroth order deflection from the AOD was launched into a 800m length of high birefringence fibre (s.m. cut off at 1100nm and N.A. = 0.15). Raman generation occured for an absorbed pump power of less than 50mW at 660nm, corresponding to 15W pulses of 40ns duration at 1.536nm. The repetition rate was 1kHz. At a pump power of 80mW it was possible to achieve almost complete conversion to the first Stokes band from 1.63μm - 1.67μm. The depleted pulse at 1.536μm is shown in Figure 5.8. The Raman pulse had a FWHM of 20ns.

The Raman threshold can be compared to the theory of Smith[18]. The critical power for equality between Stokes and pump beams is given by

$$P_{crit} = 16 \frac{A\alpha_p}{\gamma}$$

The expression is derived for the ideal case of a fibre length $\ell = 1/\alpha_p$ and identical polarisations for the Stokes and pump beams. The polarised Raman gain in fused silica

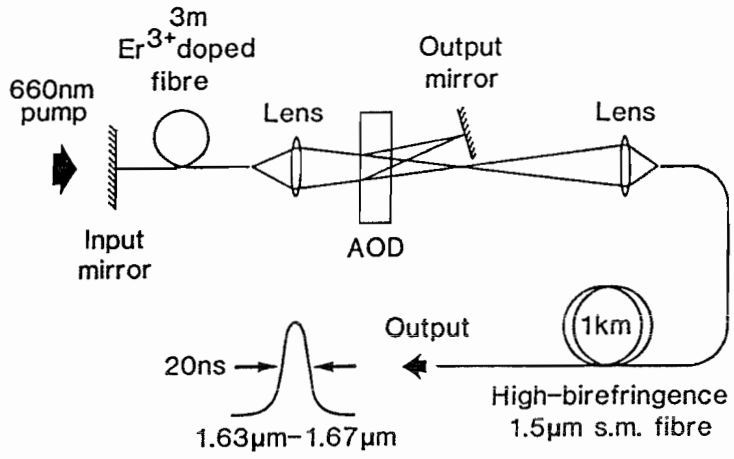

Figure 5.7. Experimental configuration for Raman generation from Q-switched erbium-doped fibre laser

(a)

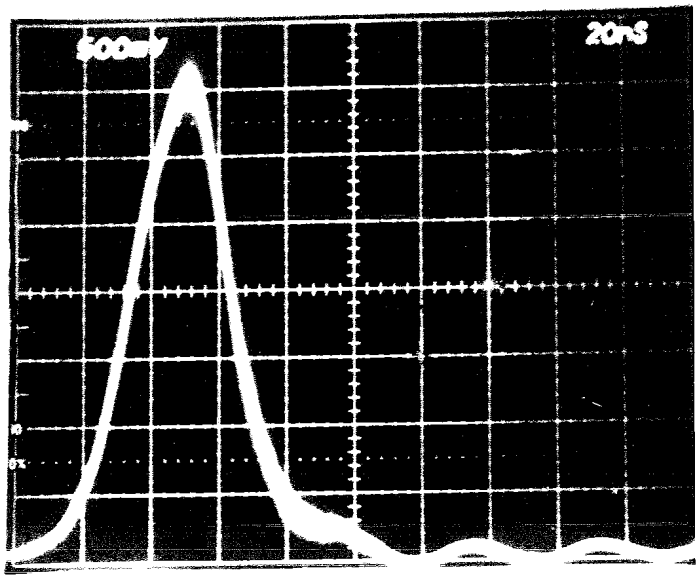

(b)

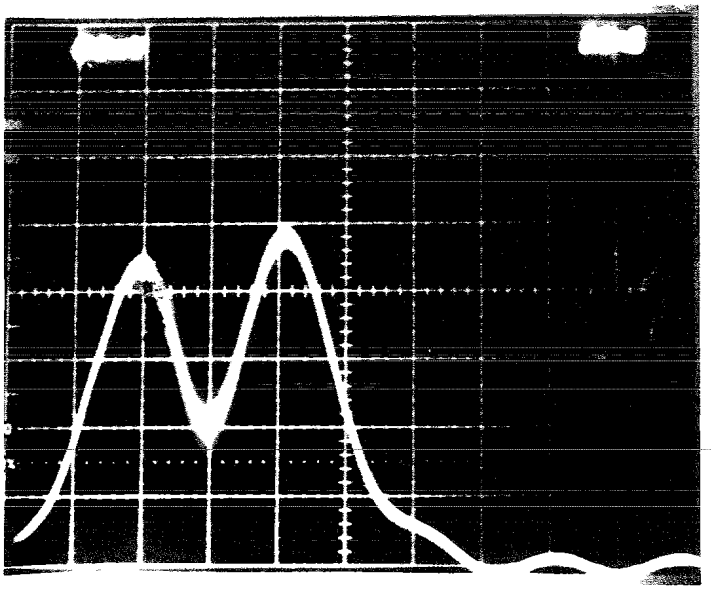

Figure 5.8. Raman generation using Er^{3+}- doped fibre laser:
(a) High-power Q-switched pulse
(b) Pulse depletion due to Raman conversion

was measured by Stolen and Ippen to be $\gamma = 1.5 \times 10^{-13}$ m/W [12]. Since the randomly-polarised output of the fibre laser excites both polarised modes of the high-birefringence fibre, it is appropriate to consider half of the pump power in each mode[19]. The fibre loss was measured to be 1dB/km at 1.6μm, i.e. $\alpha_p = 2.3 \times 10^{-4}$. The ideal length would therefore be 4km, and since such a length was not readily available, the threshold is higher by a factor $1/1-\exp(-\alpha_p \ell)$. The effective modal area at a wavelength of 1.65μm (V=1.6) is $5 \times 10^{-11} m^2$. The calculated critical power is 7.4W in each mode, or a total power of 14.8W. This value is in excellent agreement with the experimental observation.

The significance of the result is two-fold. First it demonstrates the well established technique of extending the wavelength tunability of the fibre laser by Raman shifting. Given a suitable low-loss fibre at 1.088μm, it ought to be possible to extend the neodymium tuning range in a similar manner. Secondly, and perhaps more importantly, it demonstrates the principle of a fibre laser as a source for non-linear generation.

5.1.6 Mode-locked operation

Much of the early work on the mode-locking of glass lasers was performed by DeMaria et al[20]. Active mode-locking of an Nd^{3+}-glass laser with an acousto-optic shutter produced pulses of 1ns FWHM, more than 3 orders of magnitude greater than the bandwidth limit. The discrepancy was accounted for by length variations in the rod during pumping. The best results have been obtained by passive mode-locking, which is achieved with an intra-cavity saturable absorber[21]. Unfortunately, the CW powers required to operate typical dye-cell saturable absorbers are beyond the reach of the fibre laser. Attention has therefore been focussed on active mode-locking.

5.1.6.1 Experimental configuration

The original experiments on mode-locking the Nd^{3+}-doped fibre were performed by I.P. Alcock in the Physics Department at Southampton[22]. His results indicated pulses of less than 1ns duration, but there was insufficient power to determine the pulse duration by autocorrelation techniques. Attention is restricted here to the mode-locking of the Er^{3+}-doped fibre laser. I am grateful to M. Phillips and A. Ferguson of the Physics Department for the loan of the mode-locker and birefringent plates.

The experimental configuration is given in Figure 5.9. The diffraction grating restricted the laser bandwidth to approximately 1nm, corresponding to a minimum bandwidth-limited pulse of 5ps. The mode-locker frequency was 21MHz, and after allowing for the free space and cavity elements, the fibre length was adjusted to 2.18m (42MHz free-spectral range). The cavity modal beats were clearly observable on the Marconi Spectrum analyser, and fine tuning of the cavity length was performed by mounting the end reflector on a z-axis manipulator. The mode locker was then temperature tuned until the mode-locker resonance and cavity resonance coincided.

The temporal output was measured using a TXL series Ge-APD and Tektronix sampling head. The overall rise-time for the detection system was 700ps. As the mode-locker and cavity frequencies were tuned to coincidence, the modal spectrum on the spectrum analyser increased in amplitude, and the pulse output sharpened to FWHM of 5ns, indicating partial, though very poor, mode-locking.

The mode-locker is designed for vertical polarisation, whereas the fibre and cavity provided little, or no, polarisation selection. It was therefore decided to insert two wave plates into the cavity to

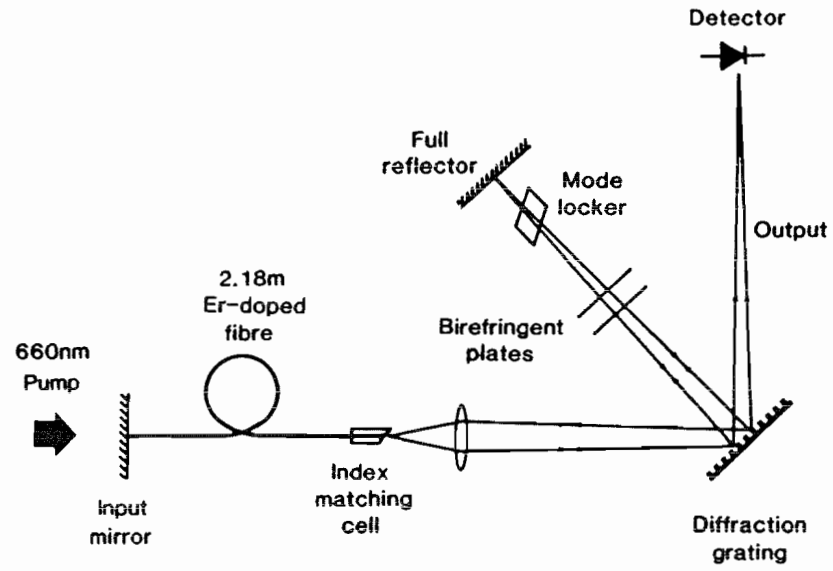

Figure 5.9. Experimental configuration for mode-locked erbium-doped fibre laser

adjust the output polarisation state. Careful adjustment of these, and the mode-locker angle and position, finally resulted in detector limited pulses of 20pJ energy, Figure 5.10. At the time of performing the experiments, an autocorrelator was not available to determine the pulse duration. The peak power under simultaneous mode-locking and Q-switching (in excess of 100W) should be sufficient to permit non-linear mixing. Further investigation is currently underway in the Physics Department.

5.2 Optical Amplifiers

Optical amplifiers are of interest not only for optical communications, but for a wide variety of sensing and signal processing applications. The advantages of a laser amplifier in a communications system have received much attention[23-25]. Examples include its configuration as a post-amplifier to boost an optical source; as a repeater to increase the distance between a source and detector; and also as a receiver preamplifier to improve sensitivity. In spite of these advantages it is only relatively recently that a concerted effort has been made to incorporate optical amplifiers into communications systems[26-28].

The usefulness of an optical fibre with gain extends beyond long-haul communications. A number of sensor schemes which are limited by fibre attenuation or component losses[29,30] would also benefit from fibre repeaters. Amplifiers could be employed to increase the number of subscribers in local loops where the loss of the taps is usually the limiting factor. Fibre amplifiers also open up opportunities in fibre circuitry and signal processing. One can conceive, for example, of active delay line memories and fibre switches. It is clear that an optical fibre with gain would have many applications.

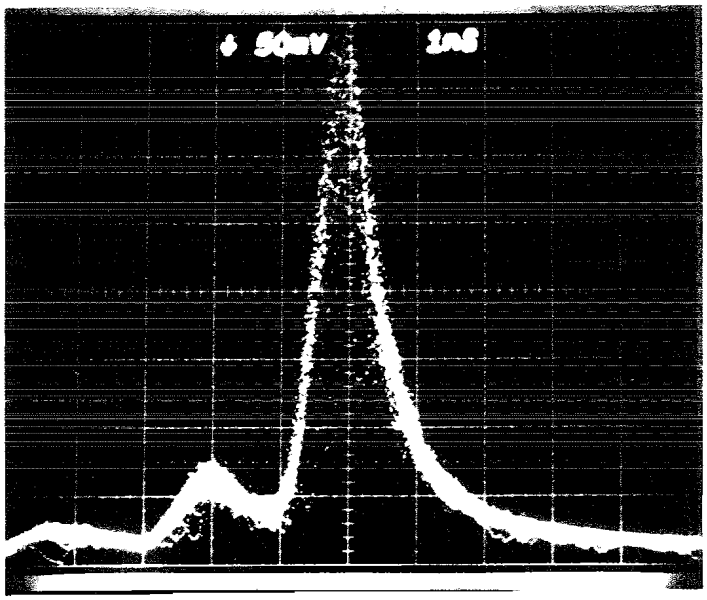

Figure 5.10. Mode-locked pulse for Er^{3+}- doped fibre laser (1ns/div.)

There are a number of methods available for demonstrating optical amplification. The technique described here is stimulated emission (i.e. a laser without feedback); but a variety of non-linear effects such as the stimulated Raman and Brillouin effects can also be employed[31-33].

The majority of current research has concentrated on semiconductor laser amplifiers which offer the advantage of a high gain/input power ratio (typically 1dB/mW electrical power)[28]. One disadvantage of this approach is that the semiconductor waveguide mode is considerably smaller than the fibre mode, so that a relatively large coupling loss (up to 10dB) is incurred when the amplifier is used as a repeater. The finite reflectivity of the facets also leads to a wavelength dependence of the gain (i.e. the amplifier is partially resonant near threshold). Precise stabilisation of the source wavelength and amplifier temperature ($\Delta T < 0.6^{o}C$ typically) is usually required to maintain a high gain.

An immediate advantage of a fibre-based amplifier is that it can be spliced with low loss and low reflectivity ($< -50dB$)[34] into a fibre system. The very low reflectivity makes possible true travelling-wave operation of the amplifier, thus reducing any temperature-dependent, or mode-pulling, effects that might occur. The gains measured are also typically of the order of 1dB/mW, although in this case the power referred to is optical, not electrical. The design and performance of fibre-amplifiers is described in the following sections.

5.2.1 Erbium-doped fibre amplifiers

Erbium-doped fibre amplifiers have attracted considerable interest[35] because they operate in the wavelength region of 1.54μm, the lowest-loss window for silica optical fibres. As is evident from the preceding

chapters, they can be optically pumped at a variety of wavelengths, but the most successful pump band to date has been from 650-680nm.

5.2.1.1 Amplifier design

The three-level nature of the transition at 1.54μm results in a pump threshold that must be exceeded in order to observe gain. Below this pump power the fibre exhibits loss. The pump threshold can be computed from equation (2.28), and the typical variation of gain with pump power is shown in Figure 2.9.

In accordance with equation (2.29) the gain increases linearly at first, as the pump is increased above the threshold value, and then begins to saturate, tending to the value $n_T \sigma \ell$. The saturation characteristics are complicated by an additional absorption from the excited level (see Chapter 3) which results in pump absorption even when the ground-state is virtually emptied. This effect prohibits pump wavelengths below 650nm, but is negligible at 665nm.

The expression for the amplifier gain (2.28) contains the term W_f, the stimulated transition rate. Any increase in W_f, either from amplified spontaneous emission or from the signal to be amplified, therefore decreases the amplifier gain. Saturation will be significant if

$$W_f \approx \frac{R + 1/T}{2} \qquad (5.1)$$

since in this case the integrand of equation (2.28) falls to half its original value. It is clear that the exact value of W at which gain saturation becomes significant depends on the pump rate R. For typical pumping conditions (P = 40mW, $A_{eff} = 2\times10^{-11}m^2$, $\sigma_p/\sigma_\ell = 0.5$) the stimulated power required is of the order of 5mW, corresponding to a signal input power of the order of 15μW for an amplifier gain of 25dB. Saturation is

restricted to the last stage of the amplifier, and since it is reduced at higher pump values it is preferable to counter-propagate the pump and signal beams.

The core diameter of the amplifying fibre is an important consideration in achieving high gains. Because of the large difference between the pump and signal wavelengths, the fibre can usually support more than one mode at the pump wavelength. Higher-order modes near cutoff have poor overlaps with the fundamental signal mode and therefore contribute little to pump efficiency. However, for a fibre with a V-value in the region 2.5-3.5 at the pump wavelength, it is relatively easy to launch the majority of the pump into the HE_{11} mode, and so ensure a good overlap. The variation of gain with fibre V-value was discussed in Chapter 2.

A further consideration is that in any systems deployment, the fibre would have to be spliced to standard telecommunications fibre, which generally has a larger spot size at the signal wavelength (~ 4μm). Techniques for splicing fibres of different spot sizes have been developed[36], and the additional gain provided by a small spot size in an amplifier fibre more than outweighs the splice losses.

The optimum fibre length depends on the dopant concentration, the pump power and the wavelength and also on the effective area. The critical condition is that the pump power at the end of the fibre should be sufficient to bleach the absorption at the signal wavelength (i.e. $\eta R = 1/T_{21}$). A knowledge of this saturation power

$$P = \frac{A_{eff}}{\eta} \frac{h\nu_p}{\sigma_p T_{21}} \qquad (5.4)$$

is experimentally sufficient to determine the correct length.

Amplifier gain is inevitably accompanied by noise in the form of spontaneous emission. The output power due to amplified spontaneous emission in a four-level amplifier can be expressed as (2.36)

$$P_{out}(\nu) = h\nu \left\{ \exp G(\nu) - 1 \right\} \tag{5.5}$$

where $G(\nu)$ is the gain at a signal frequency ν. A similar expression can be written for a three-level amplifier

$$P_{out}(\nu) = h\nu \left\{ \exp G(\nu) - 1 \right\} \left[\frac{n_2}{n_2 - n_1} \right] \tag{5.6}$$

where, because of the complicated length dependence in equation (2.34), n_2 and n_1 represent average populations in the excited state, and ground level, respectively. If a three-level amplifier is operated just above threshold, so that $n_2 \simeq n_1$, the spontaneous output is considerably higher than for an equivalent four-level amplifier. However, if the amplifier is operated in a region of high pump saturation, i.e.

$$P_{pump} \gg \frac{A_{eff}}{\eta} \frac{h\nu_p}{\sigma_p T_{21}} \tag{5.7}$$

the inversion parameter $F = n_2/n_2 - n_1$ tends to unity, and the amplifier performance is similar to that of a four-level amplifier.

Amplified spontaneous emission contributes to a mean noise photon rate N over an optical bandwidth $\Delta\nu (= \nu_2 - \nu_1)$ given by

$$N = \int_{\nu_1}^{\nu_2} F \left\{ \exp G(\nu) - 1 \right\} d\nu \tag{5.8}$$

where

$F = 1$ for a four level amplifier

$$F = \frac{n_2}{n_2 - n_1}$$ for a three-level amplifier

The mean square detector noise current due to spontaneous emission is then[37]

$$i_N^2 = 2Nh\nu\ Be\eta \qquad (5.9)$$

where

B is the detection bandwidth

e is the electron charge

η is the detector quantum efficiency

5.2.1.2 Amplifier configuration

The experimental configuration chosen for the Er^{3+}-doped amplifier is shown in Figure 5.11. Initial experiments were performed with the argon-ion laser as the pump source, but it was found to be much better to use an argon-ion laser pumped DCM dye laser, which was tunable from 620nm-690nm. The signal was provided by a 1.54μm InGaAsP DCPBH laser. The laser diode was mounted on a pair of thermoelectric coolers (Melcor Ltd) which permitted temperature tuning of the laser wavelength over an 8nm range from 1.532μm-1.540μm. A typical laser spectrum is given in Figure 5.12. It can be seen that the output power is distributed over a number of modes spaced by approximately 1nm, with about 50% of the power in the dominant longitudinal mode.

In addition to the DC power supply (C.I.R.L. Ltd.), the laser could be modulated directly with either a Marconi signal generator or a Philips pulse generator. The mounting of the laser diode prevented modulation above a few hundred MHz and the majority of the measurements were made for a signal bandwidth of 140Mbit/s.

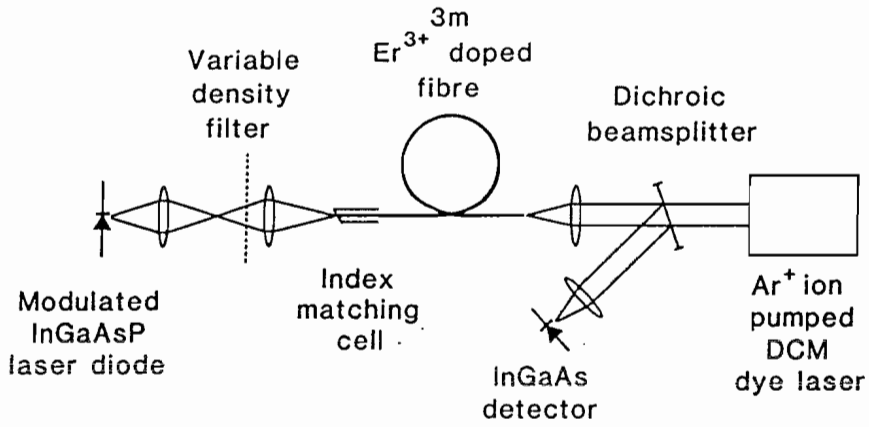

Figure 5.11. Experimental configuration of erbium-doped fibre amplifier

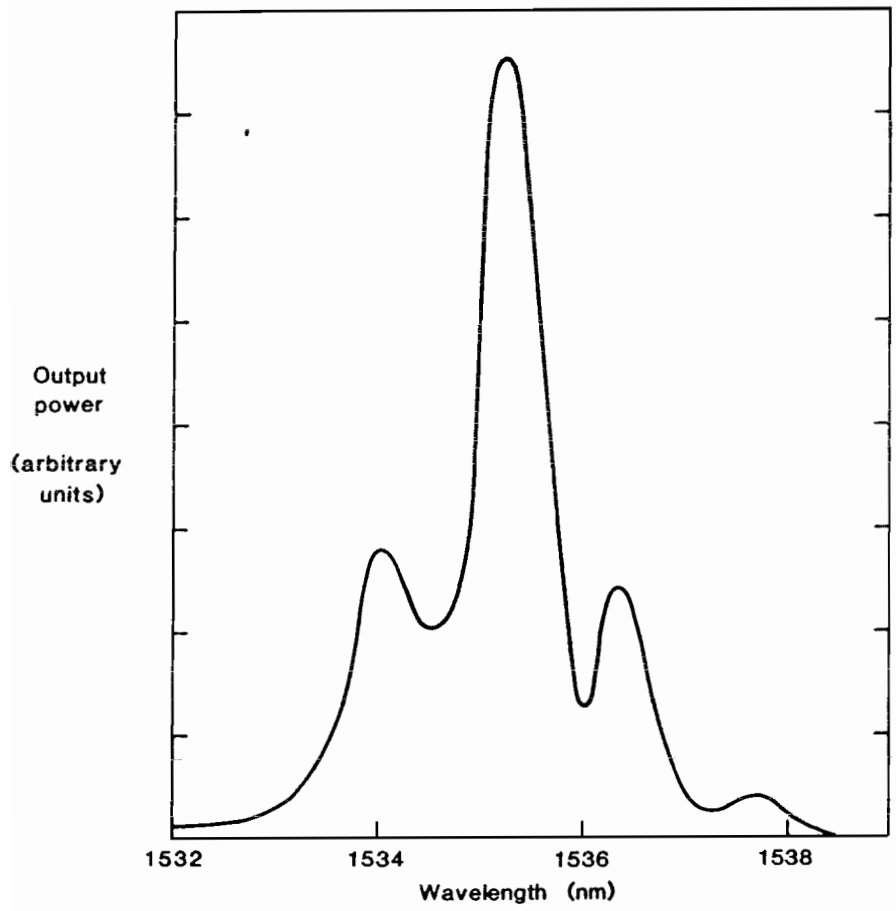

Figure 5.12. Spectrum of probe laser
(InGaAsP DCPBH) at 1.54um

In order to vary the signal power a series of neutral density filters could be inserted into the collimated signal path. The filters were calibrated at 1.54μm on a Perkin-Elmer spectrophotometer. For experimental convenience, light from the laser diode was first launched into a 1.5μm fibre coupler which had a loss of 0.5dB and a splitting ratio of 10dB at 1.54μm. The coupler was fabricated from an undoped fibre which matched the doped fibre ND263. The second output port provided a monitor for the signal power and wavelength. Light was launched into the doped fibre ND263 via an index-matched butt splice, and the splice loss was measured to be less than 1dB.

In order to prevent the onset of lasing, care must be taken to eliminate feedback, both from the fibre ends, and from plane surfaces in collimated beam paths. The signal input was index-matched as shown in Figure 5.11 and index-matching oil was inserted at the butt splice to reduce Fresnel reflection. Because of the high CW pump power (~ 100mW) it was not possible to place index-matching oil at the pump input, but the fibre was cleaved at an angle to reduce reflection.

The doped fibre used throughout these experiments was 90μm diameter ND263. The characteristics of this fibre are given in Table 3.1. The launch efficiency was 55 ± 5%, measured on a similar undoped fibre and verified by measurement of the transmitted pump power, which was monitored throughout the experiment. Counter-propagation of the pump and signal beams improves the amplifier saturation characteristics (see previous Section) and also considerably eases experimental alignment.

Output signal extraction was performed with a dichroic beamsplitter (90%R at 1.5μm; 85%T at 670nm) and a biased InGaAs p.i.n. diode. The load resistance was provided by the 50Ω input impedance of either a Tektronix

digital sampling head or a Marconi Spectrum Analyser. Although this detection scheme is simple and insensitive, it yielded excellent results in conjunction with the fibre amplifier.

5.2.1.3 Power transfer characteristic and gain saturation

Gain measurement in three-level amplifiers cannot be made by switching the pump on and off, since the fibre has an intrinsic absorption at the signal wavelength. The input signal was measured initially by placing the 1.5μm coupler output on the pump launch micromanipulator. In this way the same detection system (dichroic beam splitter, microscope objectives, detector) was used alternately to measure the input, and output, signals so that any losses in the detection were automatically compensated. The butt splice loss cannot be monitored in this way but was estimated from a cut-back measurement to be 1dB ± 0.5dB. The gain measurements presented here include the splice loss, and therefore represent a fibre/fibre signal gain. The dependence of the amplifier gain on pump power is plotted in Figure 5.13. The threshold of 12mW is in excellent agreement with the theory of Chapter 2. The total attenuation of the fibre at 1.54μm was measured in situ to be 32 ± 2dB. This corresponds well with the gain at high pump powers (28dB at 100mW), indicating a high degree of inversion; $F \simeq 1$. Note that a high gain (20dB) is available for only 20mW of absorbed power in the fibre.

The power-transfer characteristic of the amplifier is given in Figure 5.14. The measurement was made at an absorbed pump power of 60mW. The gain begins to saturate at an input power greater than -20dBm, when the output power is +5dBm. This is in good agreement with a simple saturation calculation following equation (5.1). A 3dB compression from linear gain is observed for an output power of +7dBm. For comparison, the 3dB point in a semi-

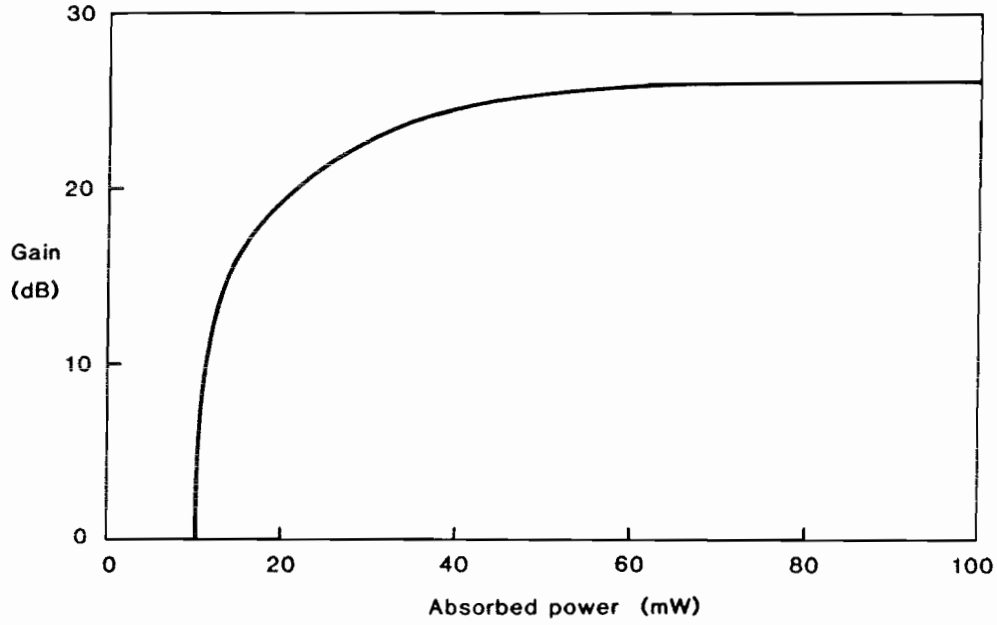

Figure 5.13. Gain versus pump-power for erbium-doped fibre amplifier

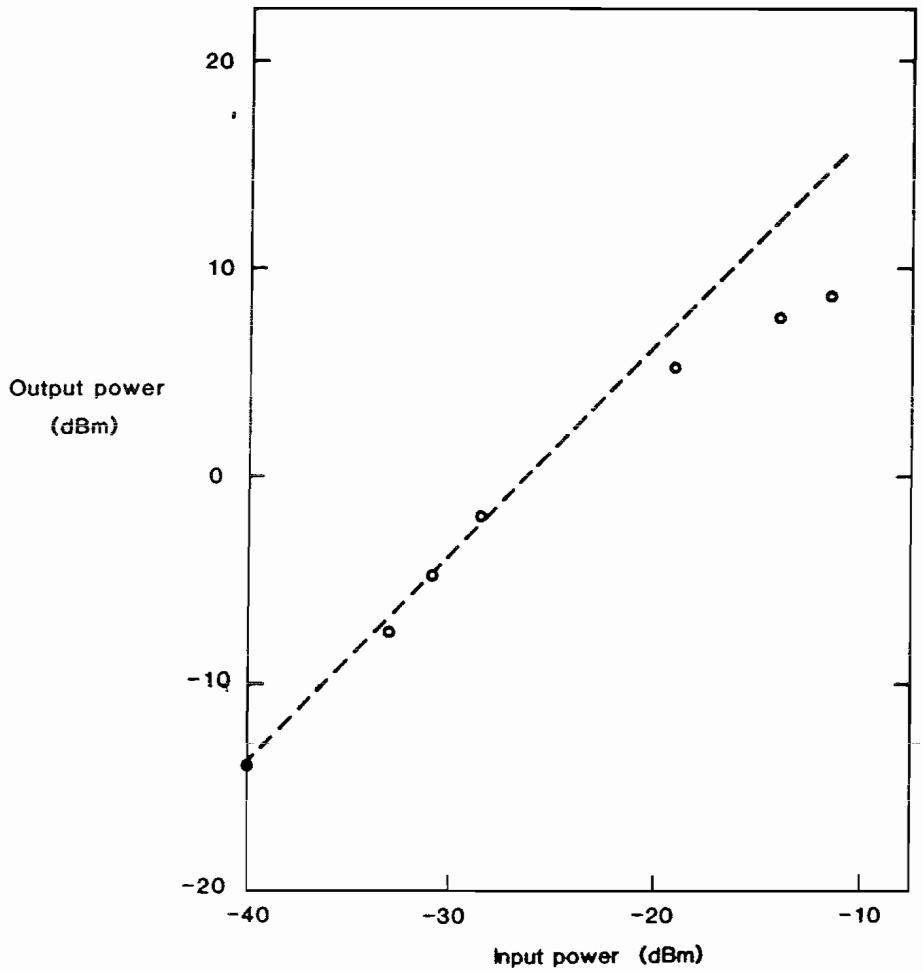

Figure 5.14. Power transfer characteristic of erbium-doped fibre amplifier

conductor laser amplifier typically occurs at output powers between -18dB and -10dBm [28]. The fibre amplifier can thus handle considerably more power.

5.2.1.4 Spectral dependence of gain

The spectral dependence of the gain is an important consideration if an amplifier is to be incorporated in wavelength-multiplexing systems. Ideally one would like as broad a bandwidth as possible.

The mounting of the laser diode permitted a temperature tuning of the wavelength over 8nm by varying the current supplied to the thermoelectric coolers. The gain was measured whilst monitoring the signal wavelength.

In Figure 5.15 the measured spectral dependence of the amplifier gain bears a close resemblance to the fluorescence spectrum (Chapter 3), as demonstrated by the dotted line superimposed on the Figure. The highest gains are available in a 300GHz bandwidth centred on 1.536μm. This would be sufficient for 30 x 10GHz spaced channels in a coherent W.D.M. system[38]. The broad fluorescence spectrum (Chapter 3) suggests that gains in excess of 10dB should be available over a much larger bandwidth of 4THz (30nm).

5.2.1.5 Pump wavelength

The measurements on Er^{3+}-doped fibre amplifiers presented in this Chapter have relied exclusively on a DCM dye laser as the pump source. The dependence of the gain on pump wavelength determines whether the dye laser might be replaced by a diode laser, such as those under development at NEC and Hitachi[39].

Figure 5.16 shows the variation in the amplifier gain as the pump was tuned from 650nm-680nm. The high degree of saturation is evident from the flat response of

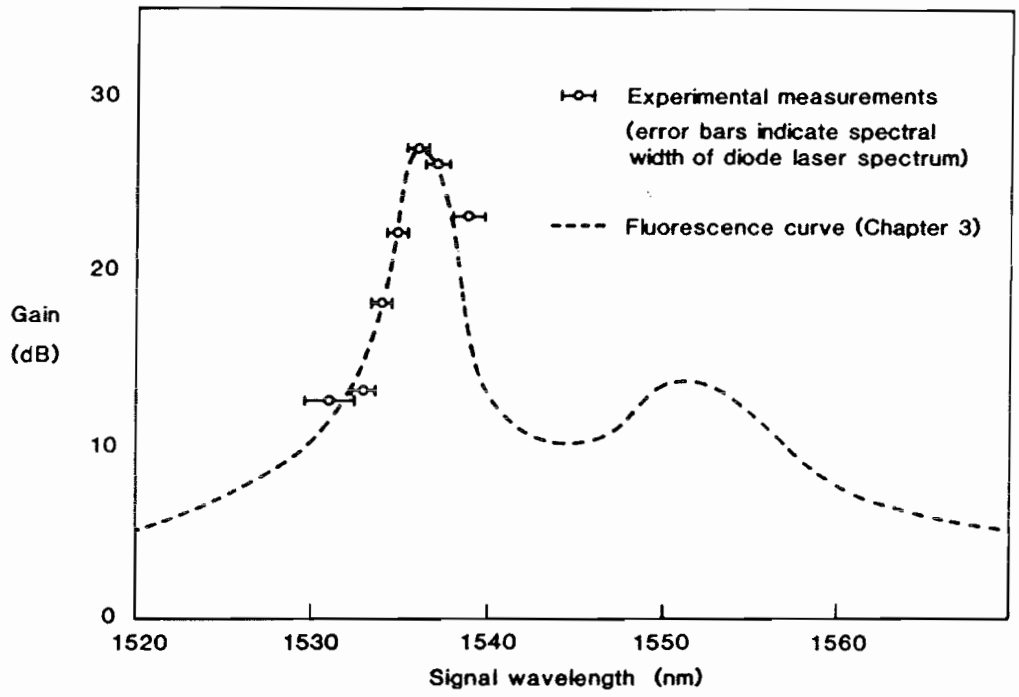

Figure 5.15. Spectral dependence of erbium-doped fibre amplifier gain

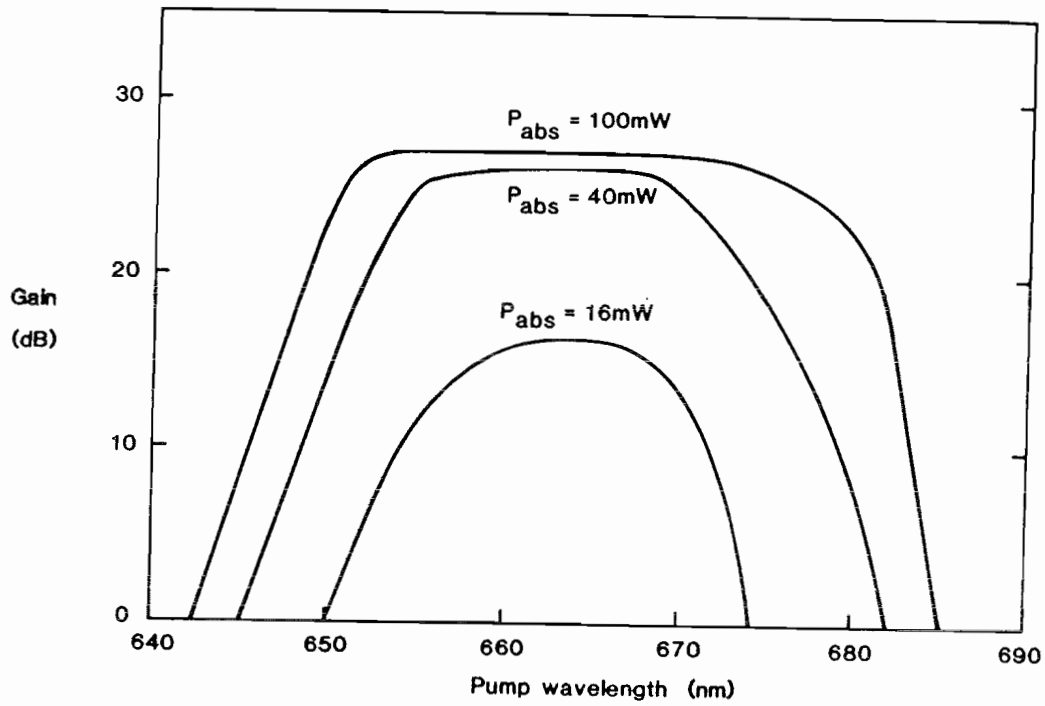

Figure 5.16. Dependence of erbium-doped fibre amplifier gain on pump wavelength

the gain over 25nm, in spite of the variation in absorption cross-section. The results suggest that it should be possible to pump the Er^{3+}-doped fibre with laser diodes having wavelengths in the range 655nm-675nm, provided the power requirements can be met.

5.2.1.6 Amplifier noise

In Section 5.2.1.1 an expression is derived relating the amplified spontaneous emission power to the spectral gain of the amplifier. Numerical integration of equation (5.8) using the spectral gain data from Figure 5.15 yields an amplified spontaneous emission power of (50±5)μW, which is in excellent agreement with the experimental measurement.

The noise associated with an amplifier determines its usefulness both as a repeater and as a receiver pre-amplifier. The amplifier noise in the region of 100MHz was measured on a Marconi Spectrum Analyser to be 200pA/√Hz, corresponding to a sensitivity of -45dBm at 140Mbit/s for a 10^{-9} bit error rate. This value compares favourably with state-of-the-art APD detectors at 1.5μm and illustrates the potential of the doped fibre as a pre-amplifier. Calculation of the shot-noise associated with the amplified spontaneous emission suggests that an even greater sensitivity of -62dBm ought to be achievable. The reasons for the discrepancy are not at present understood, but may result from residual pump leakage and additional pump noise. Further experiments are underway to pinpoint the noise source. It should be noted that the sensitivity was measured without spectral filtering of the amplified spontaneous emission. With narrow sources and spectral filters it ought easily to be possible to achieve shot-noise limited sensitivity (-70dBm at 140Mbits).

5.2.2 Neodymium fibre amplifiers

Neodymium-doped fibre amplifiers operate at 1.088μm as a four-level laser system and therefore exhibit gain at all values of the pump power. They can be pumped at a variety of wavelengths, including the important region from 750nm-850nm which is spanned by GaAlAs diode lasers.

The gain is given by the expression (2.22)

$$G = \frac{P_{abs}}{A_{eff}} \frac{1}{\eta} \frac{\sigma T}{h\nu_p} \qquad (5.10)$$

and is typically ~ 1dB/mW for a 820nm pump source. According to equation (2.20), gain saturation will be significant for

$$W \sim \frac{1}{T_{32}} \qquad (5.11)$$

since the denominator of this equation contains the term $(1 + W_{32})$. Thus in four-level amplifiers the gain saturation is not a function of pump power. Given typical fibre parameters ($A_{eff} = 10^{-11}$ m^2, $\sigma = 2 \times 10^{-24}$ m^2) the condition is fulfilled for a signal power of approximately 2mW.

The pump and signal wavelengths are sufficiently close to permit single-mode operation at both wavelengths, thereby ensuring a good spatial overlap between the population inversion and the signal mode. The optimum signal V-value appears to be in the region of 1.8. Because of the low loss of the Nd^{3+}-doped fibre, the optimum fibre length is not a critical consideration. Assuming a fibre loss of 10dB/km, and a pump wavelength of 820nm, a mere 10μW of pump power is sufficient to overcome fibre losses. Given a typical launch power of 5-10mW these figures indicate an optimum length of 6-7m for a fibre

with a dopant concentration of 10^{25} m^{-3}. It should be noted, however, that an additional 10m of fibre would only decrease the gain by 0.1dB.

So far only gain measurements have been made on Nd^{3+}-fibre amplifiers and further results will be published separately[40]. The experimental configuration for the amplifier is shown in Figure 5.17. A CW Nd^{3+}-doped fibre laser (see Chapter 3) was used as the signal source, since its operating wavelength is matched to the peak gain of the doped fibre. In order to modulate the signal, an acousto-optic deflector (Isomet 1205C) was inserted between the laser and the amplifier. The bandwidth of the A.O.D. limited the modulation rate to 4MHz. The amplifier fibre was a 5m length of ND199 pumped by a Sharp LT015 820nm laser diode. The signal was extracted with a dichroic beamsplitter (100%R at 1.088μm, 85%T at 826nm) and the detector was an InGaAs p.i.n. diode with a quantum efficiency of 0.6 at 1.088μm.

The maximum gain measured was 5dB for an absorbed pump power of 6mW. Although the gain is much smaller than for the Er^{3+}-doped fibre, it has been achieved with a compact laser-diode pump source. Recent experiments with high-power laser diodes (40mW output), and an improved launch efficiency (40%)[2], indicate that gains of the order of 10dB or more should be possible in neodymium-doped fibre amplifiers.

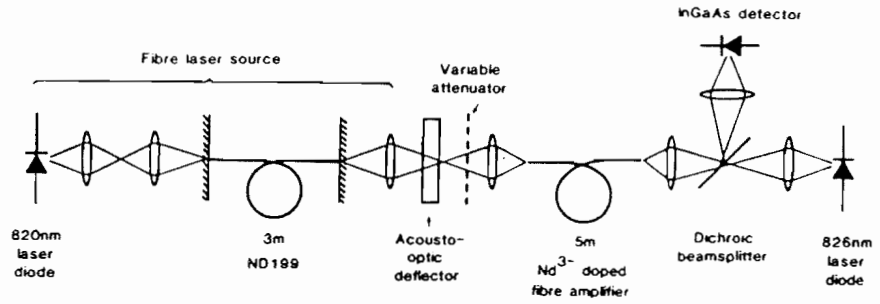

Figure 5.17. Experimental configuration of neodymium-doped fibre amplifier

5.3 Summary

The techniques of Q-switching and mode-locking fibre lasers doped with neodymium and erbium have produced pulses ranging from less than 1ns to greater than 1μs in duration. The efficiency under Q-switched operation has been demonstrated to be equal to that observed under CW conditions. It is thus possible to construct fibre lasers which usefully convert CW pump radiation into high-power pulses. The pulsed Er^{3+}-doped fibre laser has been applied to generate Raman shifted light.

The high gain of the optical fibre laser configuration has been exploited in the design of amplifiers. Gains of up to 28dB at 140 Mbit/s have been observed. The gain is exhibited over the broad fluorescence linewidths of the Er^{3+} and Nd^{3+} ions in the glass matrix, which should be useful for wavelength-multiplexed amplifiers. The doped fibre has been used as a preamplifier to considerably improve the performance of a simple optical receiver.

APPENDIX 5A : BISTABILITY IN THREE-LEVEL ER^{3+} FIBRE LASERS

The optimum length of a three-level laser such as the Er^{3+}-doped fibre laser corresponds to an output pump power at threshold which is just sufficient to saturate the absorption at the end of the fibre. If the fibre length is increased further, the additional fibre contributes to a cavity loss. Normally an increase in the rate of stimulated emission reduces the population inversion and the gain decreases. In the region of fibre where the majority of the ions are in the ground-state, however, an increase in the stimulated rate actually decreases the loss. Depending on the overall length of the fibre, the small-signal gain can therefore be less than the large-signal gain at certain pump powers. This is the origin of the bistable threshold observed in long Er^{3+}-doped fibre lasers[41].

A typical experimental result is plotted in Figure 5.18. The pump source was an argon-ion laser at 514.5nm and the fibre cavity consists of a 3m length of fibre ND263 (120μm diameter).

The pump power is increased until the (small-signal) gain is equal to the round-trip cavity loss. Thereafter, any increase in pump power results in a sharp switch-on of the laser output. As the stimulated power increases it first increases the nett round-trip gain and finally saturates it sufficiently for equilibrium to exist. The laser is now effectively well above threshold, and a reduced pump power will still support oscillation. Eventually, however, the laser reaches the unstable regime where a decrease in the stimulated rate results in a decrease in the nett gain below the threshold value, and the laser output switches off.

The behaviour is well-modelled by the theory for the Er^{3+}-laser presented in Chapter 2 and Figure 5.19 shows the theoretical variation of W, the stimulated rate,

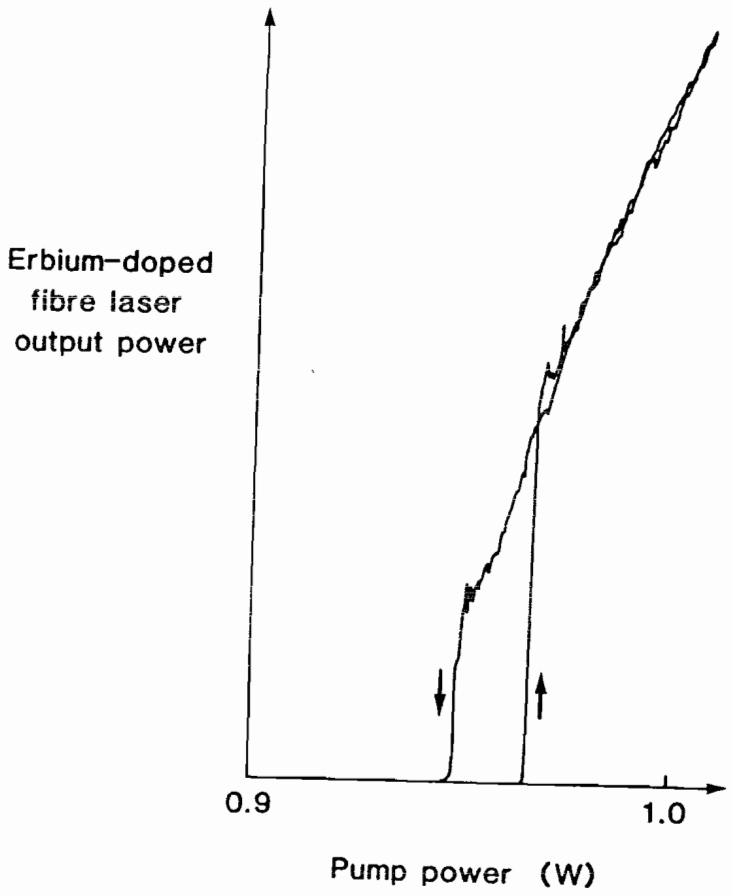

Figure 5.18. Bistable threshold of erbium-doped fibre laser

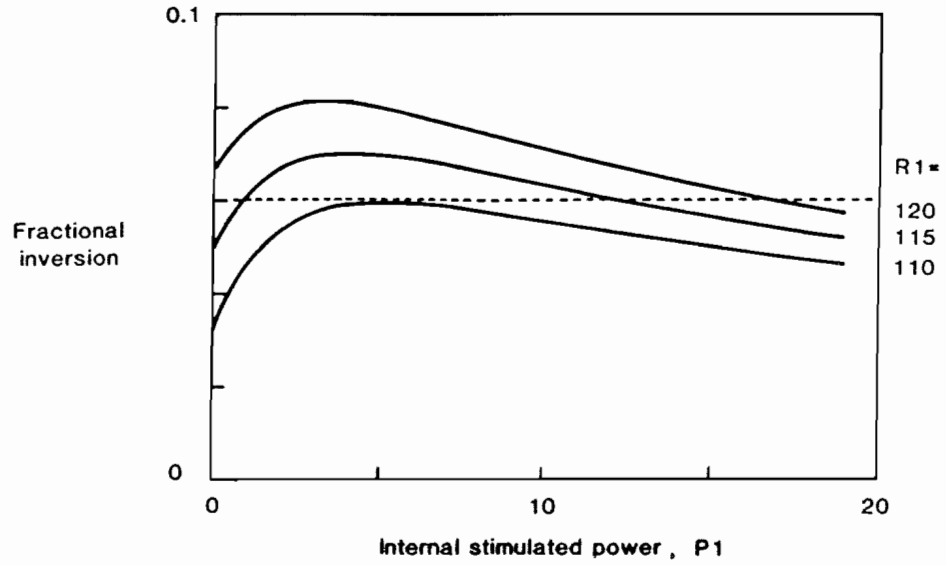

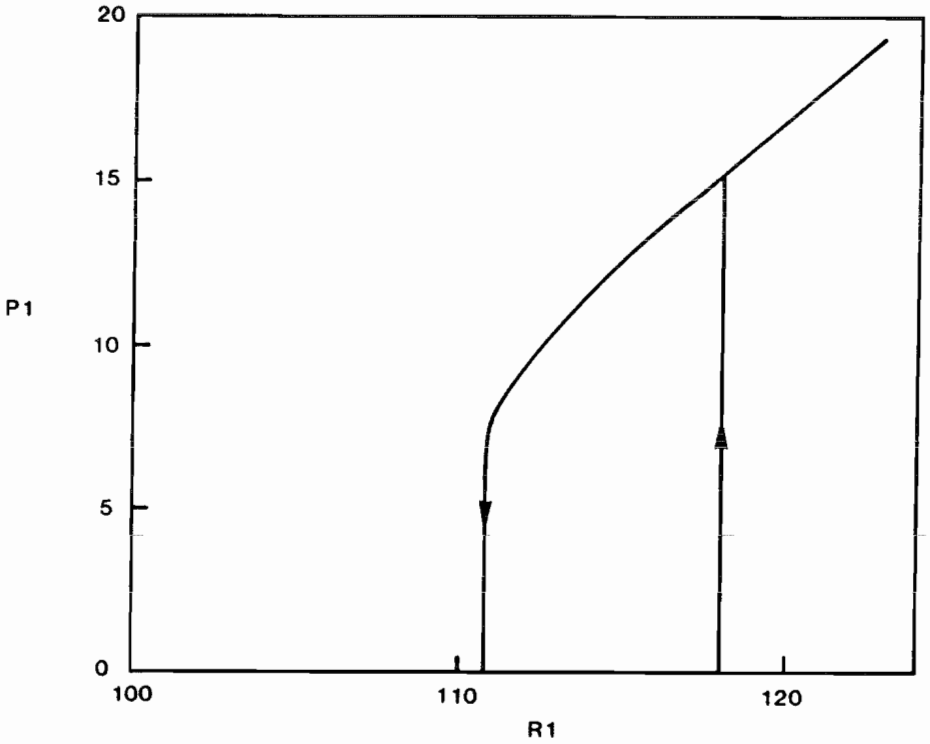

Figure 5.19. Theoretical modelling of erbium-doped fibre laser bistability

with the pump rate R, in order to maintain the gain at the value G_T. Since the pump rate R cannot be self-adjusted by the laser, the output power follows the boundary loop.

Bistability in a variety of optical systems has aroused considerable interest worldwide because it can be used as the basis of an optical logic for data-processing and computing . A measurement of the switching times has been made by L. Reekie, and the results are presented in Figure 5.20. An immediate problem observed is a delay of 2-3ms between the input pump pulse and the laser output. The delay is due to the relatively large pumping energy ($\sim$ 10μJ) required to significantly change the population inversion. The long switching time and large energy are a barrier to the practical use of this form of bistability. Nevertheless, it provides a simple demonstration of some of the properties of bistable systems.

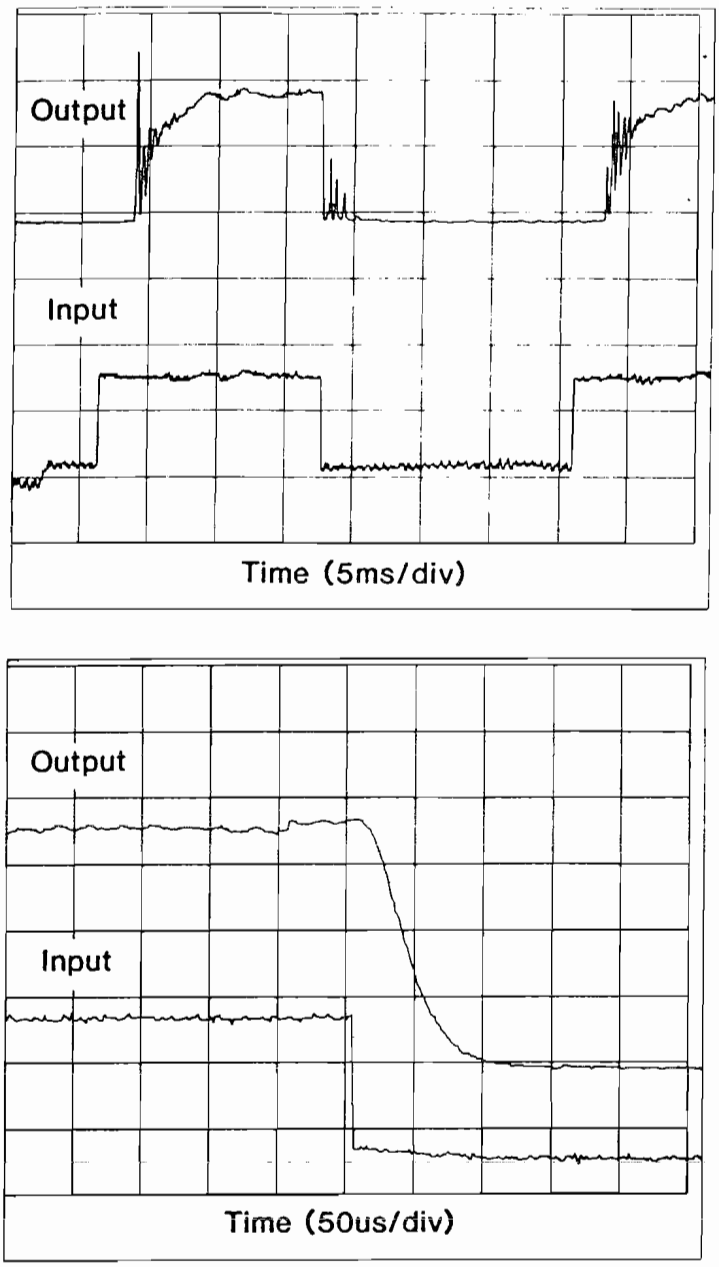

Figure 5.20. On-off switching times for bistable erbium-doped fibre laser

References to Chapter 5

1. F.J. McClung and R.W. Hellwarth:
"Giant optical pulsations in ruby",
J. Appl. Phys., 1962, 33, pp.828.

2. A.H. Hartog, A.P. Leach and M.P. Gold:
"Distributed temperature sensing in solid-core fibres",
Electron. Lett., 1985, 21, pp. 1061-1062.

3. C.C. Cutler:
"The regenerative pulse generator",
Proc. IRE., 1955, 43, pp.140-148.

4. A.J. DeMaria, W.H. Glenn, M.J. Brienza and M.E.Mack:
"Picosecond laser pulses",
Proc. IEEE., 1969, 57, pp. 2-25.

5. K.B. Eisenthal, R.M. Hochstrasser, W. Kaiser and A. Laubercau:
"Picosecond Phenomena III",
Springer-Verlag, 1982.

6. R.J. Mears and L. Reekie:
"A high-power tunable erbium-doped fibre laser operating at 1.55μm",
Proc. CLEO., 1987, Baltimore.

7. I.P. Alcock, A.C. Tropper, A.I. Ferguson and D.C. Hanna:
"Q-switched operation of a neodymium-doped monomode fibre laser",
Electron. Lett., 1986, 22, pp. 84-85.

8. I.M. Jauncey, J.T. Lin, L. Reekie and R.J. Mears:
"An efficient diode-pumped CW and Q-switched single-mode fibre laser",
Electron. Lett., 1986, 22, pp. 198-199.

9. L. Reekie, I.M. Jauncey and D.N. Payne:
"Near optimum operation of a diode-laser pumped fibre laser",
Submitted to ECOC, Helsinki, 1987.

10. R.J. Mears, L. Reekie, S.B. Poole and D.N. Payne:
"A low threshold tunable CW and Q-switched fibre laser at 1.55μm"
Electron. Lett., 1986, 22, pp. 159-160.

11. E.P. Ippen and R.H. Stolen:
"Stimulated Brillouin scattering in optical fibers",
Appl. Phys. Lett., 1972, 21, pp. 539-541.

12. R.H. Stolen and E.P. Ippen:
"Raman gain in glass optical waveguides",
Appl. Phys. Lett., 1973, 22, pp. 276-278.

13. E.P. Ippen, C.V. Shank and T.K. Gustafson:
"Self-phase modulation of picosecond pulses in optical fibres",
Appl. Phys. Lett., 1974, 24, pp. 190-192.

14. R.H. Stolen and A. Ashkin:
"Optical Kerr effect in glass waveguide",
Appl. Phys. Lett., 1973, 22, pp. 294-296.

15. Y. Fujii, B.S. Kawasaki, K.O. Hill and D.C. Johnson:
"Sum-frequency light generation in optical fibres",
Opt. Lett., 1980, 5, pp. 48-50.

16. T.Y. Chang:
"Fast self-induced refractive index changes in optical media - a survey",
Optical Engineering, 1981, 20, pp. 220-231.

17. U. Osterberg and W. Margolis:
"Dye laser pumped by Nd:YAG laser pulses frequency doubled in a glass optical fibre",
Opt. Lett., 1986, 11, pp. 516-518.

18. R.G. Smith:
"Optical power handling capacity of low loss optical fibres as determined by stimulated Raman and Brillouin scattering",
Appl. Opt., 1972, 11, pp. 2489-2494.

19. R.H. Stolen:
"Polarisation effects in fiber Raman and Brillouin lasers",
IEEE J.Q.E., 1979, QE-15, pp. 1157-1160.

20. A.J. DeMaria, C.M. Ferrar and G.E. Danielson:
"Mode-locking of a Nd^{3+}-doped glass laser",
Appl. Phys. Lett., 1966, 8, pp. 22-24.

21. D.J. Bradley and W. Sibbett:
"Streak-camera studies of picosecond pulses from a mode-locked Nd-glass laser",
Opt. Commun., 1973, 9, p. 17.

22. I.P. Alcock, A.I. Ferguson, D.C. Hanna and A.C. Tropper:
"Mode-locking of a neodymium-doped monomode fibre laser",
Electron. Lett., 1986, 22, pp. 268-269.

23. H. Steinberg:
"The use of a laser amplifier in a laser communication system",
Proc. IEEE, 1963, 51, p. 943.

24. S.D. Personick:
"Applications for quantum amplifiers in simple digital optical communication systems",
Bell Syst. Tech. J., 1973, 52, pp. 117-133.

25. G. Zeidler and D. Schicketanz:
"Use of laser amplifiers in a glass-fibre communications system",
The Radio and Electronic Engineer, 1973, 43, pp. 675-682.

26. T. Mukai and Y. Yamamoto:
"Optical direct amplification for fibre transmission",
Rev. of Elect. Commun. Labs., 1983, 3, pp. 340-348.

27. J.C. Simon:
"Semiconductor laser amplifier for single-mode optical fibre communications",
J. Opt. Comm., 1983, 4, pp. 51-56.

28. M.J. O'Mahoney, A.J. Westlake and I.W. Marshall:
"Gain measurements of laser amplifiers for optical transmission systems at 1.5μm",
British Telecom Tech. J., 1985, 3, pp. 25-29.

29. M.C. Farries, M.E. Fermann, R.I. Laming, S.B. Poole, D.N. Payne and A.P. Leach:
"Distributed temperature sensor using Nd^{3+}-doped optical fibre",
Electron. Lett., 1986, 22, pp. 418-419.

30. V. Vali and R.W. Shorthill:
"Fiber ring interferometer",
Appl. Opt., 1976, 15, pp. 1099-1100.

31. M. Ikeda:
"Stimulated Raman amplification characteristics in long span single-mode silica fibres",
Opt. Comm., 1981, 39, p. 148.

32. D.W. Smith, C.G. Atkins, D. Cotter and R. Wyatt:
"Applications of Brillouin amplification in coherent optical transmission",
Proc. OFC., 1986, Atlanta.

33. K.C. Byron:
"Simultaneous amplification and pulse compression in a single-mode optical fibre",
Electron. Lett., 1986, 22, pp. 1275-1276.

34. K.A. Fesler:
Private Communication.

35. R.J. Mears, L. Reekie, I.M. Jauncey and D.N. Payne:
"High gain rare-earth-doped fibre amplifier at 1.54μm",
Proc. OFC., 1987, Reno, Nevada.

36. D.B. Mortimore and J.V. Wright:
"Low-loss joints between dissimilar fibres by tapering fusion splices",
Electron. Lett., 1986, 22, pp. 318-319.

37. S.O. Rice:
"Mathematical analysis of random noise",
Bell System Tech. J., 1944, 23, p. 282.

38. L.G. Kazovsky:
"Multichannel coherent optical communications systems",
IEEE J. Lightwave Tech., to be published.
Proc. OFC, 1987, Reno, Nevada, USA.

39. T. Suzuki:
"Recent progress in visible light semiconductor lasers",
Proc. CLEO., 1987, Baltimore.

40. R.J. Mears, L. Reekie, I.M. Jauncey and D.N. Payne:
"Optical fibre amplifiers based on rare-earth ions",
To be submitted to the Journal of Lightwave Technology, 1987.

41. L. Reekie, R.J. Mears, S.B. Poole and D.N. Payne:
"Optical bistability at 1.54μm in a Er^{3+}-doped single-mode fibre laser",
Proc. ECOC., 1986, Barcelona.

CHAPTER 6 : OPTICAL FIBRE COUPLERS AND THEIR ROLE IN FIBRE LASERS

The hybrid fibre lasers described so far in this thesis have relied to a greater or lesser extent on discrete-optical components, dielectric mirrors, gratings etc. In this chapter experiments are described on the fundamental fibre component, the optical fibre coupler, and its application to fibre lasers. The Chapter begins with a review of the optical fibre coupler followed by the description of a coupler fabrication technique. The important features of the coupler vis-à-vis fibre lasers are its loss and wavelength characteristics. During this work, which was mainly undertaken before the development of "active" fibres, a new theory of operation was proposed, and the experimental results are modelled accordingly. The chapter ends with a description of a number of all-fibre lasers.

6.1 Optical Fibre Couplers

A schematic of the optical fibre coupler is shown in Figure 6.1. The coupler is a four-port device which can be configured as a power divider, a switch, a wavelength filter or as the basis of a variety of interferometers.

A variety of techniques have been employed to create single-mode optical fibre couplers. The first successful method was to etch two fibres and draw them closely together so that the cores of the two fibres were in close proximity[1,2] (Figure 6.2a). By varying the refractive index of the medium surrounding the etched fibres the degree of evanescent interaction, and hence the coupling, could be adjusted. The disadvantage of this type of coupler is that it is rather unstable. Another technique which also relies on an evanescent interaction between light propagating on the two fibre cores is the

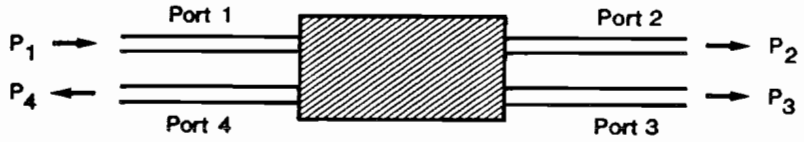

Figure 6.1. Schematic of optical fibre coupler

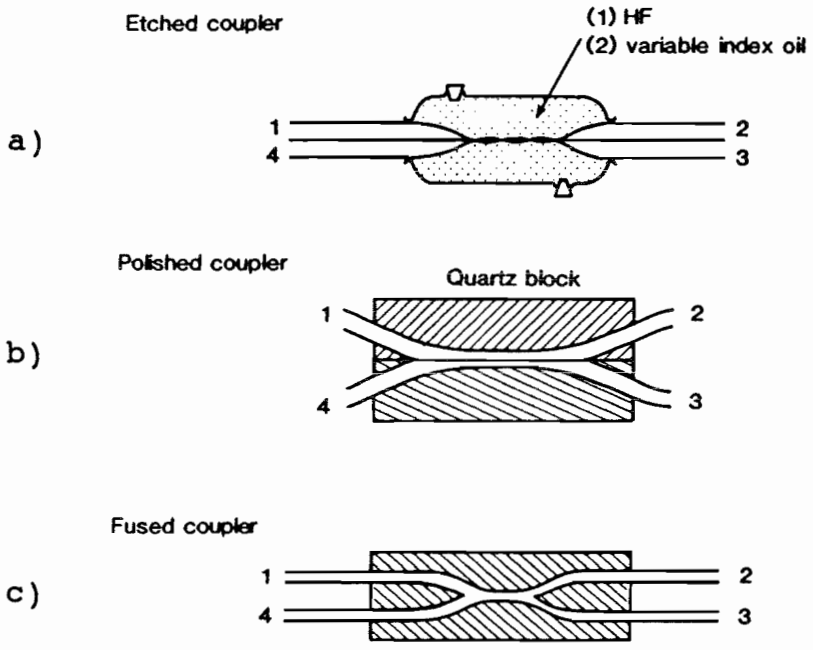

Figure 6.2. Optical fibre couplers
a) etched coupler
b) polished coupler
c) fused tapered coupler

polished coupler (Figure 6.2b). Here the fibre is mounted in a quartz block for mechanical stability, and polished to within a few microns of the core[3]. Two similar blocks are then brought into intimate contact, usually buffered with a very thin layer of index matching fluid. Small adjustments of one block relative to the other can be used to accurately vary the coupling coefficient. The polished coupler has been demonstrated to have a wavelength-dependent coupling coefficient which is the potential basis of a wavelength division multiplexer[4]. A wide variety of devices employing polished fibre couplers have already been demonstrated, including an all-fibre ring resonator[5], Michelson and Mach-Zehnder interferometers[6,7] and a fibre Sagnac interferometer for rotation sensing[8].

The third important coupler which has attracted considerable attention is the fused-tapered coupler[9-12] (Figure 6.2c). In this technique two fibres are brought together and then fused and tapered until coupling occurs. The advantage here is that the resulting coupler, after protection in a material which prevents surface flaws, is as robust and stable as the original fibre. Once a suitable heatsource has been developed, the method is quick and simple and a yield greater than 50% can be expected. For these reasons, and because it is widely considered to be the most suitable coupler for practical application, the fused tapered coupler was chosen for investigation.

The theory of operation of the fused tapered coupler has evolved slowly over the last three years. It was originally assumed that coupling occured as the result of an evanescent interaction, similar to the mechanism of the etched, and the polished coupler[13]. However it soon became apparent that the experimental results were at variance to this theory, and a new model was sought. In order to achieve coupling it was found that the V-value of the fibre had to be reduced to below the value where the core plays a significant role in the propagation of the

mode. It was proposed by the author, and by Bures et al[15], that coupling resulted from an interaction between modes of the large waveguide formed by the fibre cross-sections and the external refractive index. In fact two different models were proposed corresponding to weak and strong coupling, and subsequently a simple approximation to the strong coupling case was developed by Payne et al[16]. These models have been successful in describing the majority of the properties of single-mode fused tapered couplers. It would appear, however, that couplers with small coupling coefficients correspond more closely to evanescent devices. Recent work by Martinez et al at Southampton[17] has demonstrated the smooth transition between core mode and cladding mode that occurs in a fibre taper. This transition period is of great importance in determining the coupling and the loss characteristics of fused tapered couplers.

The primary goal of the work described in this chapter was to study the loss and coupling characteristics of the coupler with the aim of creating optical circuits and resonant cavities. During the course of this work the loss of fused tapered couplers was brought down from greater than 1dB to less than 0.2dB. The taper was identified as a major contributory loss source and great care was taken to optimise the fabrication procedure to produce smooth, gradual tapers. Subsequent work by Stewart and Love supports these findings[18]. The design of high quality optical resonant cavities requires precise control of the coupling coefficient. The original fabrication procedure could only control the coupling coefficient to within approximately ten percent and it was also discovered that the protection of the coupler in a medium of refractive index only slightly less than that of silica led to changes in this value. An investigation of the effect of changes in the refractive index of the medium surrounding the coupler was therefore undertaken. It was discovered that the influence of refractive index changes was strongly dependent on the degree of coupling;

if this was small, then so was the corresponding variation in coupling coefficient. Dramatic changes in coupling as the index of the external medium approached that of silica were observed for strongly coupled devices. This property suggested the design of a novel fibre switch, and a research programme to investigate the effect of liquid crystals on coupler behaviour has been instigated. The results for the dependence of coupling coefficient on external index have been successfully accounted for by the "high-V-guide model", although the very weakly coupled devices show a less pronounced effect than is predicted.

Single-mode fibre couplers can be operated with low loss over a wide range of wavelengths. Before this work was undertaken it had been demonstrated that polished couplers exhibit a periodic wavelength response, with a period of a few hundred nanometers[19]. A programme of measurement of the wavelength characteristics of the fused tapered coupler was therefore commenced. It was discovered that the "strongly coupled" devices had a markedly periodic response, and by elongating the coupling length and decreasing its width, periods as small as 12nm were demonstrated[14]. Subsequent work by Yataki at Southampton has yielded even smaller periods of 2nm [20]. These values are one or two orders of magnitude smaller than have been demonstrated for polished devices, which arises from the different coupling mechanism. Once again, the "high-V-guide model" has been successful in modelling the results. However, the wavelength response of standard equal splitting ratio couplers is more marked than would be predicted by the model, due to the partly evanescent nature of the coupling interaction. Recent work by Mortimore[21] to vary the excitation of the symmetric and antisymmetric modes of the coupling region has been successful in producing a largely wavelength independent coupler for telecommunications. However, the periodic splitting ratio coupler described here has a number of applications to wavelength filters, and possibly as wavelength division multiplexers[20]. The second half of this

chapter describes the use of wavelength selective couplers in a novel fibre ring laser[22]. The fibre ring laser obviates the requirement for carefully aligned resonator mirrors. The all-fibre ring resonator employs a single fused tapered coupler to provide both the input coupling of the pumping radiation and output coupling at the lasing wavelength. A major advantage of the ring laser is that the output power is automatically carried by a fibre. It is thus fully compatible with other single-mode fibre systems.

6.1.1 Fused tapered coupler fabrication

One of the primary requirements of a fabrication procedure for fused-tapered couplers is a suitable heat source. Silica has a working temperature of approximately 1800°C, which is beyond the range of the majority of resistance heaters. Graphite furnaces meet the temperature specification, but require inert atmospheres, and tend to leave deposits on the fibre surfaces, which leads to high loss. The latter problem has also been encountered with resistance heaters based on non-oxidising metals such as platinum or iridium. The heat source chosen for this work was an oxy-butane flame, which, in spite of temperature irregularities and poor reproducibility, has led to coupler losses of less than 0.2dB.

A schematic of the coupler fabrication procedure is shown in Figure 6.3. Two identical fibres were stripped of their protective coatings over a short length (approximately 10cm), cleaned with methanol and secured to two motor-controlled movable platforms. The fibres were usually given a single twist together to ensure good fusion when the flame was applied. Light was launched into one fibre from a HeNe or semiconductor laser, or from a white light source filtered by a monochromator, according to the intended operational wavelength, and the power output of both fibres was monitored. The fibres were then fused and tapered in the oxy-butane flame. Two

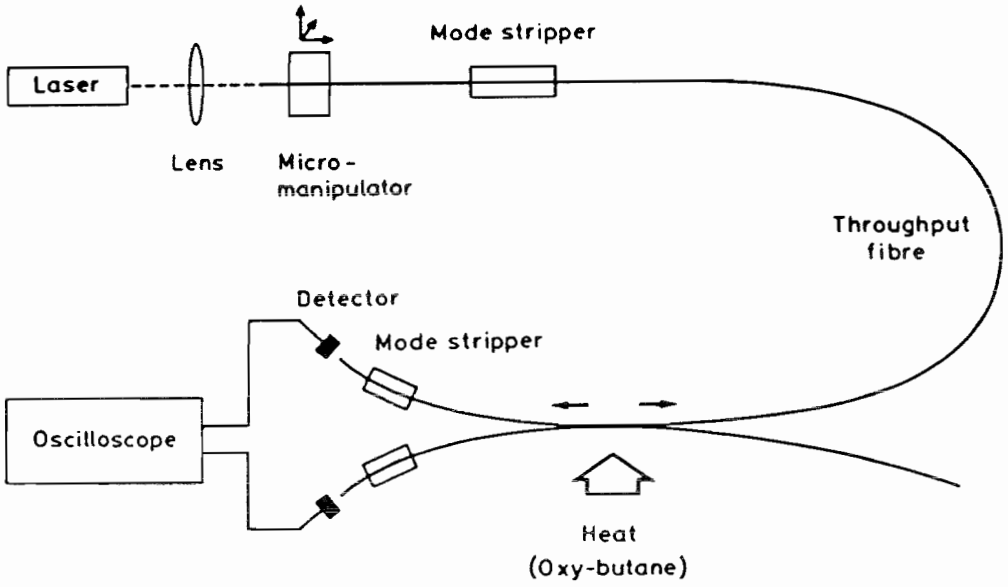

Figure 6.3. Fabrication technique for fused tapered coupler

different techniques were implemented to provide the tension necessary to taper the fibres once they had been heated to the working temperature. The majority of couplers for the experiments on refractive index and wavelength variations were fabricated using a simple d.c. motor controlled pulling rig designed and constructed by R.J. Mansfield. This rig produced gradual, symmetrical tapers, but required careful optimisation of pulling speed to match each set of flame conditions. A typical taper profile is shown in Figure 6.4a. During the course of this work a stepper-motor controlled rig was set up, with the option of translating both fibres relative to the flame during the tapering process. Although this resulted in unsymmetrical tapers, better reproducibility was achieved. A typical taper made on this rig is shown in Figure 6.4b. It is demonstrated in Section 6.4 that the symmetry of the taper is not important provided that both taper angles are less than a critical value.

During the tapering process the fundamental LP_{01} mode launched on one of the fibres expands and excites the lowest order symmetric and antisymmetric modes of the glass-air guide formed by the fusion of the two fibres. These modes have different propagation constants and thus, at the output taper, power is launched into both fibre cores. A typical power output from one coupler port during fabrication is shown in Figure 6.5. The oscillations correspond to power being transferred from one output fibre to the other as the length of the coupler is increased. Although it was not necessary to taper the coupler beyond the first complete exchange of power to achieve any desired coupling ratio, strongly coupled devices, in which power has been exchanged many times between the two fibres, exhibit a number of interesting properties, as will be shown in later sections.

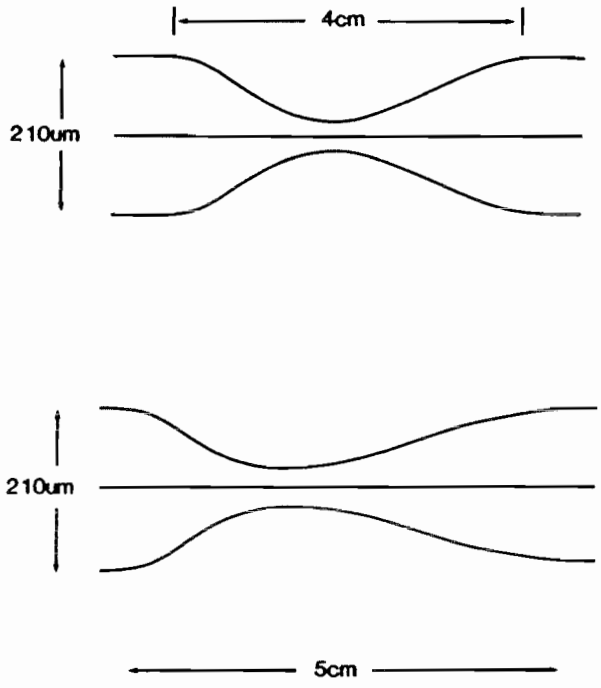

Figure 6.4. Taper profiles
a) symmetric
b) asymmetric

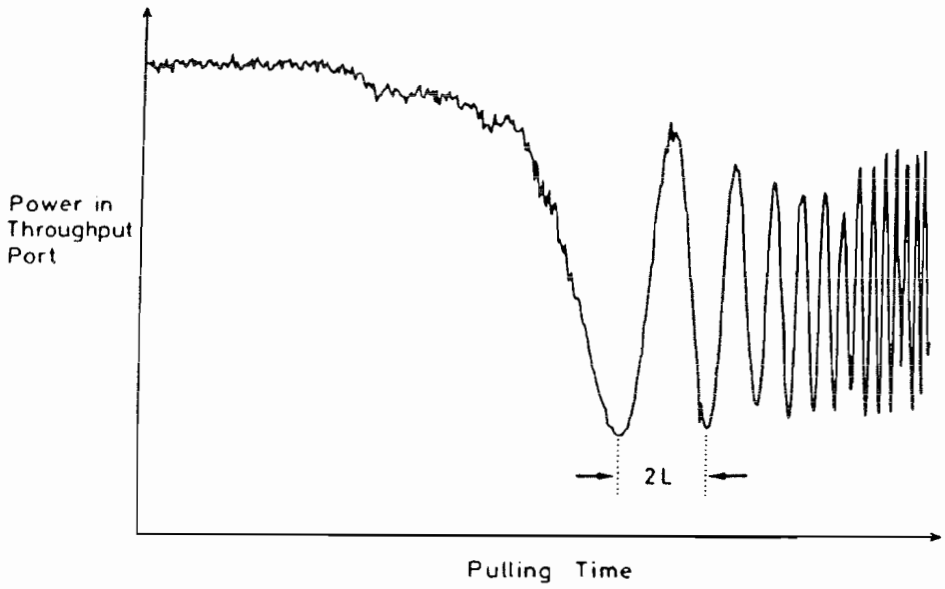

Figure 6.5. Variation of throughput power during fabrication

After fabrication the couplers were protected by potting the exposed section in a silicone rubber compound contained in a silica U-tube (Figure 6.6). The silicone rubber provided a sufficient mechanical buffer for most experimental purposes. However, for a few applications, the silica U-tube was further mounted in epoxy in a plastic or metal package and the fibre leads protected with plastic heatshrink tubing.

Since this work, fused tapered couplers have continued to be made at Southampton by M.S. Yataki. Oxy-butane flames are still providing the heat source although tapers are produced by vertical tension on the two fibres, in an attempt to eliminate motor-induced mechanical vibration. The fabrication technique and recent results are described in reference 23.

6.1.2 Dependence of couplers on external refractive index

It has been observed by other authors that the coupling coefficient for etched and for polished couplers depends on the refractive index of the intermediate medium[2,4]. This is because, for evanescent field coupling, the intermediate refractive index determines the degree of overlap between the field of one fibre and the core of the other. An investigation of the effects of refractive index changes in the medium surrounding a fused tapered coupler was therefore undertaken[12]. Prior to this work Dr. C.M. Ragdale had demonstrated that the loss of a taper is a strong function of external refractive index (Figure 6.7) reaching a maximum when the external index matched that of silica (1.458). The result clearly demonstrated that, in the centre of the taper, light propagates using all the fibre cross-section as a guide, with a propagation constant $\beta \simeq kn_{cl}$ (where $k = 2\pi/\lambda$ and n_{cl} = silica cladding index).

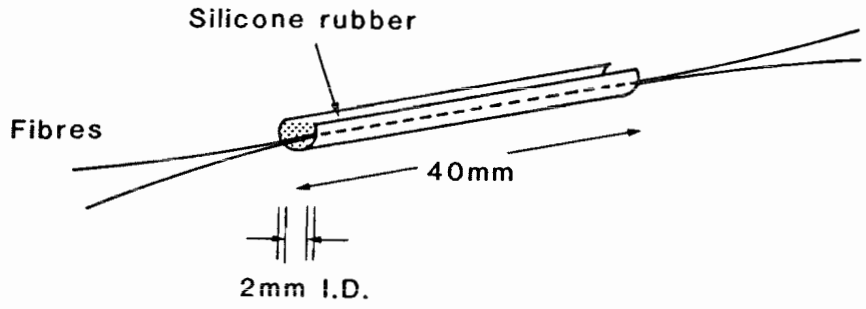

Figure 6.6. Potting technique for fused tapered coupler

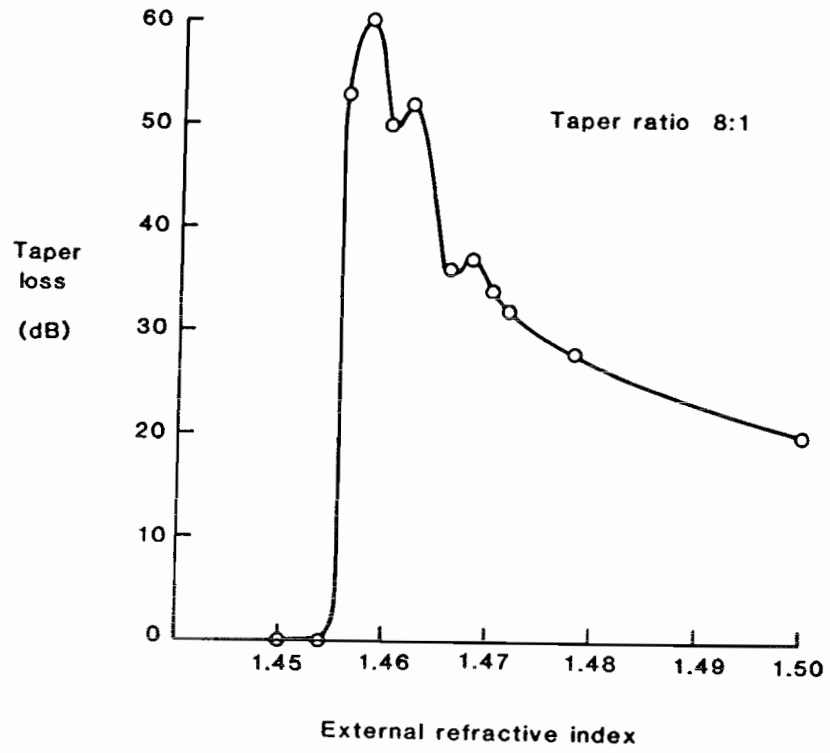

Figure 6.7. Dependence of taper loss on external refractive index

Couplers were fabricated from fibres whose parameters are listed in Table 6.1. Coupler dimensions varied from 20mm-40mm in length with taper ratios (twice diameter of one fibre : diameter of waist of tapered region) varying from 4:1 to 20:1. External refractive index variations were effected by immersing unpotted couplers in oils of differing refactive index and by temperature tuning the refractive index. The oil index was calibrated at specific temperatures using an Abbé refractometer which could be maintained at a constant temperature by a heated water supply (Gallenkampf). In this way the effect of index changes from 1.40 to 1.46 could be determined. Further experimental points were obtained with different organic liquids having refractive indices varying from 1.326 (methanol) to 1.357 (acetone) and air n=1. Figure 6.8 shows the effect of changes in external index for one fibre VD436 with taper ratios 4:1, 8:1 and 20:1.

It can be seen that for couplers with low taper ratios, little change in the coupling coefficient occurs as the external index is raised. Couplers with larger taper ratios, which were pulled through a number of oscillations in output power, exhibit an increasing dependence on external index as it approaches that of silica. All of the results in Figure 6.8 are plotted in the region where the excess loss of the coupler due to index matching is less than 1dB).

The results have been successfully modelled by assuming that the lowest order symmetric and antisymmetric modes of the fused region are excited. Variation of the external refractive index will cause the propagation constants of the two modes to change and also the beat length between them, which determines the coupling coefficient. It has been observed that the coupling is strongly dependent on the dimension of the fused cross-section, and a typical experimental taper cross-section is shown in Figure 6.9a. Different models of the tapered region have

TABLE 6.1

Fibre	NA	Diameter	Ratio of Core : cladding + substrate
VD 436	0.09	105μm	1 : 20
VD 357	0.15	105μm	1 : 30

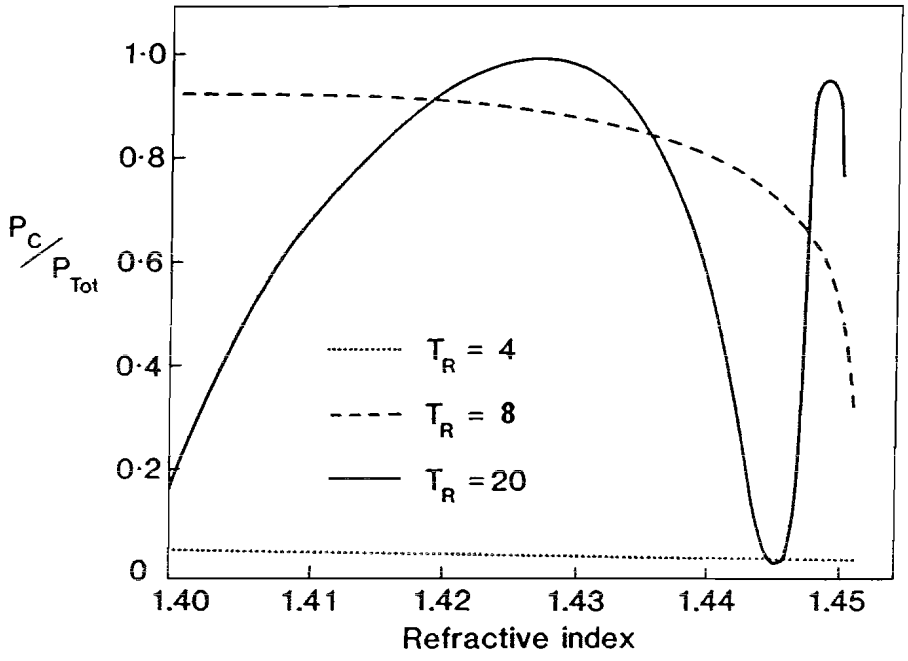

Figure 6.8. Dependence of coupled power on external refractive index

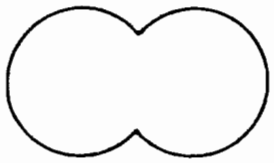

a)

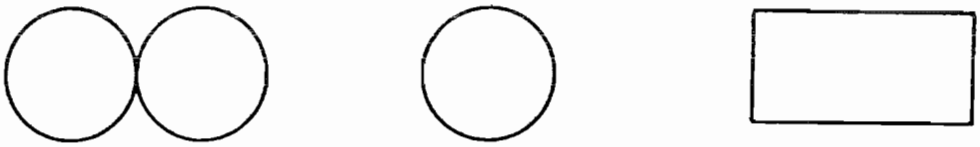

Bures model

(weakly fused)

Southampton models

(strongly fused)

b)

Figure 6.9. Experimental (a) and modelled (b) taper cross-sections

been proposed by Bures et al and by workers at Southampton and are shown in Figure 6.9b. Bures et al approximated the coupler by parallel touching cylinders and predicted that the coupling coefficient would increase as the index difference between the external medium as silica was reduced. The strongly-fused model of a single cylinder or a rectangular guide on the other hand, predicts a decrease in coupling for the same condition. It is shown in Appendix 6A that the variation in coupling is determined by the sign of

$$U_1 \frac{dU_1}{d\bar{V}} - U_2 \frac{dU_2}{d\bar{V}} \qquad \text{for } U_1 < U_2$$

where U_1 and U_2 are the modal parameters of the lowest order symmetric and antisymmetric modes of the waveguide, respectively. If this is negative, which is the case for most waveguides operated at high V-value, then the coupling coefficient decreases as the external index is raised. It is also shown, in Appendix 6A, that the coupling coefficient is proportional to $(n_{co}-n_{cl})^{-\frac{1}{2}}$, where n_{co} is the index of silica and n_{cl} is the external index. The results of Figure 6.8 have therefore been plotted against $(n_{co}-n_{cl})^{-\frac{1}{2}}$, and are shown in Figure 6.10. For couplers pulled through more than one oscillation there is an ambiguity in the sign of Δc. However, for couplers (a) and (b) the coupling coefficient clearly decreases as external index is raised, and so the other results have been plotted in the same sense. It can be seen that the gradient of the straight line fit varies dramatically with taper ratio. In Appendix 6A the constant of proportionality is shown to vary as $1/\rho^3$, where ρ is the cross-sectional radius of the tapered region. Although the coupling length varies slightly for these couplers, the agreement is striking. These results vindicate the "high V-guide model" as a description of the fused tapered coupler, and in particular the "well-fused" models developed at Southampton.

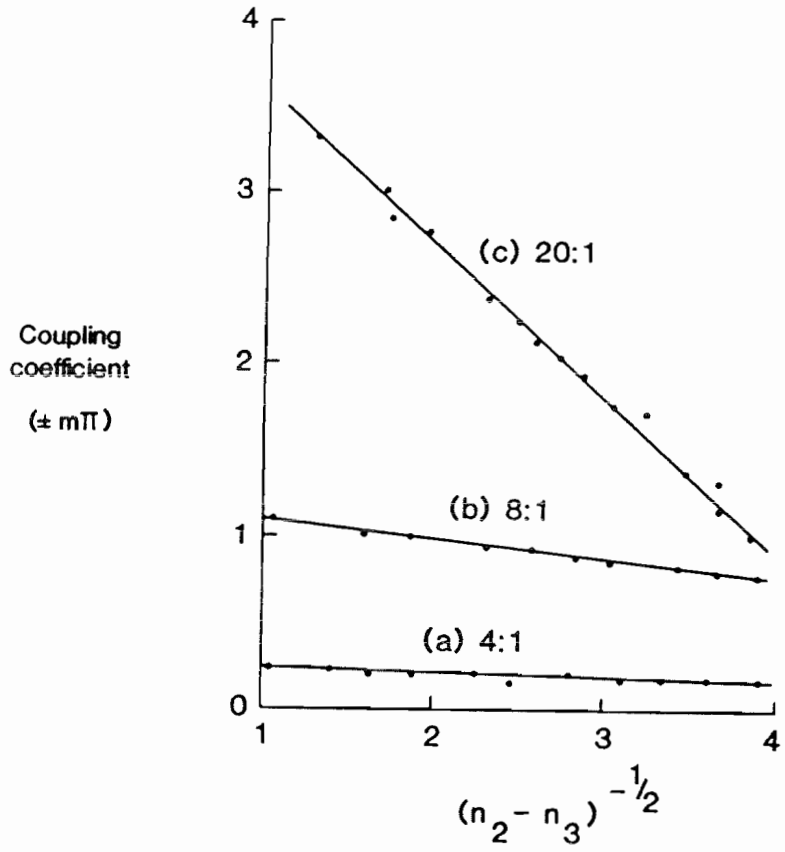

Figure 6.10. Dependence of coupling coefficient on the inverse numerical aperture of the high-V guide formed by the fused tapered coupler and the external medium

The difference in the prediction of the model of Bures et al and the "well-fused" models suggests that a coupler geometry might exist which is largely insensitive to refractive index changes. Recent work by Payne suggests that this is indeed the case[24]. However, for the couplers described in this thesis a linear variation with $(n_{co}-n_{cl})^{-\frac{1}{2}}$ is more appropriate.

6.1.3 Coupler loss

During the course of experimental work on couplers the insertion loss was reduced from greater than 1dB to less than 0.2dB. It was recognised that the fibre refractive index profile was critically important, since tapers pulled from depressed cladding fibre were shown to exhibit high loss. Results for three different depressed cladding fibres, taken from de Fornel et al[14], are shown in Figure 6.11. Matched cladding fibres were therefore used to produce low-loss couplers.

The control of the taper shape and, in particular, taper angle was also found to be important in determining the loss characteristics of fused tapered couplers. For this reason much time was spent optimising the flame length, temperature and pulling tension for each fibre, in order to produce gentle uniform tapers. Very short burners were found to produce too steep a taper angle whereas very long burners produced irregular tapers. The burner giving the best results had a hot zone of about 8mm. Low temperatures and low tensions were generally found to be advantageous, although at slow pulling speeds vibrations in the motor system led to an increased coupler loss. Most of the couplers were fabricated using pulling times varying from two to four seconds. The majority of the experimental work was carried out with the d.c. motor controlled pulling rig. However, the automated stepper motor controlled rig led to better reproducibility and, after an optimisation procedure, to the lowest losses of less than the experimental measurement limit of 0.2dB.

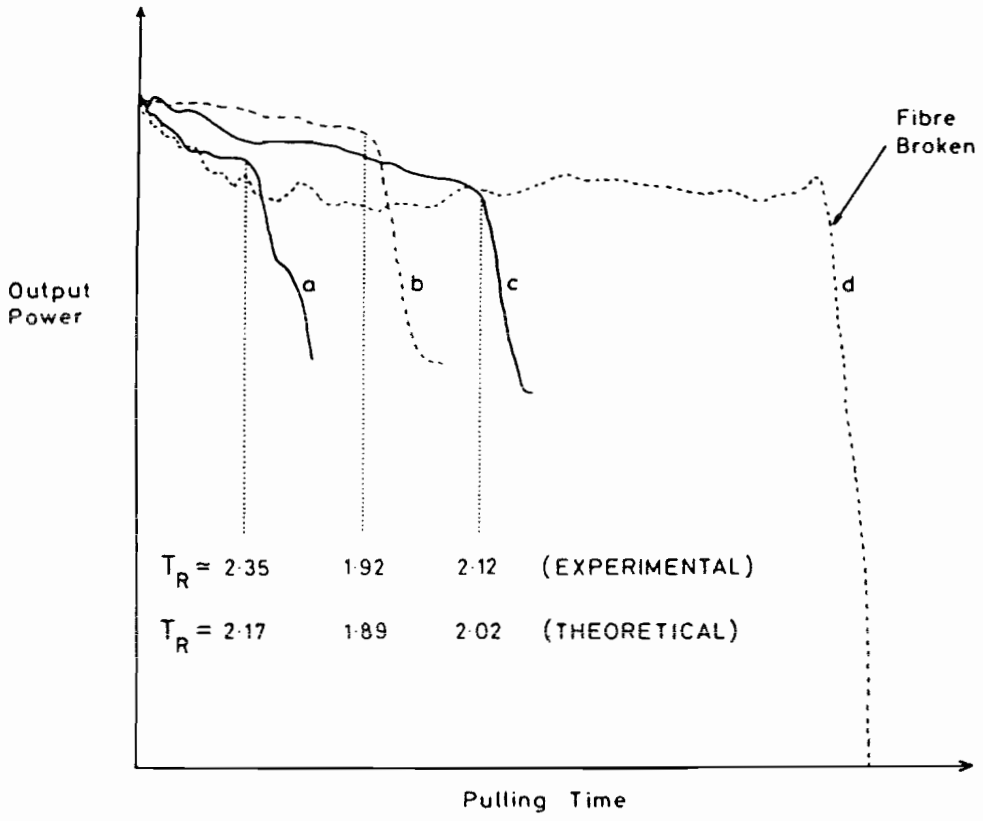

Figure 6.11. Loss of depressed cladding fibre tapers (ref. 12)

Subsequent theoretical work supports these findings. If the loss mechanism in the taper is conversion from the fundamental to higher order modes of the fibre external index guide, then a slowness criterion can be defined (see, for example, reference 25)

$$\frac{1}{\omega}\frac{d\omega}{dz} << \frac{\Delta\beta}{2\pi}$$

where

ω = modal spot size

z = distance along guide

$\Delta\beta$ = difference in propagation constants of fundamental and next highest mode of the same symmetry.

The tapering is most critical when the spot size increases rapidly, supporting the experimental observation that the coupler loss is sensitive near the end of the input taper. It is shown by Stewart and Love[18] that the slowness criterion is much less tolerant of taper angle for depressed cladding fibre than for matched cladding fibres because, at a particular value of V, the propagation constant of the fundamental mode comes very close to that of the next highest mode. The predicted V-values for this depressed cladding fibre loss agree well with the experimental results of Figure 6.11. This result has important bearing on the fabrication of couplers from highly birefringent fibre such as the "Bow-Tie" fibre. The stress-inducing sectors in these fibres are usually depressed in refractive index, and tapers made from such fibres are very lossy. By adding GeO_2 to the bow-tie sectors, approximate index matching can be achieved. Tapers pulled from "matched bow-tie" fibres have losses in the region of 1-3dB. At the time of writing it has not been possible to make low-loss highly-birefringent couplers by the fused tapered technique.

6.1.4 Wavelength dependence of couplers

The single-mode fused tapered couplers described in this chapter have a wavelength "window", where they can be operated with low loss, extending over hundreds of nanometers. An investigation of the wavelength dependence of the coupled power was therefore undertaken.

Couplers were fabricated with varying numbers of oscillations in the output power during the pulling process (ref Figure 6.5). They were potted in silicone rubber as described in section 6.2 and measured on the monochromator system described in Chapter 3. A selection of these results are shown in Figure 6.12. It was found that for couplers pulled through many oscillations in output power, a remarkable periodicity in the wavelength response was recorded, with periods as small as 12nm.

It is shown in Appendix 6A that the regular wavelength response is a feature of interference of two modes on any waveguiding structure operated at high V-value. Structural differences determine the sign and magnitude of the small changes in coupling period ($\Delta\lambda$) which are observed as wavelength is changed. The weakly fused model of Bures[15] predicts a decrease in wavelength period as wavelength is increased, whereas the strongly fused models predict an increase. Table 6.2 shows a comparison between predicted and experimental coupling periods $\Delta\lambda$. Once again it appears that the couplers are best described by the well-fused model.

A consequence of the approximate proportionality observed between the coupling coefficient and wavelength is that the coupling period is inversely proportional to the number of oscillations observed during fabrication (ref. Figure 6.5). It is shown in Appendix 6A that

$$\Delta\lambda = \frac{\pi\lambda_{monitor}}{\phi}$$

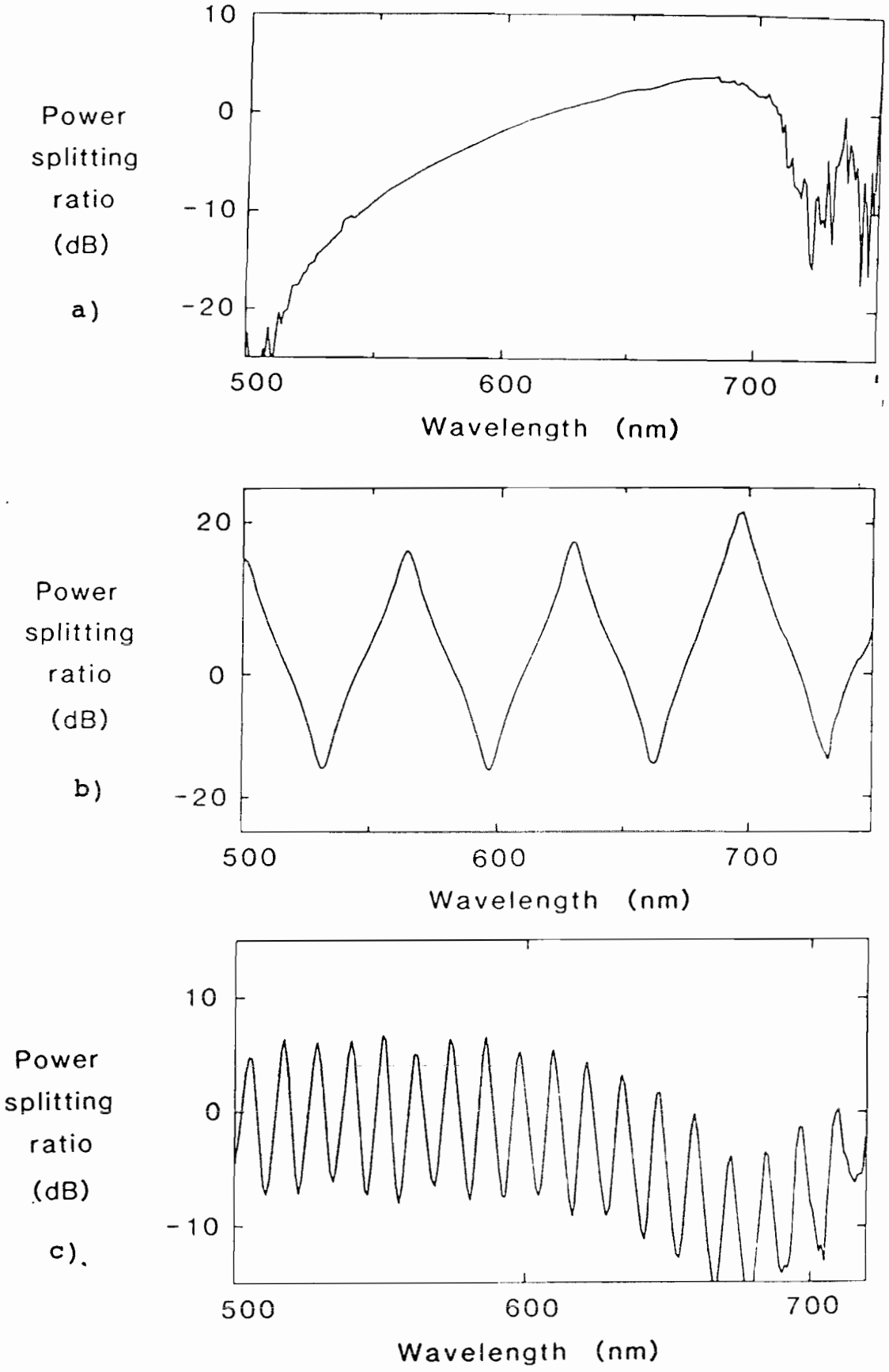

Figure 6.12. **Wavelength dependence of three couplers pulled through;**
a) 0.25 oscillations
b) 9.25 oscillations
c) >20 oscillations

TABLE 6.2

Coupler No.	1	2	3	4
No. of oscillations in output power during fabrication	0.03	1.7	7.9	8.5
Predicted $\Delta\lambda$ (nm)	2000	370	80	75
Experimental $\Delta\lambda$ (nm)	450	270	82	80

where

$\lambda_{monitor}$ is the wavelength at which oscillation are monitored

ϕ is the phase change observed during fabrication (= $m\pi$ for m oscillations).

Table 6.2 shows the measured $\Delta\lambda$ and the values predicted by measurement of ϕ at $\lambda_{monitor}$ for a selection of couplers. It can be seen that when the coupling is strong and ϕ is large, excellent agreement is obtained between the predicted and experimental results. However, for couplers pulled through much less than one oscillation, the two values are at variance. It is believed that these couplers cannot be modelled by the simple approximation developed here, and a full evanescent field analysis is necessary. Nevertheless, for couplers pulled through a number of oscillations in output power, it is possible to predict the wavelength characteristics of the coupler fairly accurately. This result has important implications for the design of wavelength selective couplers for the fibre ring laser.

6.2 Fibre Ring Lasers and Active Circuitry

The fibre lasers described in previous chapters have been based on a Fabry-Perot resonant cavity formed by the fibre and external mirrors. For many applications this is the simplest method to construct a laser resonator. The development of low-loss optical fibre couplers, however, makes possible an all-fibre ring laser, which is particularly well suited to fibre optic circuits since the output power is carried by a fibre. Furthermore, the ring configuration eliminates the need for stable mirror alignment. This section describes a fibre ring laser based on wavelength-selective couplers. Two approaches to ring fabrication have been investigated. In the first method described here, the wavelength selective coupler is made from the doped fibre itself, and two leads are spliced together to form the ring cavity. Unfortu-

nately the doped fibre is not ideal for coupler fabrication because it does not have a perfectly matched cladding. Furthermore, since the input lead to the coupler is also made from doped fibre, some of the pumping radiation is wastefully absorbed before it reaches the ring. An improved technique is to make the coupler from undoped fibre which has been optimised for low-loss coupler fabrication. The penalty here is that two splices are required to introduce doped fibre into the ring and the spot sizes of the two fibres must be well matched for the splices to have low-loss.

6.2.1 Nd^{3+}-doped ring laser

A coupler with the wavelength characteristic shown in Figure 6.13 was fabricated from the Nd^{3+}-doped fibre ND199. It was pulled through a large number of oscillations (~ 15) at the monitor wavelength of 1.08μm and adjusted to give a 10:1 splitting ratio. A moderate finesse fibre ring resonant at 1.08μm could then be formed by splicing ports 3 and 4 together, as shown schematically in Figure 6.14. To minimise pump absorption losses in the input lead, its length was reduced to less than 10cm, which corresponds to a loss at 595nm of less than 3dB. The intrinsic coupler loss was measured at 633nm (where the fibre has a negligible absorption) to be 3dB, although the loss at 1.08μm, where the ring is single-mode is less than 1dB. The coupler selectivity into the ring was estimated from Figure 6.13 to be greater than 80% in the region 580-605nm.

The fibre ring was spliced using a British Telecom prototype fusion splicer whilst monitoring the output at 633nm. Although the ring was far from optimal at this wavelength, a modulation of the output intensity caused by ring resonances gave an indication of optimum splice alignment. Monitoring was necessary because the core of the Nd^{3+}-doped fibre was not concentric. The ring was tested with a Coherent argon-ion laser pumped R6G dye

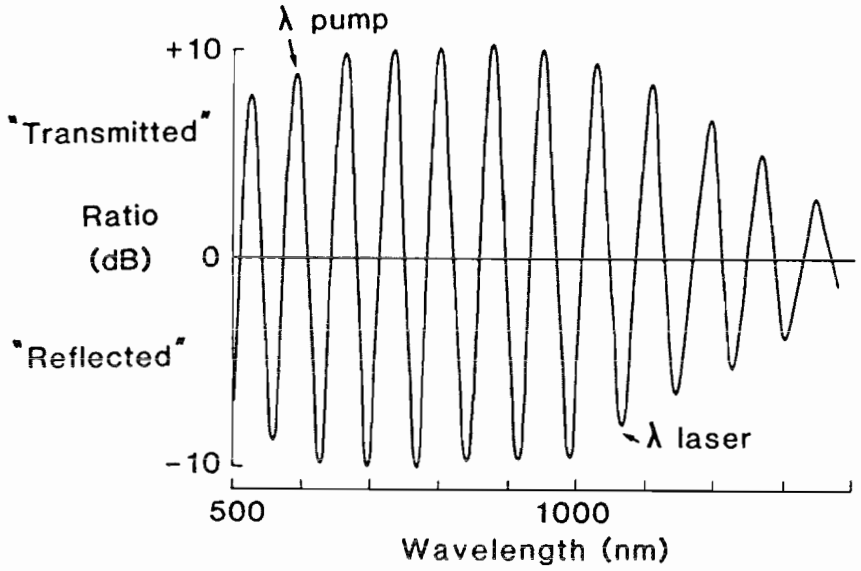

Figure 6.13. Wavelength response of coupler for neodymium-doped ring laser

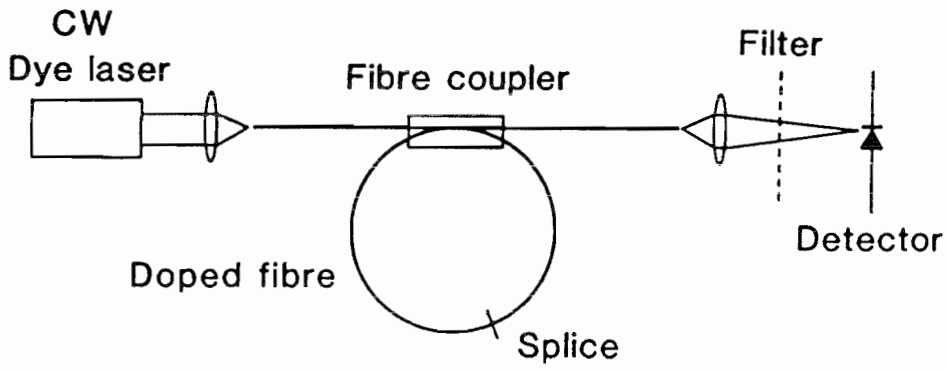

Figure 6.14. Schematic of ring fibre laser

laser which had a maximum output of 300mW in the wavelength region of 595nm. The laser was kindly loaned for this experiment by Dr. A. Tropper of the Physics Department. Lasing occured for a dye laser output of 70mW, corresponding to an estimated 14mW absorbed in the ring. The output power was measured with a calibrated reverse Peltier thermal detector designed by A. Ferguson. A maximum ring laser output of 2mW was recorded when pumping at 285mW.

The laser spectrum was measured on a 2m SPEX monochromator, which had a 0.1nm resolution. The high resolution enabled significant structure to be observed, Figure 6.15. Insertion of a polariser into the fibre output made no change to the spectrum, which was shifted by 10nm from the gain maximum due to a mismatch with the coupler selectivity (Figure 6.13). The structure is probably a result of residual gain competition, and has been observed previously in a linear cavity[26].

6.2.2 Improved Nd^{3+}-doped ring laser

The performance of the neodymium-doped ring laser has been improved by fabricating the coupler from an undoped matched cladding fibre. The coupler was chosen to have a coupling ratio greater than 10:1 in the wavelength region 580nm-610nm and 2:3 at the lasing wavelength of 1088nm, and the fibre was matched in numerical aperture and cut-off wavelength to the doped fibre ND199. The coupler loss at the lasing wavelength was measured to be 0.7 ± 0.2dB. Although the fibre was multimode at the pump wavelength ($V \sim 3.8$), it was relatively easy to launch the majority of the light into the fundamental mode. The maximum power available at the output of the coupler was measured to be 200mW.

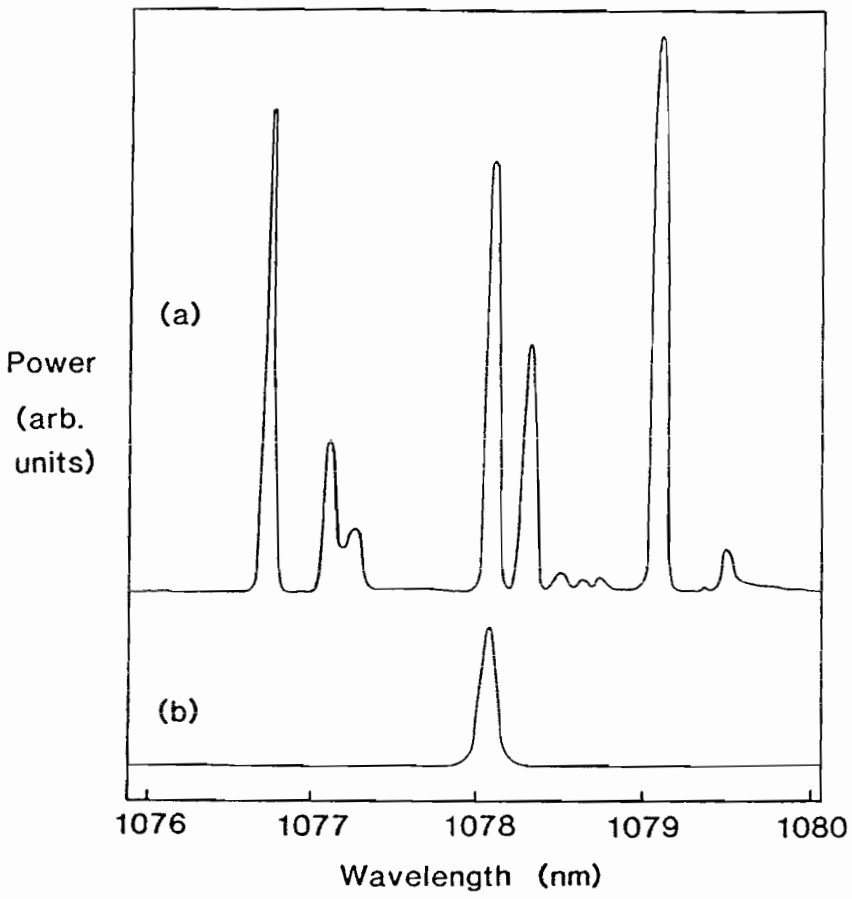

Figure 6.15. Output spectrum of neodymium-doped ring fibre laser

Two metres of fibre ND199 (110μm diameter) were spliced to the coupler output whilst monitoring the power at 630nm (where the fibre absorption is low). The loss was measured to be 0.9dB. Allowing for residual absorption of the doped fibre, the splice loss is estimated to be ~ 0.2dB. The ring was completed by splicing the doped fibre to the redundant input port of the coupler. Monitoring was still possible via the remaining output port of the coupler. The measured loss was 1.7dB. Allowing for the coupler loss at 630nm (~ 1.5dB; higher than at the lasing wavelength because the coupler is multimode), the splice loss was estimated to be 0.2dB. Optical monitoring of the splicing process was essential because the fibre cores were not concentric, and therefore alignment of the outer surfaces does not guarantee a low-loss splice.

The lasing characteristic and spectral output are shown in Figures 6.16 and 6.17. A maximum total output power of 12mW was obtained in a bidirectional output, an order of magnitude increase on the ring laser using a doped fibre coupler.

The spectrum was measured on a monochromator having a resolution of 1nm. Thus it was not possible to corroborate the previous high-resolution measurements. The FWHM was measured to be 6nm at a pump rate $P/P_{TH} \sim 15$. The extent of the broadening is less than observed in the Fabry Perot cavities, probably because of the wavelength selectivity of the coupler.

6.2.3 Er^{3+}-doped ring laser

An erbium-doped fibre ring laser has also been constructed following the technique of the previous section. The undoped coupler was the same as for the amplifier experiments in Chapter 5. The lasing characteristic and spectrum are given in Figures 6.18 and 6.19 respectively. It is interesting to note that it was

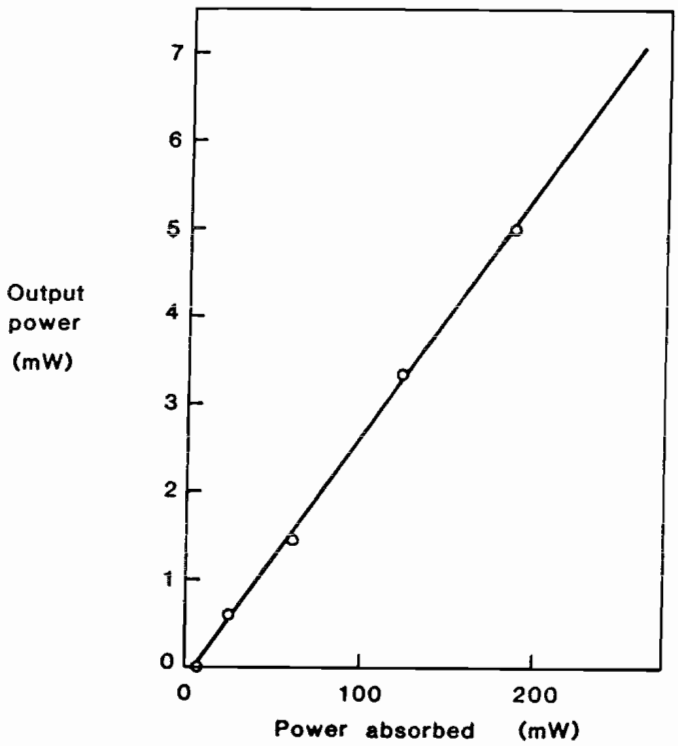

Figure 6.16. Lasing characteristic of improved neodymium-doped ring fibre laser

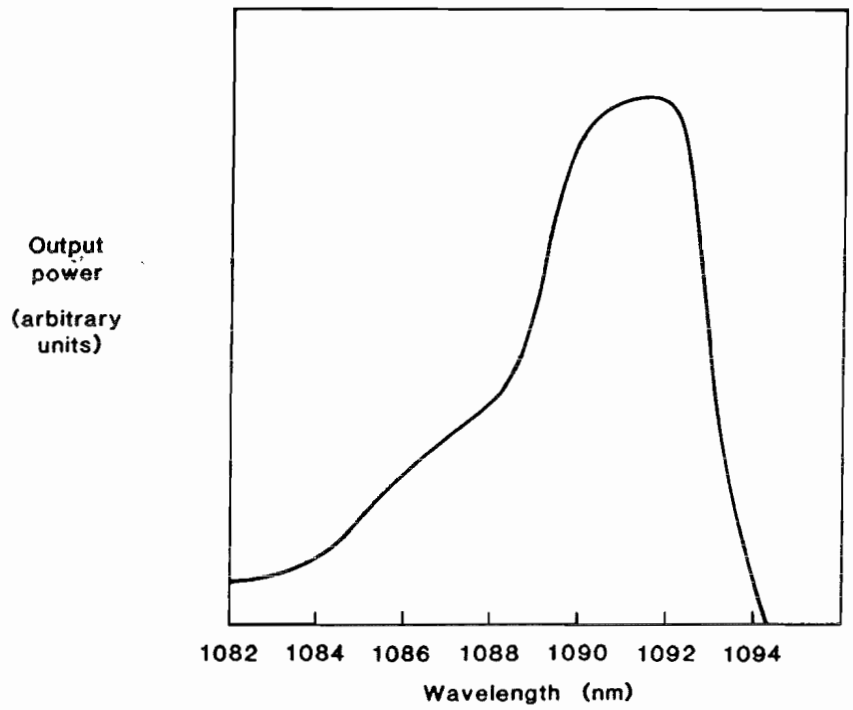

Figure 6.17. High power output spectrum of improved neodymium-doped ring fibre laser

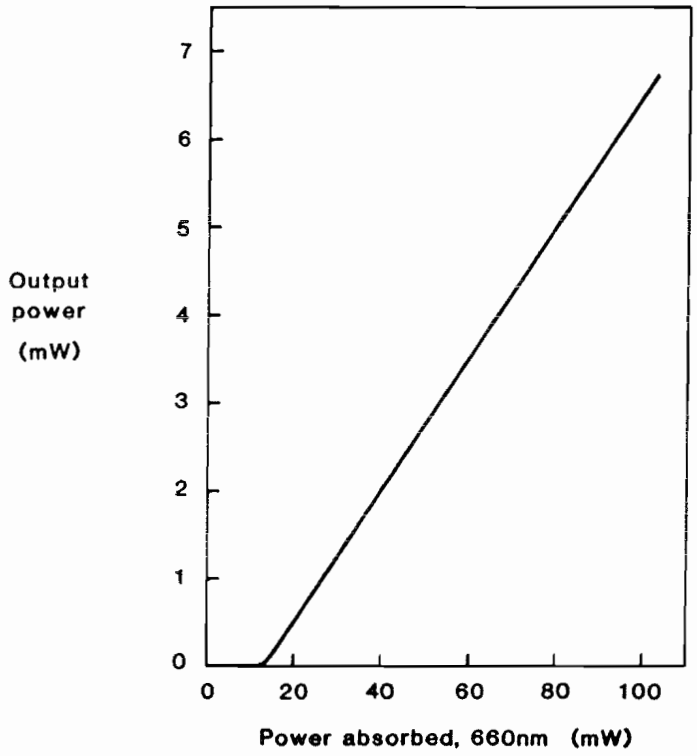

Figure 6.18. Lasing characteristic of erbium-doped ring fibre laser

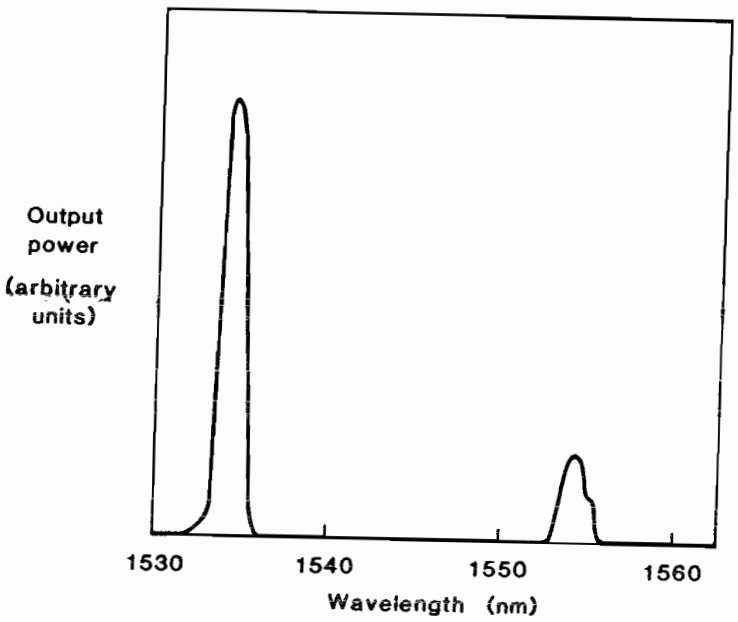

Figure 6.19. Output spectrum of erbium-doped ring fibre laser

possible to observe lasing on both transitions, at 1.536μm and 1.552μm, simultaneously. The maximum total output power was 14mW, in a bidirectional output.

6.3 Summary

A fabrication technique for fused-tapered couplers has been described. The method has resulted in low-loss couplers of variable splitting ratio. The dependence of the coupling strength on external refractive index and wavelength has been shown to correspond to a simple model appropriate to a well-fused taper cross-section.

The couplers have been used to construct fibre ring lasers at both 1.08μm and 1.54μm. The ring lasers have been shown to have a high efficiency, and eliminate the need for dielectric mirrors.

APPENDIX 6A :

In this section a general simplified model of the fused tapered coupler is presented. It is based on the assumption that coupling results from the interference of the lowest order symmetric and antisymmetric modes of the glass/external refractive index waveguide which forms the fused section of the coupler. These modes are excited by the input taper and excite core modes of both fibres in the output taper. A useful approximation of the fibre cross section as a rectangular waveguide by Payne et al[16] has led to simple analytic expressions of the dependence of coupling on external refractive index and wavelength which agree well with experimental results.

The general expression for the propagation constant of a waveguide mode is

$$\beta = \frac{1}{\rho}\left\{\frac{V^2}{2\Delta} - U^2\right\}^{\frac{1}{2}} \qquad (6A.1)$$

where

ρ is a typical linear dimension in the core cross section (ρ = core radius for cylindrical fibre waveguide)

$$V = \frac{2\pi\rho}{\lambda}\,(n_{co}^2 - n_{cl}^2)^{\frac{1}{2}}$$

n_{co} = maximum core refractive index

n_{cl} = uniform cladding index

λ = wavelength

$$\Delta = \frac{(n_{co}^2 - n_{cl}^2)}{2n_{co}^2}$$

U = dimensionless modal parameter

If the power exchange in a coupler results from interference between two modes on the waveguide then the coupling coefficient is given by the difference in propagation constants of the two modes.

$$C = \beta_1 - \beta_2 \qquad (6A.2)$$

when 1 denotes lowest order symmetric mode
2 denotes lowest order antisymmetric mode

Thus

$$C = \frac{1}{\rho}\left[\left\{\frac{V^2}{2\Delta} - U_1^2\right\}^{\frac{1}{2}} - \left\{\frac{V^2}{2\Delta} - U_2^2\right\}^{\frac{1}{2}}\right] \qquad (6A.3)$$

Equation (6A.3) can be evaluated for any waveguide once the values of U_1 and U_2 have been calculated from the eigenvalue equation. Payne has shown that if the coupler cross section is modelled by a rectangular waveguide a simple analytic expression for the coupling coefficient can be derived[16], viz

$$C = \frac{3\pi\lambda}{32\, n_{co}\, \rho^2} \cdot \frac{1}{(1 + 1/V)^2} \qquad (6A.4)$$

The agreement between the experimental results described in this Chapter and Equation (6A.4) is excellent. Since V is large, the coupling coefficient can also be expressed as

$$C = \frac{3\pi\lambda}{32\, n_{co}\, \rho^2}\left[1 - \frac{\lambda}{\pi\rho}\,(n_{co}-n_{c1})^{-\frac{1}{2}}\right] \qquad (6A.5)$$

Thus a plot of C against $(n_{co}-n_{cl})^{-\frac{1}{2}}$ is expected to yield a straight line with a gradient proportional to $1/\rho^3$. It should be noted that ρ in this model is the diameter of a single fibre at the centre of the taper i.e. $\rho/d = T_R$, where d is the diameter of one of the fibres and T_R is the taper ratio.

The form of equation (6A.4) is common to wide variety of waveguide cross-sections operated at high V-value, and expressions for the dependence of coupling on external refractive index and wavelength are, to first order, independent of coupler cross-section as will be shown. Provided that $k\rho >> U$, equation (6A.3) can be written

$$C \simeq \frac{\lambda}{4\pi\rho^2 n_{co}} \left\{ U_2^2 - U_1^2 \right\} \qquad (6A.6)$$

Typical coupler sectional dimensions are of the order of 10μm, and thus at a wavelength of 1μm $k\rho$ is of the order of 60. At high V-values U_2 and U_1 tend to their asymptotic values $U_{2\infty}$ and $U_{1\infty}$ such that $dU/dV = U_\infty/V^2$ i.e. $dU/dV << 1$.

Under these conditions the coefficient is proportional to wavelength in first order, which explains the observed periodicity in the coupling characteristic. Note too that the coupling coefficient should be proportional to the square of the taper ratio. The second order changes in $(U_2^2-U_1^2)$ as the wavelength, and hence the V-value varied, account for the small dependence of the coupling period, $\Delta\lambda$, on wavelength. The dependence of the coupling coefficient on external refractive index changes and on wavelength can be evaluated from equation (6A.5)

$$\frac{\partial C}{\partial n_{cl}} = \frac{\lambda}{4\pi\rho^2 n_{co}} \left\{ 2U_2 \frac{dU_2}{dV} - 2U_1 \frac{dU_1}{dV} \right\} \frac{\partial V}{\partial n_{cl}} \qquad (6A.7)$$

For "well-fused" waveguides $dU_2/dV > dU_1/\partial V$ and $U_2 > U_1$.

Therefore, since $\partial V/\partial n_{cl}$ is negative, the coupling coefficient decreases with increasing external refractive index. This result is in agreement with the experimental results of section 6.3. The positive $\partial C/\partial n_{cl}$ predicted by Bures arises for waveguides satisfying

$$U_2 \frac{\partial U_2}{\partial V} < U_1 \frac{\partial U_1}{\partial V} \qquad \text{for } U_2 > U_1 \tag{6A.8}$$

In physical terms the positive coefficient arises from the increased overlap between the two parallel sections of the waveguide (see Figure 6.9) as the refractive index is raised. However, for the majority of waveguides, the increase in refractive index leads to a reduction in the V-value and a corresponding reduction in the difference of the propagation constants as they both tend to kn_{cl}. The wavelength period $\Delta\lambda$ can be evaluated from equation (6A.5)

$$\frac{\partial C}{\partial \lambda} \simeq \frac{U_2^2 - U_1^2}{4\pi n_{co}\rho^2} + \left[2U_2 \frac{dU_2}{dV} - 2U_1 \frac{dU_1}{dV} \right] \frac{\lambda \partial V/\partial \lambda}{4\pi n_{co}\rho^2} \tag{6A.9}$$

and making the approximation that

$$\frac{dU}{dV} \rightarrow \frac{U_\infty}{V^2} \quad \text{as} \quad U \rightarrow U_\infty$$

$$\frac{\partial C}{\partial \lambda} \simeq \frac{U_{2\infty}^2 - U_{1\infty}^2}{4\pi n_{co}\rho^2} \left[1 - \frac{2}{V} \right] \tag{6A.10}$$

If the wavelength period $\Delta\lambda$ is defined as the wavelength change for which $\Delta C \ell = \pi$, where
ℓ is the length of the coupling region, then

$$\Delta\lambda = \frac{\pi}{\ell} \frac{4\pi n_{co}\rho^2}{U_{2\infty}^2 - U_{1\infty}^2} \frac{1}{(1-2/V)} \tag{6A.11}$$

Thus for well fused waveguides at high V-value the wavelength period $\Delta\lambda$ is expected to increase as wavelength is increased. Measurements of $\Delta\lambda$ for coupler (c) of Figure 6.12 do indeed indicate a small increase as wavelength is increased[16].

Equation (6A.11) can be reexpressed to give

$$\Delta\lambda \simeq \frac{\pi\lambda}{C\ell} \frac{1}{(1-2/V)} \qquad (6A.12)$$

At the monitor wavelength $\lambda_{monitor}$, $C\ell$ is the phase change ϕ observed during fabrication (i.e. $\phi = \pi$ x no. of oscillations observed). Thus for large V,

$$\Delta\lambda = \frac{\pi\ \lambda_{monitor}}{\phi} \qquad (6A.12)$$

The significance of equation (6A.12) is that the wavelength period $\Delta\lambda$ can be estimated from the number of power oscillations observed during fabrication. It is evident from Table 6.2 that for values of ϕ in excess of approximately 2π, good agreement between the predicted and experimental wavelength periods has been obtained.

References to Chapter 6

1. S.K. Sheem and T.G. Giallorenzi:
"Single-mode fibre-optical power divider : encapsulated etching technique",
Opt. Lett., 1979, 4, pp. 29-31.

2. F.J. Liao and J.T. Boyd:
"Single-mode fibre coupler",
Appl. Opt., 1981, 20, pp. 2731-2734.

3. R.A. Bergh, G. Kotler and H.J. Shaw:
"Single-mode fibre optic directional coupler",
Electron. Lett., 1980, 16, pp. 260-261.

4. M.J.F. Digonnet and H.J. Shaw:
"Analysis of a tunable single-mode optical fibre coupler",
IEEE J. Quant. Electron., 1982, QE-18,
pp. 746-754.

5. L.F. Stokes, M. Chodorow and H.J. Shaw:
"All single-mode fiber resonator",
Opt. Lett., 1982, 7, pp. 288-290.

6. R. Kashyap and B.K. Nayar:
"An all-single-mode fibre Michelson interferometer sensor",
IEEE J. Lightwave Tech., 1983, LT-1, pp. 619-624.

7. M.C. Brierly, C.A. Millar and B.J. Ainslie:
"Fundamental characterisation of polished fibre half-couplers in contact with variable refractive-index media",
Proc. OFC., 1986, Atlanta.

8. R.A. Bergh, H.C. Lefevre and H.J. Shaw:
"All-single-mode fibre-optic gyroscope",
Opt. Lett., 1981, 6, pp. 198-200.

9. B.S. Kawasaki, K.O. Hill and R.G. Lamont:
"Biconical-taper single-mode fibre couplers",
Opt. Lett., 1981, 6, pp. 327-328.

10. C.A. Villarruel and R.P. Moeller:
"Fused single-mode fibre access coupler",
Electron. Lett., 1981, 17, pp. 243-244.

11. M.H. Slonecker:
Proc. OFC., 1982, Phoenix, USA., p. 36.

12. C.M. Ragdale, D.N. Payne, F. de Fornel and R.J. Mears:
"Single-mode fused biconical taper fibre couplers",
Proc. 1st OFS., 1983, London.

13. P.D. McIntyre and A.W. Snyder:
"Power transfer between optical fibres",
J. Opt. Soc. Amer., 1973, 63, pp. 1518-1527.

14. F. de Fornel, C.M. Ragdale and R.J. Mears:
"Analysis of single-mode fused tapered fibre couplers",
IEE Proc. H, 1984, 131, pp. 221-227.

15. J. Bures, S. Lacroix and J. Lapierre:
"Analyse d'un coupleur bidirectionnel à fibres optiques monomodes fusionées",
Appl. Opt., 1983, 22, pp. 1918-1922.

16. F.P. Payne, C.D. Hussey and M.S. Yataki:
"Modelling fused single-mode fibre couplers",
Electron. Lett., 1985, 21, pp. 461-462.

17. F. Martinez:
Minithesis,
University of Southampton, 1987.

18. W.J. Stewart and J.D. Love:
"Design limitation on tapers and couplers in single-mode fibres",
Proc. ECOC., 1985, Venice.

19. M.J.F. Digonnet and H.J. Shaw:
"Single-mode fibre-optic wavelength multiplexer",
Proc. OFC., 1982, Phoenix, USA.

20. M.S. Yataki, D.N. Payne and M.P. Varnham:
"All-fibre wavelength filters using concatenated fused-taper couplers",
Electron. Lett., 1985, 21, pp. 248-249.

21. D.B. Mortimore:
"Wavelength-flattened fused couplers",
Electron. Lett., 1985, 21, pp. 742-743.

22. R.J. Mears, L. Reekie, S.B. Poole and D.N. Payne:
"Neodymium-doped silica single-mode fibre lasers",
Electron. Lett., 1985, 21, pp. 738-740.

23 M.S. Yataki:
Minithesis,
University of Southampton, 1987.

24 F.P. Payne:
Private communication.

25. A.W. Snyder and J.D. Love:
"Optical Waveguide Theory",
Chapman and Hall, 1983.

26. E. Snitzer and C.G. Young:
"Glass Lasers",
Advances in Lasers, Vol. 2, A. Levine Ed.,
New York : Dekker, 1968, pp. 191-256.

CHAPTER 7 : DISCUSSION AND CONCLUSION

The advent of single-mode optical fibre lasers and amplifiers[1-3] is widely recognised as a significant advance for optical fibre communications and related measurements. Throughout the thesis attention has been restricted to the characterisation of two ions, Nd^{3+} and Er^{3+}, in a single glass host. In this chapter the widening potential of rare-earth-doped fibre lasers is examined and topics for further research are discussed.

7.1 The Potential for Rare-Earth-Doped Fibre Lasers

Lasers based on rare-earth ions, and in particular the Nd:YAG laser, already play a major role in laboratory, diagnostic and sensor applications. Two factors which restrict the even more widespread usage of such lasers are their high power requirements and large size. By virtue of their reduced thresholds, waveguide lasers look set to revolutionise this field. Slab- and fibre-waveguide Nd-crystal lasers have undergone considerable development and are now commercially available.

It is reasonable to compare the performance of the new optical fibre lasers with crystal waveguide lasers such as the mini-YAG laser. Table 7.1 summarises the present results and contrasts them with the typical specifications of a mini-YAG[4]. It is evident that in both classes of laser very high slope efficiencies can be obtained. For a GaAlAs laser diode pump source electrical/ optical conversion efficiencies of 5-10% can be obtained, compared to ~ 0.1% for a typical solid-state laser pumped by a flash tube.

The real difference between the two lasers lies in their spectral properties. Optical fibre lasers are broadly tunable[5] (over 80nm at 1.088μm) and typically run on many longitidunal modes. Crystal fibre lasers do not

have the tunability, but can be operated on a single longitudinal mode. Recent results on spectral narrowing with fibre gratings suggest that operation of optical fibre lasers in a single longitudinal mode should also be possible with more highly-doped, and thus shorter, fibres.

The tunability of optical fibre lasers makes them well suited to a variety of spectroscopic and wavelength-division multiplexing applications. For example, in excess of fifty, one-nanometer-spaced, channels could be obtained from the Nd^{3+}-doped fibre laser given suitable wavelength-selective feedback. With the inclusion of broad-band amplifiers it is evident that extremely high bandwidth communications networks could be maintained.

A further feature of the optical fibre laser is the variety of different ions which can be incorporated by the same fabrication procedure. Already neodymium[1], erbium[2] and praseodymium[7] ions have lased in the fibre configuration, and many more are possible (e.g. Ho^{3+}, Yb^{3+})[8-10]. The Er^{3+}-doped fibre laser, lasing at a wavelength of 1.54μm that coincides with the lowest-loss region of silica-based optical fibres, is well in advance of any crystal-fibre laser at this wavelength. As a three-level system it is ideally suited to the small-cored optical fibre configuration because of the high pump intensity which is required to deplete the ground-state. In addition to efficient CW operation, pulsed outputs with peak intensities well into the non-linear regime ($\sim 1GW/cm^2$) have been obtained[11]. These results open the way for new non-linear devices based on fibre lasers.

Optical amplification is optimised in the single-mode fibre configuration because the gain, for a given input power, is inversely proportional to the cross-sectional area of the waveguide. The results of Chapter 5 indicate that gains of the order of 1dB/mW are attainable at 1.5μm, the preferred wavelength for long-distance telecommunications. It is believed that fibre amplifiers

can play an important role not only in communications, but for a variety of sensors and components where fibre loss is an important consideration. At present the pulsed performance of crystal fibre lasers exceeds that of the optical fibre lasers at 1.06μm/1.08μm although at 1.5μm the situation is reversed. The reason is not one of efficiency, but simply because of the higher pump powers possible in the crystal configuration. The optical fibre laser usually requires the pump to be launched into the HE_{11} mode, whereas the radiation from high-power laser diode arrays can only be launched efficiently into multi-mode fibres. A number of designs for single-mode selection in large core fibres have been put forward, and the author is confident that pulsed operation at much higher powers is possible. The real advantage of the optical fibre lies, once again, in its ability to produce tunable pulses, a specification frequently met in laser applications.

The linewidth broadening mechanisms in glass result in the potential for very short mode-locked pulses. To date this has remained merely a potential - the shortest pulses observed in optical fibre lasers are still measured in hundreds of picoseconds. It is believed that fibre dispersion is largely responsible, and it is hoped that with shorter, more highly doped fibres, bandwidth limited operation will result.

7.2 Further Research

There are a number of topics still to be addressed which will, hopefully, form the subject matter of subsequent theses.

The solution technique for the fabication of doped fibres[12], discussed briefly in Chapter 3, has great potential for the development of new fibres. In particular there is considerable scope for the optimisation of the

glass composition in a manner similar to the evolution of the glasses for bulk-glass lasers over the past twenty years. Laser wavelength, stimulated cross-section, and excited state absorptions, are all dependent on glass composition and, although trends have been noted, laser glass technology is still very much an empirical science.

One refinement not discussed at length in this thesis is the use of co-dopants to enable the use of convenient pump wavelengths. For example, in bulk glasses, a cocktail of Yb^{3+} and Er^{3+} ions absorb at 900nm and resonantly transfer the energy to the $^4I_{13/2}$ level of the erbium ion[13]. This has an obvious application to a diode-pumped Er^{3+}-doped fibre laser.

In order to achieve successful codoping, higher dopant concentrations are required, and this necessitates a change in glass composition from the germanoscilicate glass studied in this thesis because of the quenching and ion-clustering that is observed[14]. Higher dopant concentration will also be advantageous to the production of short Q-switched, and mode-locked, pulses and in the effort to obtain operation in a single longitudinal mode. The fibre lasers described in this thesis are randomly polarised, and in the amplifier experiments, the gain has not been observed to be dependent on signal polarisation. Nevertheless, a small degree of polarisation anisotropy is observed when, for example, a polarisation-maintaining fibre is pumped, on one axis, with a polarised source. The results are consistent with an excitation of randomly-orientated dipoles and a partial depolarisation between the upper pump level and the upper laser level. This has important consequences for the design of polarised fibre lasers, and will be discussed in a later publication. The investigation forms part of a doctoral study by J.T. Lin[15].

Raman generation using a Q-switched Er^{3+}-doped fibre laser was discussed in Chapter 4. It is one example of a variety of non-linear effects which should be attainable using the fibre laser configuration. The importance of the result lies in the fact that the absorbed pump power is only a few tens of milliwatts. One restriction to the application of non-linear effects in devices is the high power required to generate the non-linearity. Fibre lasers would appear to be an attractive method for using low power (and hence inexpensive) pump sources to generate the intensities necessary for the utilisation of non-linear effects. There remains much research to be done in this field, but it is noted that the peak intensity in the diode-pumped Nd^{3+}-fibre Q-switched laser is already of the order of $1GW/cm^2$ [16].

In Chapter 6, the foundation of an all-fibre laser technology based on optical fibre couplers is discussed. As further optical fibre components are developed, new applications to fibre lasers will be pursued. A special fibre design has already resulted in polarised laser action[17], and the spectral properties of fibre lasers can be controlled with fibre gratings. There is a philosophy that it would be preferable to perform any temporal or spectral modification on the laser without the light leaving the fibre. To this end there is a general requirement for fibre switches and modulators. The fibre beam expander[18] could be the key to maintaining a guided mode whilst interacting with, for example, acoustic modulators or filters. Beam expanders could also be incorporated to obtain a collimated laser output, and to minimise surface damage in high-power lasers.

In conclusion, whilst this thesis considers two ions in a specific glass host, there remain ninety other elements in the periodic table and innumerable glasses! Nevertheless, it is hoped that the thesis provides an intelligible introduction to this new technology and gives an indication of the potential for the future.

TABLE 7.1 : Comparison of Optical Fibre Laser, and Crystal Fibre Laser, Specifications.

Nd^{3+}-ion

CW Operation	Optical Fibre Laser	Mini-YAG[4]
Threshold	High finesse : 100μW Typical : 2mW	4mW - 10mW
Slope efficiency	35% - 45%	~40%
Highest output power (HE_{11} mode)	6mW (40mW diode)	15mW (SLM; 200mW diode)
Linewidth	1GHz - 3THz multilongitudinal mode 1MHz SLM	<100kHz single longitudinal mode
Tunable	over 80nm (1059-1140nm)	~1nm
Other lines	899nm - 944nm	1.32μm [19]
Pulsed Operation		
Q-switched	1.6μJ, 120ns, 400Hz repetition (40mW diode)	10μJ, 30ns 1kHz (200mW diode)
Mode-locked	1mW (av), 1ns (40mW diode)	20mW (av), 150ps (200mW diode)
Amplifier	5dB, (40mW diode)	40dB (200mW diode)

Er^{3+}-ion

CW Operation	Optical Fibre Laser	Er^{3+}-YAG
Threshold	High finesse : 4mW (660nm pump) Typical : 6mW	no data available at 1.55μm
Slope efficiency	20%	
Highest output power (HE_{11} mode)	25mW (200mW pump)	
Linewidth	5GHz - 200GHz (multilongitudinal mode)	
Tunable	over 35nm (1.529-1.564μm)	
Other lines	No	2.8μm, 1.66μm [20] 0.85μm

Pulsed Operation

Q-switched	100W, 30ns, 1kHz repetition (200mW pump)
Mode-locked	10mW, 1ns
Nonlinear generation	Raman 1.62-1.66μm
Amplifier	20dB (40mW diode)

References to Chapter 7

1. R.J. Mears, L. Reekie, S.B. Poole and D.N. Payne: "Neodymium-doped silica single-mode fibre lasers", Electron. Lett., 1985, 21, pp. 738-740.

2. R.J. Mears, L. Reekie, S.B. Poole and D.N. Payne: "A low threshold tunable CW and Q-switched fibre laser operating at 1.55μm", Electron. Lett., 1986, 22, pp. 159-160.

3. R.J. Mears, L. Reekie, I.M. Jauncey and D.N. Payne: "High-gain rare-earth-doped fibre amplifier at 1.55μm", Proc. OFC., 1987, Reno, Nevada.

4. John Gerkin (Photon Control): Private communication.

5. L. Reekie, R.J. Mears, S.B. Poole and D.N. Payne: "Tunable single-mode fibre lasers", Journal of Lightwave Technology, 1986, LT-4, pp. 956-960.

6. I.M. Jauncey, L. Reekie, J.E. Townsend, D.N. Payne and C.J. Rowe: "Single longitudinal mode operation of a Nd^{3+}-doped fibre laser", Submitted to Optics Letters.

7. L. Reekie, R.J. Mears, S.B. Poole and D.N. Payne: "A Pr^{3+}-doped single-mode fibre laser", IOP/IEE Symposium on Advances in Solid State Lasers, Imperial College, May 1986.

8. H.W. Gandy and R.J. Ginther:
"Stimulated emission from holmium activated silicate glass",
Proc. IRE., 1962, 50, pp. 2113-2114.

9. H.W. Etzel, H.W. Gandy and R.J. Ginther:
"Stimulated emission of infra-red radiation from ytterbium activated silicate glass",
Appl. Opt., 1962, 2, pp. 534-536.

10. H.W. Gandy, R.J. Ginther and J.F. Weller:
"Stimulated emission of Tm^{3+} radiation in silicate glass",
J. Appl. Phys., 1967, 38, pp. 3030-3031.

11. R.J. Mears and L. Reekie:
"A high-power tunable erbium-doped fibre laser operating at 1.55μm",
Proc. CLEO., 1987, Baltimore.

12. J.E. Townsend, S.B. Poole and D.N. Payne:
"Solution-doping technique for fabrication of rare-earth-doped optical fibres",
Electron. Lett., 1987, 23, pp. 329-331.

13. E. Snitzer and R. Woodcock:
"Yb^{3+} - Er^{3+} glass laser",
Appl. Phys. Lett., 1965, 6, pp. 45-46.

14. H. Namikawa, K. Arai, K. Kumata, Y. Ishii and H. Tanaka:
"Preparation of Nd-doped SiO_2 glass by Plasma Torch CVD",
Jap. Journal Appl. Phys., 1982, 21, pp. 360-362.

15. J.T. Lin:
Minithesis,
University of Southampton, 1987.

16. L. Reekie, I.M. Jauncey and D.N. Payne:
"Near optimum operation of a diode-laser pumped fibre laser",
To be presented at ECOC, Helsinki, 1987.

17. J.T. Lin, P.R. Morkel, L. Reekie and D.N. Payne:
"Polarisation effects in fibre lasers",
To be presented at ECOC, Helsinki, 1987.

18. K.P. Jedrzejewski, F. Martinez, J.D. Minelly, C.D. Hussey and F.P. Payne:
"Tapered-beam expander for single-mode optical-fibre gap devices",
Electron. Lett., 1986, 22, pp. 105-106.

19. A.I. Ferguson:
"Single-frequency operation of an optically pumped monolithic Nd:YAG laser at 1.3μm",
Electron. Lett., 1985, 21, pp. 853-854.

20. L.J. Johnson, J.E. Geusic and L. G. Van Uitert:
"Coherent oscillations from Tm^{3+}, Ho^{3+}, Yb^{3+} and Er^{3+} ions in yttrium aluminium garnet",
Appl. Phys. Lett., 1965, 7, pp. 127.

CHAPTER 8 : PERSONAL PUBLICATIONS, CONFERENCE PRESENTATIONS AND AWARDS

1. C.M. Ragdale, D.N. Payne, F. de Fornel and R.J. Mears:
"Single-mode fused biconical taper fibre couplers",
Proc. 1st International Conference on Optical Fibre Sensors, 1983, London.

2. F. de Fornel, C.M. Ragdale and R.J. Mears:
"Analysis of single-mode fused tapered couplers",
IEE Proc. H., 1984, 131, pp. 221-228.

3. R.J. Mears, M.P. Varnham, D.N. Payne and A.J. Barlow:
"Polarisation control in resonant-ring fibre gyroscopes",
Proc. 2nd OFS, 1984, Stuttgart.

4. R.J. Mears:
"Birefringence in the resonator gyroscope",
IEE Colloquium on Optical Fibre Sensors and Components, 1984, Glasgow.

5. R.J. Mears, L. Reekie, S.B. Poole and D.N. Payne:
"Neodymium-doped silica single-mode fibre lasers",
Electron. Lett., 1985, 21, pp. 738-740.

6. S.B. Poole, D.N. Payne, M.E. Fermann, R.I. Laming and R.J. Mears:
"Characterisation of fibres containing rare-earth-ions",
JOERS Optical Fibre Measurements Symposium, 1985, London.

7. R.J. Mears, D.N. Payne, S.B. Poole, L. Reekie, I.P. Alcock, A.I. Ferguson, D.C. Hanna and A.C. Tropper:
"Single-mode neodymium fibre lasers",
Seventh National Quantum Electronics Conference, 1985, Great Malvern.

8. A.J. Barlow, D.N. Payne, M.P. Varnham and R.J. Mears:
"Birefringent fibre polarisation components for sensor applications",
Proc. SPIE, 1985, San Diego.

9. L. Reekie, R.J. Mears, D.N. Payne and S.B. Poole:
"Tunable single-mode fibre lasers",
Conference on Integrated Optics and Optical Fibre Communication/11th European Conference on Optical Communiction, October 1985, Venice.

10. D.N. Payne, R.J. Mears, L. Reekie and S.B. Poole:
"Rare-earth doped fibre lasers",
10th Australian Conference on Optical Fibre Technology, Perth, Australia, December 1985 (Invited).

11. R.J. Mears, L. Reekie, S.B. Poole and D.N. Payne:
"A low threshold tunable CW and Q-switched fibre laser operating at 1.55μm",
Electron. Lett., 1986, 22, pp. 159-160.

12. I.M. Jauncey, J.T. Lin, L. Reekie and R.J. Mears:
"An efficient diode-pumped CW and Q-switched single-mode fibre laser",
Electron. Lett., 1986, 22, pp. 198-199.

13. R.J. Mears, L. Reekie, S.B. Poole and D.N. Payne:
"Rare-earth doped fibre lasers",
Optical Fibre Communication/Integrated and Guided Wave Optics, Atlanta, February 1986.

14. R.J. Mears, L. Reekie, S.B. Poole and D.N. Payne: "Development of rare-earth doped fibres and single-mode fibre lasers", Anglo-Chinese Symposium on Optical Communications, Beijing, May 1986.

15. L. Reekie, R.J. Mears, S.B. Poole and D.N. Payne: "A Pr^{3+}-doped single-mode fibre laser", IOP/IEE Symposium on Advances in Solid State Lasers, Imperial College, May 1986.

16. I.M. Jauncey, J.T. Lin, L. Reekie, R.J. Mears and D.N. Payne: "A diode laser pumped single-mode fibre laser", JOERS Advanced Fibre Waveguide Devices Symposium, May 1986.

17. D.N. Payne, L. Reekie, R.J. Mears, S.B. Poole, I.M. Jauncey and J.T. Lin: "Rare-earth doped single-mode fibre lasers, amplifiers and devices, CLEO, San Francisco, June 1986, (Invited).

18. S.B. Poole, D.N. Payne, R.J. Mears, M.E. Fermann and R.I.Laming: "Fabrication and characterisation of low-loss optical fibres containing rare-earth ions", Journal of Lightwave Technology, 1986, LT-4, pp. 870-876.

19. L. Reekie, R.J. Mears, S.B. Poole and D.N. Payne: "Tunable single-mode fibre lasers", Journal of Lightwave Technology, 1986, LT-4, pp. 956-960.

20. L. Reekie, R.J. Mears, S.B. Poole and D.N. Payne: "Optical bistability at 1.54μm in a Er^{3+}-doped single-mode fibre laser", European Conference on Optical Communication, 1986, Barcelona.

21. F.P. Payne, T. Finegan, M.S. Yataki, R.J. Mears and C.D. Hussey: "Dependence of fused taper-couplers on external refractive index", Electron. Lett., 1987.

22. R.J. Mears, L. Reekie, I.M. Jauncey and D.N. Payne: "High-gain rare-earth-doped fibre amplifier at 1.55μm", OFC, 1987, Reno, Nevada.

23. I.M. Jauncey, L. Reekie, R.J. Mears, D.N. Payne, C.J. Rowe, D.C.J. Reid, I. Bennion and C. Edge: "A narrow linewidth fibre laser with integral fibre grating", Electron. Lett., 1986, 22, pp. 987-988.

24. I.M. Jauncey, L. Reekie, R.J. Mears and C.J. Rowe: "A narrow linewidth fibre laser operating at 1.55μm", To be published in Optics Letters.

25. R.J. Mears and L. Reekie: "A high-power tunable erbium-doped fibre laser operating at 1.55μm", Proc. CLEO, Baltimore, 1987.

In June 1986 the author took up a Junior Research Fellowship in the Electronics Department at The University of Southampton. In February 1987 the author was elected to the Maudslay Research Fellowship at Pembroke College, Cambridge.